Freie Universität Berlin

Fachbereich Geowissenschaften / Institut für Geologische Wissenschaften

und

Deutsches GeoForschungsZentrum GFZ - Helmholtz Zentrum Potsdam

Department 4 Chemie und Kreisläufe der Erde / Sektion 4.4 Sedimentbeckenanalyse

---

Lithospheric-scale 3D structural and thermal modelling and the assessment of the origin of thermal anomalies in the European North Alpine Foreland Basin

Dissertation
zur Erlangung des Doktorgrades der Naturwissenschaften
„doctor rerum naturalium“
(Dr. rer. nat.)

eingereicht am
Fachbereich Geowissenschaften
der Freien Universität Berlin

von

Anna Maria Przybycin

Berlin, September 2015

Erstgutachter: Prof. Dr. Michael Schneider (Freie Universiät Berlin)

Zweitgutachterin: Prof. Dr. Magdalena Scheck-Wenderoth (RWTH Aachen)

Datum der Disputation: 27. November 2015

... just because…

Content

Content I

List of figures III

List of tables VI

Declaration of Originality VII

Acknowledgement VIII

Summary 1

Zusammenfassung 3

1 Introduction 4

1.1 State of the Art 6

1.2 Objectives of the thesis 7

1.3 Overview over the thesis 11

2 Assessment of the isostatic state and the load distribution of the European Molasse Basin by means of lithospheric-scale 3D structural and 3D gravity modelling 14

2.1 Abstract 14

2.2 The European Molasse Basin 14

2.3 The starting model 17

2.4 Gravity modelling 28

2.5 Load calculation 31

2.6 Interpretation and Discussion 33

2.7 Conclusions 38

3 The 3D conductive thermal field of the North Alpine Foreland Basin: influence of the deep structure and the adjacent European Alps 39

3.1 Abstract 39

3.2 Background 39

3.3 The lithospheric-scale 3D structural model 43

3.4 Method 48

3.5 Results 51

3.6 Sensitivity Analysis with respect to thermal properties 57

3.7 Interpretation and Discussion 61
3.8 Conclusions 66
4 The origin of deep geothermal anomalies in the Germany Molasse Basin assessed by 3D numerical modelling of coupled fluid flow and heat transport 67
4.1 Abstract 67
4.2 Introduction 67
4.3 The hydrogeological model 72
4.4 The numerical approach 77
Governing Equations 77
The FE model 79
Parametrisation 81
Boundary Conditions and Initial Conditions 81
4.5 Results and Interpretation 84
4.6 Discussion 95
4.7 Conclusions 98
5 Summarising Discussion 99
6 Summarising Conclusions 110
7 References 113
8 Appendix 1 Publications related to this thesis ..... a

List of figures

Fig 1 The model area (red frame) superposed on the topography ETOPO1 in the Molasse Basin and Alpine area and the implemented data. **15**

Fig 2 Thickness maps of the sediments and the Alpine and Tauern Body implemented into the 3D structural model. **19**

Fig 3 Depth map of the top basement (= top crystalline crust) implemented into the model. **21**

Fig 4 The Moho depth implemented into the structural model (Moho depth after Grad et al. 2009). **22**

Fig 5 Calculated lateral density distribution (left) in the crystalline crust according to the approach of isostatic equilibrium of Pratt (1855) and the thickness of the crystalline crust (right). **24**

Fig 6 Thickness maps of the upper (left) and lower (right) crustal layer before (above) and after (below) the modification of the structural model by means of 3D gravity modelling. **26**

Fig 7 Depth map of the Lithosphere-Asthenosphere Boundary (LAB) in the Molasse Basin area constructed following Tesauro (2009), Geissler et al. (2010), Karousova et al. (2013), Seiberlich et al. (2013) and Bianchi et al. (2014). **27**

Fig 8 Map a shows the measured Bouguer gravity, which was used to evaluate the structural model and the position of the cross section shown in Fig 10. Map b shows the first gravity response of the starting model before the modification of the layer interfaces. Map c shows the calculated Bouguer gravity response and map d the associated residual anomaly of the best fit model after the modification of the layer geometry and the densities. Map e displays the difference between the first model response and the best-fit model and therewith the deviation of the best-fit model from the isostatically calculated starting model. **30**

Fig 9 Calculated load distribution at different depths in the area of the European Molasse Basin. **32**

Fig 10 Cross-section through the lithospheric-scale model (below) and a zoom-in into the crustal part (middle). Above, the measured Bouguer Gravity (black) and the best-fit model response (red) are shown for this cross-section. **33**

Fig 11 The North Alpine Foreland Basin in its topographic environment. The model area is marked with a red square. The basin is highlighted in green, the position of the Tauern Body is marked with yellow. **40**

Fig 12 The lithospheric-scale 3D structural model used for the calculation of the present-day conductive thermal field (modified after Przybycin et al. 2015a). First kind boundary conditions have been used at the surface (variable mean surface temperature, Fig 16) and at the LAB (1,300°C, Fig 15) for the thermal calculation. **44**

Fig 13 Thickness maps (a-f) of the sedimentary units resolved in the 3D structural model (modified after Przybycin et al. 2015a). **45**

Fig 14 Thickness maps of the Alpine units (a-b) and the crustal units (c-d) resolved in the 3D structural model (modified after Przybycin et al. 2015a). **46**

Fig 15 Depth of the Lithosphere-Asthenosphere Boundary (modified after Przybycin et al. 2015a) used for this study as the lower thermal boundary to which a temperature of 1,300°C is assigned for the calculation of the 3D thermal field. **48**

Fig 16 The mean annual surface temperature used as upper thermal boundary condition at the model surface for the calculation of the 3D thermal field (modified after DWD 2013, InMeteo 2013, HISTALP 2013). Locations of the 24 geothermal energy production sites (Tab 4) are depicted, for which observed temperatures are available, to which our calculated temperature results have been compared **50**

Fig 17 The resulting present-day lithospheric-scale 3D conductive thermal field of the Molasse Basin area. Subpanels a and b zoom into areas of specific thermal effects with a) thermal blanketing effect and b) chimney effect (shown with higher temperature resolution, scale shown at zoom-in b). **52**

Fig 18 Temperature maps (a-d) at different depths extracted from the 3D thermal model of which maps a-d have been compared to respective temperature-depths maps of the GeotIS thermal model (Agemar et al. 2014b, purple dashed lines). Maps e-f show depths for which no observed data was available as comparison. **54**

Fig 19 Temperature maps for larger depths (a-b) extracted from the 3D thermal model. **55**

Fig 20 Depth maps a and b showing the depths of the 100°C and 450 °C isotherms. **56**

Fig 21 Temperature distribution at a depth of 3,000 m bsl predicted for different ranges of thermal properties as assessed in a sensitivity analysis. Maps a to d show the influence of the thermal conductivity of specific model units on the temperature distribution. **58**

Fig 22 Temperature distribution at a depth of 3000 m bsl predicted for different ranges of thermal properties as assessed in a sensitivity analysis. Maps a - d show the influence of the thermal conductivity of the upper and lower crystalline crust on the temperature distribution. **59**

Fig 23 Temperature distribution at a depths of 3000 m bsl. Maps a and b show the impact of the radiogenic heat production of the upper crystalline crust on the thermal field. **60**

Fig 24 The model area (red frame) shown on the topography ETOPO1 (after Amante and Akins 2009) **68**

Fig 25 Thickness maps of lithostratigraphic units implemented into the coupled model **73**

Fig 26 The hydraulic conductivity of the Malm Gamma-Zeta following Birner (2013) implemented into the 3D numerical model. **76**

Fig 27 The 3D numerical model used for the coupled simulations of fluid flow and heat transport. The different horizontal mesh resolution was chosen according to the facies distribution of the Malm aquifer (StMWIT 2010). **80**

Fig 28 The upper thermal boundary condition implemented into the numerical model. The map shows a variable mean annual surface temperature over the last 30 years (DWD 2013) and was assigned as Dirichlet boundary condition to the topography. **82**

Fig 29 Temperature distribution at a depth of 7,500 m bsl which has been extracted from the 3D lithospheric-scale conductive thermal model of Przybycin et al. (2015b) and prescribed as lower thermal boundary condition (Dirichlet) to the base slice of the model. **83**

Fig 30 Predicted temperatures by the coupled fluid flow and heat transport simulations without considering faults in the system (model 1) shown with temperature maps at different depths. **86**

Fig 31 Temperature map at a depth of 3,500 m bsl showing the temperature distribution calculated considering only conductive heat transport following the approach of Przybycin et al. (2015b). **89**

Fig 32 The predicted temperature distribution shown on profiles through the model area.. ..... **91**

Fig 33 The temperature distribution at a depth of 3,500 m bsl calculated using a lower (by two dimensions) hydraulic conductivity of the Folded Molasse Sediments compared to model 1 ..... **92**

Fig 34 Temperature maps at a depth of 3,500 m bsl showing the influence of different hydraulically conducive testfaults on the thermal field, which have been included stepwise and subsequently all together in model 3.. ..... **93**

List of tables

Tab 1 Input data for the structure model of the North Alpine Foreland Basin. **18**

Tab 2 The lithologies and the averaged bulk densities assigned to the distinguished lithostratigraphic units. **22**

Tab 3 Thermal properties assigned to the lithostratigraphic units and the range of values tested in the sensitivity study. **49**

Tab 4 Geothermal energy production sites with their measured temperature and the respective calculated temperatures. The production sides are additionally depicted on the map in Fig 16. ..... **63**

Tab 5 The thermal and hydraulical properties prescribed to the layers of the numerical model. **75**

Tab 6 Comparison of observed and calculated temperatures for the location of 20 geothermal production sites at different depths. The locations of measurements are shown in figure 28 ..... **88**

Declaration of Originality

I hereby certify, as the author of this thesis and as the main author of the publication involved, that the work presented in this thesis was composed by and originated from me, except as acknowledged in text and related reference list. The work was not submitted previously to any other institutions.

Anna Maria Przybycin

Acknowledgement

I would like to thank Prof. Dr. Michael Schneider from the Freie Universität Berlin and Prof. Dr. Magdalena Scheck-Wenderoth from the German Research Centre for Geosciene GFZ - Helmholtz Centre Potsdam for their supervision, the great discussions and their sustained support during this thesis. Furthermore, I thank the LFU of Bavaria, the LIAG in Hannover and the AQUASOIL GmbH for providing me the requirend data and their support during the preparation of this thesis.
Furthermore, I would like to thank the DHI WASY and the TRANSINSIGHT GmbH for providing the academic licenses for the software FEFLOW and the software IGMAS+, respectively, and their constant support.

I am grateful to the present and former members of the section 4.4 of the GFZ for the time spent together and their constant encouragement. Special thanks go to Leni, who never failed to show me her confidence and always reached out a helping hand when needed. I owe you a lot.
Namely I would like to thank Jessi, Alex, Ingo, Lew, Max, Vera, Yvonne and Bo for their patience, support and help during the time of this thesis. I will always remember what you did for me.

My personal thanks go to my family who always supported me, even when times were tough. You earthed me and cheered me up when I needed it.

Moreover, my thanks go to my friends since many years, especially Maike, Susi and Stefi, which were there for me when I needed them.
Furthermore, I would like to thank my friends Tobias, Janine, Christin and Ulrike, which I found during my time at the GFZ. You made my live much more pleasant and became an important part of my live on and off the hill. I could not imagine completing this work without all your constant support.

Summary

The European North Alpine Foreland Basin, also known as the European Molasse Basin, is a Tertiary wedge-shaped foreland basin at the northern front of the European Alps and extends over parts of France, Switzerland, Germany and Austria. In the basin, the Molasse Sediments are underlain by Mesozoic sedimentary successions, which include the Upper Jurassic aquifer (Malm), a major target for geothermal energy production.
The Molasse Basin has been explored and used for geothermal energy production since decades due to its specific thermal configuration. The thermal field of the basin shows increasing temperatures from north to south at all depths and pronounced positive and negative thermal anomalies, especially in the area around the city of Munich at depths of exploration interest. Between these anomalies, temperature differences of more than 40 K may occur at 3,500 m bsl over a small horizontal distance of just a few kilometres, a phenomenon which could so far not be explained based on the present-day knowledge.

From previous exploration efforts and related studies, a high amount of data about the structure as well as the distribution of temperatures and thermal properties in the European Molasse Basin exists. Unfortunately, the spatial distribution and lateral data coverage is non-uniform in the basin. Modelling techniques are useful tools to overcome such appearing data gaps by combining databased knowledge with physically reliable assumptions to generate a complete picture of the thermal field of the basin. However, knowing the temperature distribution is not enough to reduce the exploration risk in the European Molasse Basin. Rather, an understanding of the heat driving mechanisms and the origin of the pronounced temperature anomalies is of high importance to reduce the uncertainty in predicting the extraction temperature and discharge of geothermal power plants.

The aim of this thesis was to contribute to the understanding of the structural configuration of the basin and the heat transport processes acting therein and with that to explain the origin of the pronounced thermal anomalies in the German Molasse Basin.

To achieve this goal, first a lithospheric-scale 3D structural model was constructed which includes the Molasse Basin as well as the South German Scarpland and some parts of the Alps. This structural model was based on freely available depth and thickness information for different lithostratigraphic units in the basin area from wells, seismic experiments and surface geology. Areas not covered with measured data were constrained with isostatic calculations and 3D gravity modelling. The calculated 3D load distribution shows significant lateral load variations down to the depth of the Lithosphere-Asthenosphere Boundary. Furthermore, the assessment of the isostatic state shows that the German Molasse Basin area is not isostatically equilibrated and that the gravity field is strongly influenced by the configuration of the crystalline crust on lithospheric-scale.

In a second step, the present-day 3D steady-state conductive thermal field of the German Molasse Basin was calculated based on the gravity constrained lithospheric-scale 3D structural model. For this, the

temperature distribution was assumed to be controlled only by the structural configuration, the distribution of thermal properties and the boundary conditions. After comparing the resulting conductive thermal field to published temperature maps based on measured data, areas with a good match between predicted and observed temperatures were considered as dominated by conductive heat transport. In areas with a poor temperature fit an additional influence of fluid flow on the thermal field was assumed. The predicted temperature distribution indicates that the thermal field is controlled by conductive heat transport in the lithospheric mantle and the crystalline crust. Shallower parts of the thermal field are strongly controlled by a thermal interdependence between the Alpine area and the basin itself and by the underlying crystalline crust related to their contrasting thermal properties. Furthermore, the results indicate that the distinct thermal anomalies in the German Molasse Basin are partly triggered by the structural configuration of the crust and the presence of the Tauern Body, though not excluding an additional influence of fluid flow.

To assess the influence of fluid flow on the shallow thermal field of the German Molasse Basin, coupled fluid flow and heat transport simulation were conducted. A basin-scale 3D structural model of the sedimentary part of the German Molasse Basin was built which was based largely on the upper part of the lithospheric-scale 3D structural model. To adapt the basin-scale model to the needs of numerical simulations, the hydrogeological model was transferred into a 3D finite element model. Using a 3D finite element method, the thermal field of the basin was predicted with simulations of coupled fluid flow and heat transport, which succeeded to reproduce the observed thermal anomalies in the German Molasse Basin. In contrast to assumptions of previous studies no permeable faults were needed to reproduce these thermal anomalies.
The resulting coupled thermal field indicates that the temperature distribution is primarily controlled by conductive heat transport, but also strongly affected by basin-wide as well as local fluid flow especially at shallower depths. In particular, the results show that the positive and negative thermal anomalies are caused by a combination of conductive and advective heat transport and may be correlated to the permeability of the Molasse Sediments, to the facies controlled permeability distribution in the Upper Jurassic aquifer (Malm) and to the spatial distribution of the Cretaceous Purbeck formation.

Summarising, the thesis was successful in reproducing the observed thermal field of the German Molasse Basin with a multi-scale approach of different modelling techniques for the first time, based on which an explanation for the distinct thermal anomalies occurring in the basin could be derived. In addition, the results of this study provide reliable thermal and hydraulic boundary conditions for local- and reservoir-scale models to further reduce the exploration risk of future geothermal energy drillings in the German Molasse Basin area.

Zusammenfassung

Das Europäische Nordalpine Vorlandbecken, auch bekannt als Europäisches Molassebecken, ist ein keilförmiges, tertiäres Vorlandbecken im Norden der europäischen Alpen. Es erstreckt sich über Teile Frankreichs, der Schweiz, Deutschlands und Österreichs und ist gefüllt mit Molassesedimenten. Diese *Molasse* wird unterlagert von mesozoischen Sedimentfolgen, einschließlich des oberjurassischen Malm-Grundwasserleiters, welcher ein Hauptzielhorizont für die geothermische Energieexploration ist. Aufgrund seiner speziellen thermischen Beschaffenheit wird das Sedimentbecken seit Jahrzehnten für die geothermische Energieproduktion erkundet und genutzt. Die Temperaturen im Becken steigen von Nord nach Süd in allen Tiefen an und es treten ausgeprägte positive und negative thermische Anomalien, vor allem im Gebiet um die Stadt München, in explorationsrelevanten Tiefen auf. Der horizontale Temperaturunterschied zwischen diesen Anomalien von mehr als 40 K innerhalb weniger Kilometer konnte jedoch bis heute noch nicht vollständig erklärt werden. Durch die Exploration und die daran angebundenen Studien in der Vergangenheit konnten viele Daten zur Struktur sowie zur Temperatur- und Parameterverteilung im Europäischen Molassebecken angesammelt werden. Diese sind jedoch ungleichmäßig im Becken verteilt. Die dadurch auftretenden Datenlücken können jedoch mit Modellierungsansätzen bestehend aus einer Kombination von datenbasiertem Wissen und physikalisch belastbaren Annahmen überbrückt werden, um ein vollständiges Bild der Temperaturverteilung im Becken zu erhalten. Das reine Wissen über die Temperaturverteilung im Untergrund ist jedoch nicht ausreichend, um das Explorationsrisiko im Europäischen Molassebecken nachhaltig zu senken. Vielmehr ist ein umfassendes Verständnis der Wärmetransportmechanismen nötig, um den Ursprung der ausgeprägten Temperaturanomalien zu erklären und die Vorhersageunsicherheit bezüglich Fördertemperatur und Entnahmemenge geothermischer Bohrungen zu reduzieren.

Das Ziel dieser Doktorarbeit war es, zum Verständnis der strukturellen Beschaffenheit und der Wärmetransportprozesse im Deutschen Molassebecken beizutragen und damit die Entstehung der ausgeprägten thermischen Anomalien zu erklären.

Um dies zu erreichen, wurde zunächst ein lithosphärenskaliges 3D-Strukturmodel des Molassebeckens, des Süddeutschen Schichtstufenlandes und Teile der Alpen konstruiert. Dieses basierte auf frei zugänglichen Informationen zu Tiefen und Mächtigkeiten unterschiedlicher lithostratigraphischer Einheiten aus Bohrkernuntersuchungen, aus seismischen Experimenten und aus der Oberflächengeologie. Bei der Modellkonstruktion wurden Areale, die nicht mit Beobachtungen abgedeckt waren, mit Hilfe isostatischer Berechnungen und mit 3D-Schwerefeldmodellierung vervollständigt. Die mit dem Modell berechnete 3D-Lastenverteilung zeigt wesentliche laterale Lastenvariationen bis zur Lithosphären-Asthenosphärengrenze. Die Ergebnisse der 3D-Schwerefeldmodellierung deuten auf einen isostatisch nicht ausgeglichenen Zustand des Deutschen Molassebeckens hin, sowie auf eine starke Beeinflussung des Schwerefeldes durch die Konfiguration der kristallinen Kruste.

In einem zweiten Schritt wurde, basierend auf dem lithosphärenskaligen 3D-Strukturmodel, das heutige konduktive thermische Feld des Deutschen Molassebeckens berechnet. Dabei wurde angenommen, dass die Temperaturverteilung nur durch die strukturelle Konfiguration, die damit einhergehende Verteilung von thermischen Eigenschaften und durch bestimmte thermische Randbedingungen kontrolliert wird. Nach einem Vergleich der Ergebnisse mit publizierten, auf Beobachtungen basierenden Temperaturkarten, wurden Gebiete mit guter Temperaturübereinstimmung als dominiert durch thermische Konduktion angesehen. Für Gebiete, in denen gemessene und modellierte Temperaturen stark von einander abwichen, wurde eine zusätzliche Beeinflussung durch advektiven Temperaturtransport in Zusammenhang mit Fluidfluss angenommen. Aus der Berechnung des thermischen Feldes ergibt sich, dass die Temperaturen im lithosphärischen Mantel sowie in der kristallinen Kruste durch die Tiefe der Lithosphären-Asthenosphärengrenze und die radiogene Wärmeproduktion der Oberkruste kontrolliert werden. Flachere Bereiche werden dagegen stark von einer thermischen Wechselwirkung der Sedimente der Alpen und des Beckens mit der kristallinen Kruste und dem Tauernkörper beeinflusst. Diese Wechselwirkung wird durch den Kontrast zwischen den thermischen Eigenschaften der einzelnen Strukturen hervorgerufen.

Um abzuschätzen, wie stark das flache thermische Feld durch advektiven Wärmetransport in Zusammenhang mit Fluidfluss beeinflusst wird, wurden gekoppelte Fluidfluss- und Wärmetransportsimulationen durchgeführt. Hierfür wurde ein beckenskaliges numerisches 3D FE-Modell des Deutschen Molassebeckens basierend auf dem oberen Teil des lithosphärenskaligen Strukturmodells konstruiert, welches an die Anforderungen numerischer FE-Simulationen angepasst wurde. Das erechnete thermische Feld reproduziert die beobachteten thermischen Anomalien im Deutschen Molassebecken erfolgreich. Anders als in früheren Studien, war dafür kein Einbau hydraulisch durchlässiger Störungen in das Model nötig. Die Ergebnisse der gekoppelten Simulationen zeigen, dass die Temperaturverteilung im Molassebecken primär durch konduktiven Wärmetransport erzeugt wird, aber auch stark beeinflusst ist durch beckenweiten Fluidfluss. Insbesondere zeigen die Ergebnisse, dass die positiven und negativen thermischen Anomalien im Becken durch eine Kombination von konduktiven sowie lokalen und beckenweiten advektiven Wärmetransport erzeugt werden und mit der Verteilung der hydraulischen Durchlässigkeit der Molassesedimente und des Malms, sowie der räumlichen Verteilung der Purbeckformation korreliert werden können.

Insgesamt ist es in dieser Doktorarbeit gelungen, das beobachtete thermische Feld des Deutschen Molassebeckens mit einem mehrskaligen Ansatz und mit unterschiedlichen Modellierungstechniken zu reproduzieren. Basierend auf den Ergebnissen konnte eine mögliche Erklärung für die ausgeprägten thermischen Anomalien im Becken formuliert werden. Zusätzlich stellen die Ergebnisse dieser Doktorarbeit verlässliche thermische und hydraulische Randbedingungen für zukünftige lokale und reservoirskalige Untersuchungen bereit, um das Explorationsrisiko zukünftiger geothermischer Bohrungen weiter zu senken.

1. Introduction

In times of decreasing reserves of hydrocarbon, the provision of renewable energy is a key topic of the present-day society. Geothermics is such a renewable energy, whose energy source is the earth itself. Depending on the geothermal gradient, areas suitable for geothermal exploitation can be recognized by studying the thermal field of the subsurface.

One area, which has been explored for geothermal energy production since decades is the European North Alpine Foreland Basin, also known as the European Molasse Basin. It evolved due to the Euro-Adriatic continental collision since the Cretaceous and extends over parts of France, Switzerland, Germany and Austria. Today, the basin has a wegde shape and is filled with clastic sediments originating from erosional processes of the Alps, *the Molasse* (Berge and Veal 2005). These sediments are underlain by a Mesozoic sedimentary succession, which includes the Upper Jurassic Malm aquifer (Birner et al. 2009, Birner 2013). The exploration and exploitation of this aquifer for geothermal energy production have lead to a large amount of data, with which a picture of the temperature distribution in the subsurface could be generated (GeotIS, Schulz et al. 2009). This picture shows pronounced negative and positive thermal anomalies in the shallow part of the basin, between which the temperature may change rapidly by more than 40 K within a few kilometers of horizontal distance (StMWIT 2010). Such strong temperature variations at the same depth over a small lateral extent cause a high risk for geothermal energy exploitation and may reduce the willingness of further investment into geothermal energy production in the European Molasse Basin. To decrease the exploration risk and improve the prediction of extraction temperature and fluid quantity, a better understanding of the heat driving mechanism causing the distinct thermal anomalies in the basin is of high significance, which in turn is depending on the availability of data. Though the basin has been an object of investigations in many studies of different scales in the past (Roeder and Bachmann 1996, Kempf et al. 1999, Berge and Veal 2005, Jodocy and Stober 2009, Pamer and Diepolder 2010, Böhm et al. 2011, Reischenbacher and Sachsenhofer 2011, Birner et al. 2012, Cacace et al. 2013, GeoMol Team 2015) its temperature distribution and the origin of the pronounced thermal anomalies could not be explained with the present-day knowledge.

One crucial aspect to understand the thermal configuration and the origin of the thermal anomalies in the basin is having sufficient information about the structural configuration, the distribution of physical properties and about the temperatures within the basin. Even though the exploitation interest has lead to a large amount of data, the spatial distribution of this data is highly non-homogeneous in the basin area. In contrast to successful exploration in areas of positive thermal anomalies and strong fluid inflow, unsuccessful geothermal exploration campaigns with poor extraction temperatures or fluid quantities in the past (Moeck et al. 2013) have lead to a decreased effort of exploration and with that data gaps in the respective areas. Modelling techniques are useful tools to overcome such data gaps by combining databased knowledge with physical assumptions to create a three-dimensional model of the area of interest. However, the sheer knowledge about the complex temperature distribution at depth in the

European Molasse Basin is not enough to reduce the exploration risk. Though the interpolated temperature measurements of GeotIS (Jodocy and Stober 2009, Schulz et al. 2009, StMWIT 2010) give an insight into the subsurface temperature distribution at depth, they are not explaining the heat driving processes creating the distinct temperature distribution. To estimate the potential production rate of geothermal power plants confinable, a better understanding of the coupled fluid and heat transport in the basin is necessary.

1.1 State of the Art

In the past different studies have used different modelling approaches to reproduce the thermal and flow field and with that to explain the thermal anomalies in the European Molasse Basin of which Frisch and Huber (2000), Vosteen (2003), Rühaak (2009, 2015), Rühaak et al. (2010) and Birner (2013) are just some examples. Unfortunately, all of these studies failed to explain those thermal anomalies satisfactorily due to different limitations of the chosen approach. Such limitations were a two-dimensionality of the model, consideration of only conductive heat transport or fluid flow, respectively, or a model size too small to capture the process of basin-wide heat transport. In fact, heat transport in a sedimentary basin is a three dimensional process, acts on a basin-scale and can even be influenced by thermal effects related to deeper seated or long distance structures and fluid flow, a fact that has already been proven for other areas as e.g. the North German Basin (e.g. Cacace et al. 2010, Noack et al. 2010, Kaiser et al. 2011) and the Po Plain (e.g. Pasquale et al. 2013). However, it is unclear which structural elements of which size and at which depths influence the thermal field of the European Molasse Basin, how strong fluid flow in general and/or along permeable faults is modifying the temperature distribution caused by conductive heat transport on which scale and whether the observed temperature distribution of the Molasse Basin can be reproduced with a three dimensional modelling approach of heat transport at all. Although many studies have dealt in the past with large-scale to local geological or tectonic features and processes, as e.g. the continental collision, the distribution of facies or faults (e.g. Persaud and Pfiffner 2004, Berge and Veal 2005, D´Agostino et al. 2008, Champagnac et al. 2009, Brückl et al. 2010, Böhm et al. 2012, Birner 2013, Cacace et al. 2013, Homuth et al. 2014 and 2015), and the stress field in the Molasse Basin (e.g. Heidbach et al. 2008, Reinecker et al. 2010, Seithel et al. 2015), the influence of such factors on the thermal field of the Molasse Basin is still not fully deciphered (e.g. Rühaak et al. 2010, Agemar et al. 2012). In fact, a combined consideration of the basin with the adjacent mountians has never been done befor in 3D for the Molasse Basin to assess the thermal field.

A steady-state conductive approach of heat transport to explain the pronounced negative and positive thermal anomalies has been followed by Rühaak (2009) and Rühaak et al. (2010), which were not able to reproduce the observed thermal field in the basin. By comparing the predicted conductive thermal field to observed data presented by GeotIS (Schulz et al. 2009, StMWIT 2010), areas of temperature mismatch were identified, for which an additional influence of fluid flow on the temperature distribution

was assumed. However, it is unclear if the Molasse Basin can be regarded as mechanically, thermally and hydraulically equilibrated, a requirement to assume steady-state conditions in e.g. the calculation of the thermal field. Furthermore, it remains questionable whether the resulting mismatch between the calculated and the observed temperatures by Rühaak (2009, 2015) and Rühaak et al. (2010) can truly be explained with fluid flow related cooling, or whether other deep seated and/or large-scale temperature influencing parameters, e.g. laterally varying heat input from larger depths, are underestimated.

Nevertheless, an effect of fluid flow related cooling in general on the thermal field of the Molasse Basin is supported by Birner et al. (2012), Böhm et al. (2012) and Birner (2013) who investigated the hydrogeological configuration of the Upper Jurassic Malm aquifer in the German Molasse Basin and its geothermal usage, and should therefore not be excluded. Moreover, a possible influence of fluid flow related cooling along permeable faults has been shown in the past for a reservoir-scale model of a fractured carbonate geothermal reservoir in the Molasse Basin by Cacace et al. (2013) and for the area of Brandenburg in north-eastern Germany by Cherubini et al. (2014). Though, it is unclear how strong such an influence of fluid flow in general and along permeable fault zones may be on the basin-wide thermal field of the German Molasse Basin.

Hence, before the thermal field and the possible fluid flow related cooling effect itself can be adressed, the lithospheric structural configuration of the European Molasse Basin, its state of isostatic, thermal and hydraulical equilibration as well as its structural and thermal interdependence with the adjoining Alps and the South German Scarpland have to be understood first.

Based on the state of the art with respect to the knowledge about the Molasse Basin and the arising need for research one major question with several subquestions has been formulated to which this thesis proposes answers. Those questions are presented in the following chapter.

1.2 Objectives of the thesis

The aim of this thesis was to investigate the nature and causing mechanisms of the pronounced thermal anomalies and with that to improve the understanding of the thermal field of the European Molasse Basin area.

For this, the incentive of this thesis was premised on one major question:

What is the origin of the prominent positive and negative thermal anomalies in the European North Alpine Foreland Basin (= European Molasse Basin)?

To answer this main question, three principal questions with several associated subquestions have to be addressed before, of which the first principle question deals with the structural configuration of the European Molasse Basin:

1. How does the lithospheric-scale 3D structure of the European Molasse Basin look like?
    - How is the distribution of geological units on lithospheric-scale?
    - Which influence results from this distribution with respect to the distribution of mechanical, thermal and hydraulical properties?
    - Is the European Molasse Basin isostatically equilibrated?
    - If not, where and how strong does it deviate from the isostatic equilibrium? How does the isostatic state affect the distribution of vertical stress in the European Molasse Basin?
    - Is it reasonable to assume steady-state conditions for the calculation the vertical load distribution and the thermal field?

Based on the results of the structural investigations the following questions about the conductive thermal field were stated:

2. What controls the lithospheric-scale 3D conductive thermal field of the European Molasse Basin?
    - How far do the structural configuration and related heterogeneities in thermal properties lead to heat refraction effects affecting the thermal field of the basin?

- Is there an interdependence between the basin and the Alps related to the lithospheric-scale 3D conductive thermal field?

- Which conductive thermal effects can be recognized in the lithospheric-scale 3D conductive thermal field? How do the conductive thermal effects affect the shallow thermal field of the European Molasse Basin?

- How far can a steady-state conductive model reproduce observed temperatures and can areas be identified for which a probable additional influence of fluid flow on the thermal field should be considered?

After assessing the resulting conductive thermal field, questions about the contribution of advektive heat transport related to fluid flow to the thermal field of the model area were formulated:

3. Which heat driving mechanisms cause the present-day thermal field of the German Molasse Basin?

- Can the present-day temperature distribution of the German Molasse Basin be reproduced by coupled fluid flow and heat transport simulations?

- What is the impact of fluid flow on the basin-scale thermal field of the German Molasse Basin?

- Which heat transport mechanism is dominant at which depth?

- What is the influence of hydraulically conductive fault zones on the temperature distribution in the German Molasse Basin?

To answer these questions, a five-step workflow was followed in this thesis:

- The construction of a databased lithospheric-scale 3D structural model of the European North Alpine Foreland Basin including the adjoining South German Scarpland as well as parts of the Alps with an adequate vertical and horizontal resolution for isostatic, load and conductive thermal calculations.

- The calculation of the 3D lithospheric-scale load distribution and the present-day 3D conductive thermal field.

- The assessment of the three dimensional interaction of large-scale structural and tectonic features with respect to the isostatic state and the conductive thermal field of the basin area.

- The simulation of coupled fluid and heat transport with a basin-scale 3D numerical model.

- The assessment of the influence of fluid flow related cooling on the temperature distribution in the basin.

1.3 Overview over the thesis

Since the chapters 2, 3 and 4 of this thesis are presented as papers published in peer-reviewed ISI-journals or at present under review in such, this chapter gives an overview over the following parts of the thesis. Thereby, the work done is summarised in short statements and the main scientific contributions of the co-authors are mentioned. Further, the links to the principal questions of the thesis are given.

Chapter 2: Assessment of the isostatic state and the load distribution of the European Molasse Basin by means of lithospheric-scale 3D structural and 3D gravity modelling.

The first publication consists of three subparts and focuses on the building of the databased lithopsheric-scale 3D structural model and the density distribution within the European Molasse Basin, the South German Scarpland and parts of the Alps. The resulting 3D model features a vertical as well as horizontal resolution which was not shown before for such spatial extend in 3D.

In the first part of the paper, the data implementation and calculation of the respective lithostratigraphic units in the sedimentary part of the basin is described and the isostatic approach for the calculation of the crustal layers is explained. The second part deals with the 3D gravity modelling which was applied to constrain the crustal structure and the density distribution as well as to assess the isostatic state of the European Molasse Basin. Finally, in the third part the 3D load distribution was calculated from which the vertical stress was derived for the model area.

As the first author, I was the main contributor to the manuscript of this publication. I constructed the 3D structural model, carried out the 3D gravity modelling and calculated the load distribution. Furthermore, I prepared the figures and wrote the text with minor contribution from my co-authors Magdalena Scheck-Wenderoth and Michael Schneider. Both co-authors contributed with fruitful discussions to the interpretation of the modelling results. The resulting publication deals with the first principal question and the respective subquestions of the thesis´ objectives.

The manuscript was published after peer-review as:

Przybycin AM, Scheck-Wenderoth M and Schneider M (2015a) Assessment of the isostatic state and the load distribution of the European Molasse Basin by means of lithospheric-scale 3D structural and 3D gravity modelling. International Journal of Earth Sciences 104/5: 1405-1424, doi: 10.1007/s00531-014-1132-4.

Chapter 3: The 3D conductive thermal field of the North Alpine Foreland Basin: influence of the deep structure and the adjacent European Alps.

In chapter 3 the work addressing the second principle question and its subquestions is presented. In this work step the gravity constrained lithospheric-scale 3D structural model presented in chapter 2 was used to calculate the present-day lithospheric-scale 3D conductive thermal field of the European Molasse Basin area. Therefore, all layers of the model have been characterised by thermal properties. By solving the conductive heat equation for steady-state conditions, the temperature distribution was predicted for the model area and the main conductive thermal effects were identified. The resulting temperatures were compared to measured and published data and areas of possible influence of fluid flow on the thermal field were identified. This work represents the first description of the 3D thermal field on lithospheric-scale for the area of interest and provides thermal boundary conditions for subsequent regional and local-scale studies.

As in chapter 2, I am the main contributor to this publication. I have applied the modifications of the 3D model to adapt it to the needs of thermal calculations, and have calculated the thermal field. I have evaluated and have interpreted the results with the help of my co-authors. The manuscript, for which I prepared the figures and tables, was drafted by me with minor contributions of the co-authors.

The manuscript was published after peer-review as:

Przybycin AM, Scheck-Wenderoth M and Schneider M (2015b) The 3D conductive thermal field of the North Alpine Foreland Basin: influence of the deep structure and the adjacent European Alps. Geothermal Energy 3:17, doi 10.1186/s40517-015-0038-0.
The final publication is available at link.springer.com (reproduced with kind permissions from Springer): http://www.springer.com/-/1/AU_YT8Y3nYabzt6n2O4A

Chapter 4: The origin of deep geothermal anomalies in the Germany Molasse Basin – results from 3D numerical models of coupled fluid and heat transport

The third publication, presented in chapter 4, describes the results from simulations of coupled fluid flow and heat transport processes in the German Molasse Basin and their possible relation to the observed prominent geothermal anomalies. To address the third principle questions of this thesis and its subquestions, the lithospheric-scale 3D structural model presented in chapter 2 and 3 was used to build a basin-scale 3D hydrogeological model of the German Molasse Basin between the Danube river in the north and the Alps in the south down to a depth of 7,500 m bsl. To adapt this model to the needs of coupled fluid flow and heat transport simulations, the resolution of the basin-scale model has been increased by distinguishing six different Upper Jurassic Malm-layers and the Cretaceous Purbeck-formation. All layers have been characterised by thermal and hydraulic properties and appropriate upper and lower thermal and hydraulic boundary conditions have been prescribed to the model. For the lower

thermal boundary condition, temperatures from the lithospheric-scale conductive thermal model were extracted at a depth of 7,500 m bsl. The temperature distribution predicted by the coupled fluid flow and heat transport simulations was compared to measured and published temperatures, and sensitivity analyses were carried out to determine the influence of different properties and lithological units on the thermal field. Furthermore, three different testfaults have been implemented successively to test the influence of faults permeable for fluid flow on the thermal field of the basin.

As the first author of the manuscript, I constructed the basin-scale model and conducted the coupled fluid flow and heat transport simulations. I evaluated and interpreted the results, and prepared the figures and tables for the manuscript. The text was mainly written by me with minor help of the co-authors.

The manuscript is under peer-review as:

Przybycin AM, Scheck-Wenderoth M and Schneider M: The origin of deep geothermal anomalies in the Germany Molasse Basin – results from 3D numerical models of coupled fluid and heat transport. Submitted to Geothermics.

Chapter 5: Summarising Discussion

In this chapter the individual results of this thesis are cumulatively discussed with respect to the principle questions asked in chapter 1.2 and the stepwise derived answers are summarized. Thereby, the results are set into context. Ultimately the limitations of the adapted approach are addressed and an outlook is given on further possible applications of the results as well as on further investigation requirements.

Chapter 6: Summarising Conclusions

In this chapter, final conclusions are drawn, which provide an answer to the main question of this thesis.

Chapter 7: References

In this chapter the combined references of all chapters are given.

Appendix 1 List of Publications related to this thesis

In this appendix the publications, published and under review, bound to this thesis are listed.

2. Assessment of the isostatic state and the load distribution of the European Molasse Basin by means of lithospheric-scale 3D structural and 3D gravity modelling

2.1 Abstract

The European Molasse Basin is a foreland basin situated at the northern front of the European Alps and has formed as a consequence of the Euro-Adriatic continental collision since the Tertiary. Today it is underlain by Mesozoic sedimentary successions on top of a Paleozoic crust. To investigate the deep structure, the isostatic state, as well as the load distribution in the basin and the adjacent Alpine area, we constructed a lithospheric-scale, 3D structural model by implementing available surface, well and seismic data. Subsequently, the structure of the model was constrained by means of 3D gravity modelling. Complementary, the isostatic state has been assessed based on the calculation of the 3D load distribution. Our results show that the Molasse Basin is not in isostatic equilibrium and that the gravity field of the area is strongly controlled by the configuration of the crystalline crust. Furthermore, we show that the area is influenced by significant lateral load variations down to a depth of -150 km, which are considerably larger than commonly assumed for this level. Furthermore, our results allow a first order assessment of the minimum compensating horizontal stress required to prevent gravitational collapse.

2.2 The European Molasse Basin

Sedimentary basins are reservoirs for hydrocarbons and geothermal heat and have been explored worldwide for energy resources since decades. With increasing knowledge about the basins, gained from studies conducted by both academia and industry, estimates of possible production rates could be improved independently whether it concerns petroleum or geothermal heat. An example for a basin standing in the focus of interest since a long time is the European Molasse Basin which is situated at the northern rim of the European Alps and extends over parts of France, Switzerland, Germany and Austria (Fig 1).

This basin evolved due to the continental collision of Europe and Adria since the Tertiary. Thereby, the underlying continental plate responded to the load of the orogen and the progressing compression with a flexure creating the wedge shaped depression of the basin. With its characteristic configuration the European Molasse Basin has stored the tectonic record of the Alpine collision and provides the possibility to study the Alpine evolution of the past. Today the basin is filled with continental clastic sediments derived from erosional processes of the adjoining Alps (Roeder and Bachmann 1996), called *Molasse*. These Molasse Sediments are underlain by Mesozoic sedimentary successions, which include a fractured and partly porous and karstified aquifer of mainly Upper Jurassic (Malm) age and a crystalline crust of Paleozoic age (Lemcke 1973, Freudenberger and Schwerd 1996, Schmid et al. 2004a

and b, Berge and Veal 2005, Schmid et al. 2008). This Jurassic aquifer is today intensively used for geothermal energy production (Birner et al. 2011 and 2012). However, locally partly unexplained temperatures have been encountered at depths of a few kilometers and pressures that entail a significant economic risk for the geothermal exploration (Rühaak et al. 2010, Agemar et al. 2012, Schulz and Thomas 2012, Birner 2013). To reduce the economic risk for geothermal energy production in this basin, its structural configuration and the consequence of the latter for the regional stress field have to be understood in 3D and on a basin-scale, firstly.

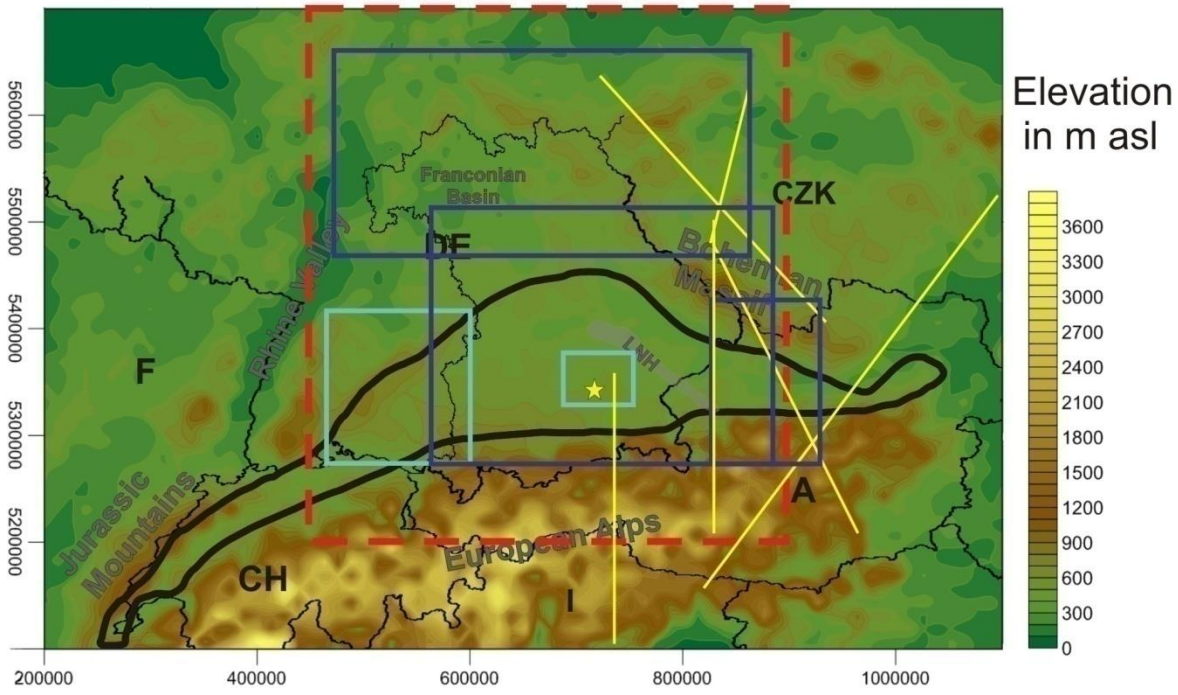

Fig 1 The model area (red frame) superposed on the topography ETOPO1 in the Molasse Basin and Alpine area and the implemented data. Dark Blue squares → Surface Maps (LFU, StMWIT 2010); Light Blue squares → local 3D structural models (Schulz and Thomas 2012 and Rupf & Nietsch 2008); Yellow lines → seismic profiles: Transalp (Gebrande and the TRANSALP working Group 2001), CELEBRATION2000 (Hrubcová et al. 2002), ALPASS (Mitterbauer et al. 2011), ALP2002 (Brückl et al. 2010). LNH = Landshut-Neuöttinger High. Map is shown in UTM32N. (Topography modified after Amante and Eakins 2009).

To investigate the processes acting in the basin, it is crucial to have a three dimensional conception of the model area. Unfortunately, available well data cover mostly the shallow parts of the system (max. 5 km depth), and seismic data is restricted to 2D or cover only local subareas (3D seismic) in the Molasse Basin. For this reason, modelling techniques provide useful tools to overcome the problem of data gaps. Such approaches combine geologically reasonable interpolation of observations in the shallow part of the system with methods to constrain the deeper structure by physical assumptions.

Accordingly, a lithospheric-scale 3D structural model of the European Molasse Basin has been developed in this study that has been used to assess the present-day physical state of the model area. This model provides a base for further investigations addressing the temperature and pressure conditions. It is based on published depth and thickness information for geological layers in the sedimentary part of the model and on results from seismic and seismological studies for the deeper parts of the lithosphere. The conditions for areas and depths not covered by data were constrained by means of isostatic calculations and 3D gravity modelling. Area wise, this work is focused on the German part of the basin (Fig 1), which comprises the widest and deepest parts of the foredeep. Furthermore, the sedimentary successions of this basin part are reasonably well constrained by available borehole data. Northward, the model extends beyond the Molasse Basin margin to cover the wavelength of the lithospheric flexure caused by the continental collision and to include the outcropping Triassic, Jurassic and Cretaceous sediments of Southern Germany and the Franconian Basin. Below the Molasse Basin, these Mesozoic units are bent downward and extend southward far under the basin proper. To the south the Northern Calcareous Alps, the Central Eastern Alps as well as the uplifted crystalline body of the Tauern Window (Schmid et al. 2004a and b) were included into the model. Along its eastern boundary the model area covers the outcropping crystalline crust of the Bohemian Massif, and cuts into the northernmost part of the Rhine Valley along its western boundary. The model encompasses an area of 500 x 450 km (N-S x E-W).

With the 3D model we address the lithospheric-scale structural configuration of the Molasse Basin with a higher vertical resolution than previously published and analyze the density distribution in the crystalline crust and the thickness of the lithospheric mantle. Accordingly, we quantify the three-dimensional gravity effect of the Alpine Body in relation to the foreland basin on a lithospheric-scale. To construct the model, we follow a 2-step workflow: First we integrate available observations and isostatic considerations to derive a starting model that, in a second step, is re-evaluated using 3D gravity modelling. In addition, we derive the 3D load distribution in this part of the continental collision zone which provides a first insight into the horizontal stress needed to sustain the actual configuration of the orogen-basin-system. Thereby, already existing knowledge about the structure and the state of isostatic compensation of the European Alps by Ebbing (2002, 2004), Braitenberger at al. (2002) and Ebbing et al. (2006) was taken into consideration during model construction. The common result of these 2D studies already indicated an isostatically non-equilibrated state of the European Eastern Alps. However, all previous studies were restricted to those parts of the European Alps covered by the Transalp seismic campaign (Gebrande and the TRANSALP working group 2001). Therefore, these studies did not include the entire Molasse Basin to the north and the adjacent South German Scarpland and thus, failed to capture the full wavelength of the related lithospheric flexure. Furthermore, in contrast to previous studies, we have integrated a large amount of observations (well data, seismic lines, surface geology) for the sedimentary fill that have not been combined before in 3D.

Accordingly, this new model has a higher vertical resolution, especially in the sedimentary parts, than existing studies and thus, the 3D load distribution could be calculated more accurately than before.

Information about the stress field in the Molasse Basin area has been derived from field observations and modelling studies presented e.g. by Gölke and Coblentz (1996), by Heidbach et al. (2009) in the World Stress Map (WMS08), by Reinecker et al. (2010) as well as lately by Carafa and Barba (2013). However, while the first two studies underestimate the impact of intraplate heterogeneities on the stress field (Reinecke et al. 2010), the latter two emphasize that intraplate stress sources, like lateral density heterogeneities, may generate stresses in the magnitude of tectonic stress which can overrule the far-field stress pattern locally (Reinecke et al. 2010) and may result in a reorientation of the main stress orientation (Carafa and Barba 2013). Since continental convergence is still ongoing (Persaud and Pfiffner 2004, D´Agostino et al. 2008, Champagnac et al. 2009) accompanied by active compression, the Molasse Basin area is not expected to be isostatically balanced. Nevertheless, it is unclear how far the isostatic state deviates from the state of equilibrium and how this may influence stress changes with depth in the basin area. With this study we want to contribute to a better understanding of these aspects and estimate the deviation from the isostatic equilibrium based on the analysis of the load distribution down to the depth of the Lithosphere-Asthenosphere Boundary (LAB).

2.3 The starting model

The database

Since no existing dataset covers the whole model area for all units resolved in the later model, different datasets had to be combined to construct a 3D structural model on a basin-wide scale. The 3D structural model of this study is primarily based on data published by the Geological Survey of Bavaria LFU (Freudenberger and Schwerd 1996) and by the State Ministry of Bavaria for Economy, Infrastructure, Traffic and Technology StMWIT (2010) for the Bavarian part of the Molasse Basin. These data include 2D depth and thickness maps of geological layers based on observations from the oil and gas industry, from geothermal drilling projects as well as from seismic campaigns. The respective maps also integrate information about faults at different depths. Additionally, these datasets were complemented by information on the depth of the Upper Marine Molasse Sediments and of the crystalline basement in Bavaria kindly provided by the Geological Survey of Bavaria LFU, the 3D structural model of the area of Munich (Schulz and Thomas 2012) and by depth information taken from the 3D structural model of Baden-Württemberg (Rupf and Nitsch 2008). Furthermore, results from several seismic experiments were considered during the construction of the model obtained by the TRANSALP seismic survey (e.g. Gebrande and the TRANSALP working group 2001), the CELEBRATION2000 survey (e.g. Hrubcová et al. 2002), the ALP2002 experiment in 2002 (e.g. Brückl et al. 2010) and the ALPASS passive seismic monitoring project (e.g. Mitterbauer et al. 2011) (Fig 1). The upper boundary of the model was defined by the topography ETOPO1 (Amante and Eakins 2009). The data coverage varies for different units

depending on the interest of exploration in the unit. An overview on the stratigraphic units resolved in the model, the associated data types as well as the related horizontal resolution and the respective references is given in table 1.

Tab 1 Input data for the structure model of the North Alpine Foreland Basin.

Lithostratigraphic Unit	Type of Data	Horizontal resolution	Reference
Topography	grid data	1 arc-minute	ETOPO1 (Amante & Eakins 2009)
Nördlinger Ries	well data	one research well	Jankowski (1977)
Alpine Body	seismic data		Transalp (Gebrande & TRANSALP working group 2001)
			CELEBRATION2000 (Hrubcová et al. 2002)
			ALP2002 (Brückl et al. 2010)
			ALPASS (Mitterbauer et al. 2011)
Folded Molasse Sediments	scattered data	1:250,000	Geothermal Atlas of Bavaria (StMWIT 2010)
	seismic data		Transalp (Gebrande & TRANSALP working group 2001)
			ALP2002 (Brückl et al. 2010)
			ALPASS (Mitterbauer et al. 2011)
Foreland Molasse Sediments	scattered data	1:250,000	Geothermal Atlas of Bavaria (StMWIT 2010)
	seismic data		Transalp (Gebrande & TRANSALP working group 2001)
			ALP2002 (Brückl et al. 2010)
			ALPASS (Mitterbauer et al. 2011)
Cretaceous	scattered data	1:250,000	Geothermal Atlas of Bavaria (StMWIT 2010)
		1:2,000,000	Freundenberger & Schwerd (1996)
Upper Jurassic Malm	scattered data	1:250,000	Geothermal Atlas of Bavaria (StMWIT 2010)
		1:2,000,000	Freundenberger & Schwerd (1996)
		1:500,000	LRGB (Rupf & Nitsch 2008)
	grid data	300 m	3D structrure model Munich (Schulz et al. 2012)
PreMalm Mesozoic Sediments	scattered data	1:500,000	Geothermal Atlas of Bavaria (StMWIT 2010)
		1:2,000,000	Freundenberger & Schwerd (1996)
		1:500,000	LRGB (Rupf & Nitsch 2008)
Tauern Body	seismic data		Transalp (Gebrande & TRANSALP working group 2001)
			ALP2002 (Brückl et al. 2010)
			ALPASS (Mitterbauer et al. 2011)
Crystalline Crust	scattered data	1:500,000	Geothermal Atlas of Bavaria (StMWIT 2010)
		1:2,000,000	Freundenberger & Schwerd (1996)
		1:500,000	LRGB (Rupf & Nitsch 2008)
	grid data	300 m	3D structure model Munich (Schulz et al. 2012)
	seismic data		Transalp (Gebrande & TRANSALP working group 2001)
			CELEBRATION2000 (Hrubcová et al. 2002)
			ALP2002 (Brückl et al. 2010)
			ALPASS (Mitterbauer et al. 2011)
Moho	grid data	0.1 degree	Grad et al. 2009

Model construction

To construct the 3D model all available depth information for each of the lithostratigraphic units have been assembled in one file, using the software Petrel (Schlumberger, Version 2011.1). For the lithostratigraphic units and the areas where no depth information was available, thickness and/or seismic

data were consulted, if available. The resulting files were interpolated using a minimum tension gridding algorithm with the software Earth Vision (Dynamic Graphics Ltd., Version 8.0.1).

For the calculation of the resulting 2D grids, faults, where known, were considered as interpolation barriers. Inconsistencies between the constructed surfaces, due to the interpolation and extrapolation in areas not covered by data, were removed.

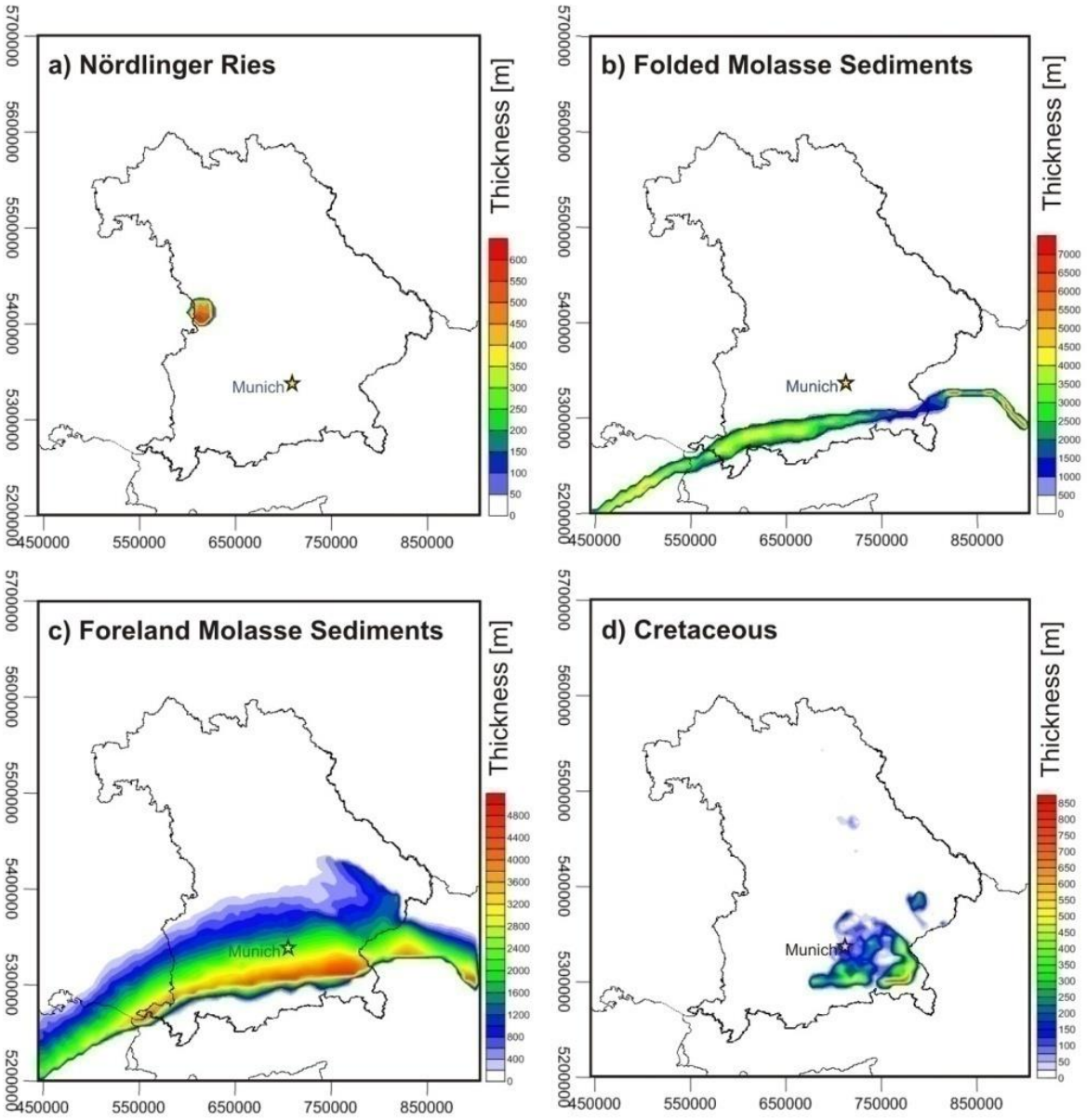

Fig 2 Thickness maps of the sediments and the Alpine and Tauern Body implemented into the 3D structural model. Maps are shown in UTM32N.

For this correction the top Upper Jurassic (Malm) and the top crystalline crust were chosen as reference surfaces as these surfaces extend over most parts of the model area and are the ones that are best-constrained in terms of data coverage and distribution.

After all inconsistencies were corrected, thicknesses of all lithostratigraphic units were calculated by subtracting the depths of successive units. In case no depth information was available for a specific unit, available data on the respective thicknesses were considered.

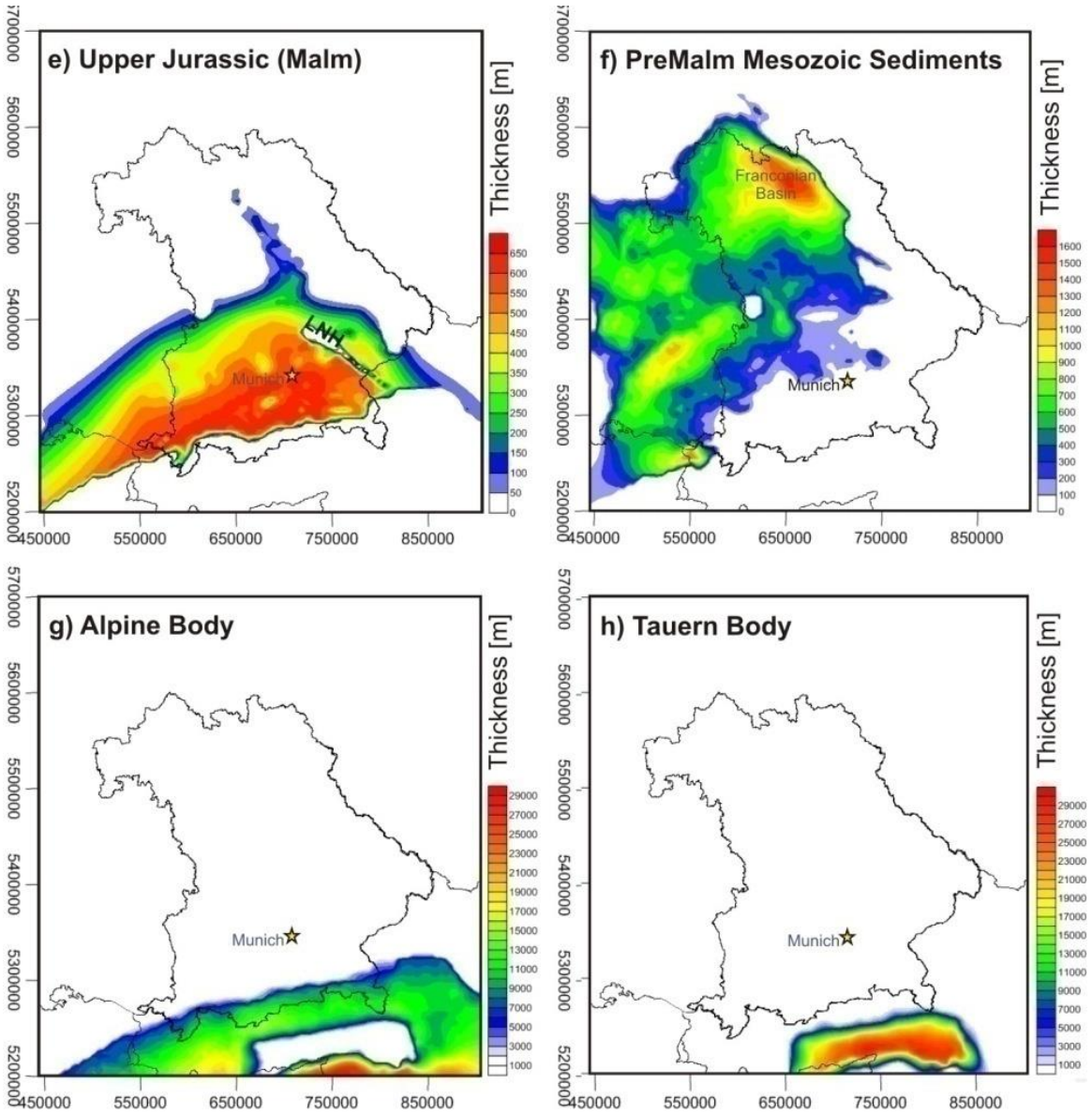

Fig 2 continued

Following this principle, the thicknesses of 8 lithostratigraphic units were calculated that include (from the top downward) the Nördlinger Ries, the Folded Molasse Sediments, the Foreland Molasse Sediments, the Cretaceous, the Upper Jurassic (Malm), the PreMalm Mesozoic Sediments, the Alpine Body and the Tauern Body (Fig 2).

The lower boundary of the initial model was defined by the top crystalline crust in the northern part of the model area and below the Molasse Basin and the Alpine Body as well as by the Subtauern Ramp below the Tauern Body (Fig 3).

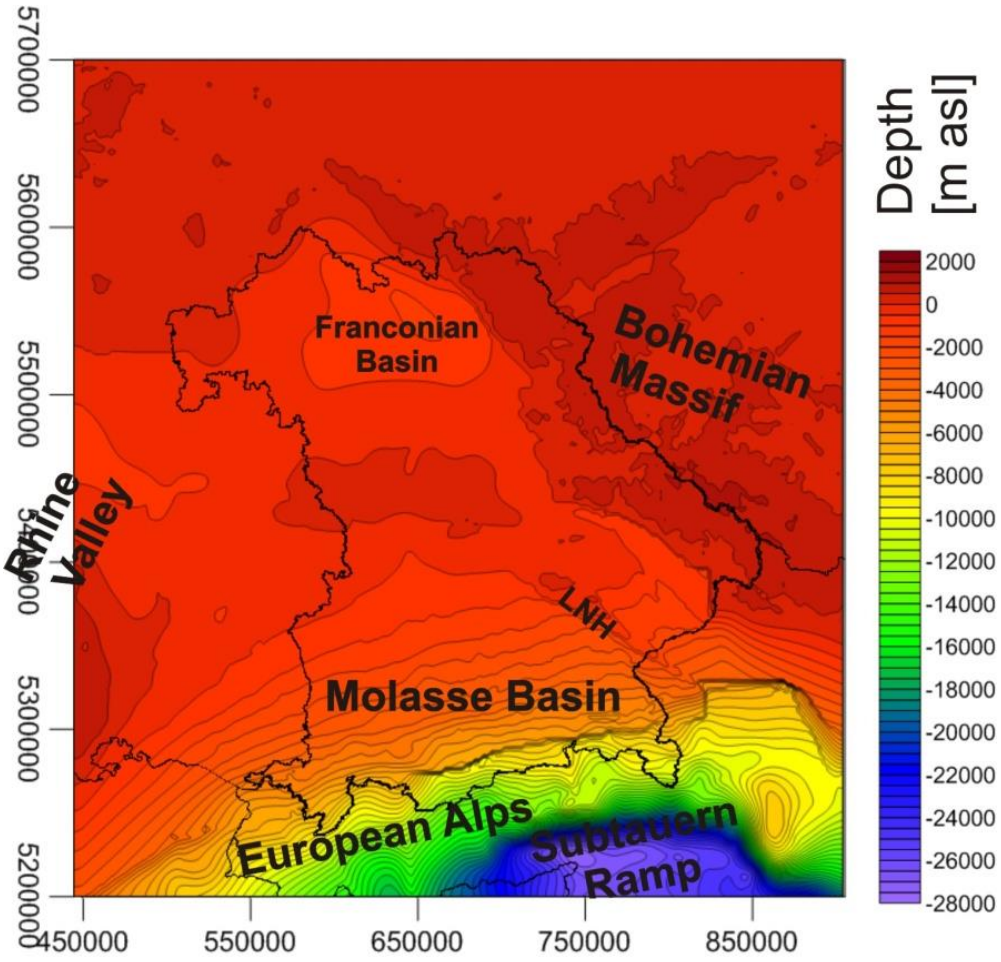

Fig 3 Depth map of the top basement (= top crystalline crust) implemented into the structural model. Map is shown in UTM32N.

The calculated thicknesses (Fig 2) were finally integrated into a consistent 3D structural model from the topography down to the top of the crystalline crust using GMS (**G**eological **M**odelling **S**ystem, in-house software Helmholtz Centre Potsdam - GFZ German Research Centre for Geoscience). To extend our model further downwards we implemented the Moho (Grad et al. 2009, Fig 4) as the next-deeper depth level of the model and calculated the thickness of the crystalline crust as the difference between the top of the crystalline basement and the Moho.

Afterwards each unit of the sedimentary part was parameterised with an average bulk density according to its dominant lithology taken from literature (Tab 2). Where available, measured density values were favoured (sediments, Tauern Body).

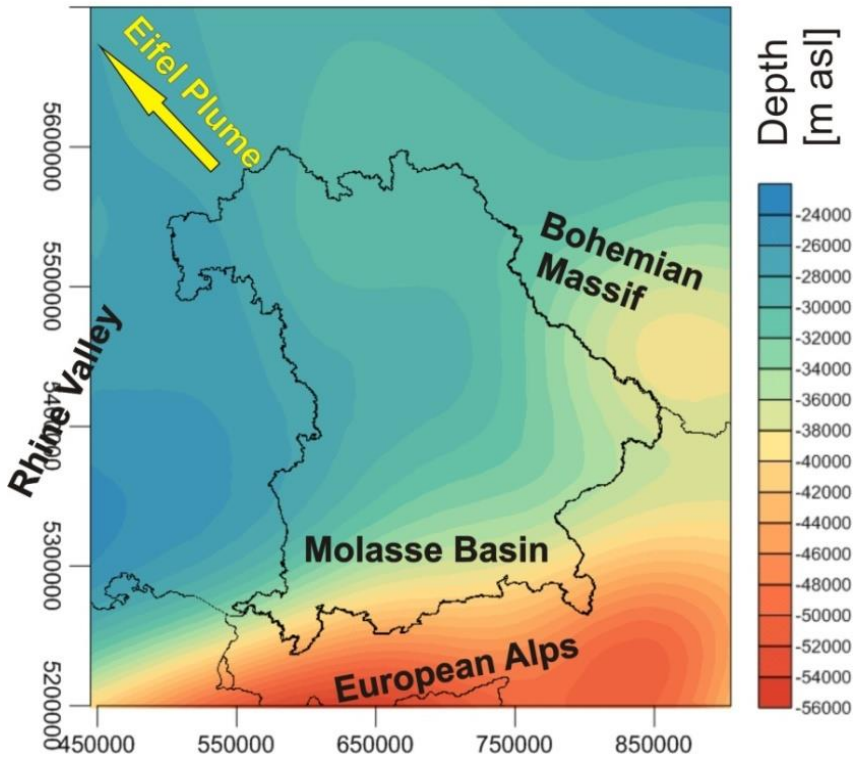

Fig 4 The Moho depth implemented into the structural model. Map is shown in UTM32N. (after Grad et al. 2009)

Tab 2 The lithologies and the averaged bulk densities assigned to the distinguished lithostratigraphic units. References (1) Ernstson and Pohl 1977, (2) Freudenberger and Schwerd 1996, (3) Granser et al. 1989, (4) Ebbing 2002 (modified), (5) Koch et al. 2009. (6) Scheck 1997 (modified). * modified density during 3D gravity modelling

Lithostratigraphic Unit	dominant Lithology	averaged Bulk Density [kg/m^3]
Nördlinger Ries	lacustrine sediments, impact breccia (1)	2000 (1)
Alpine Body *	limestone, dolomite, marl, clay, silt, conglomerate (2)	2700 (4) 2730*
Folded Molasse Sediments	conglomerate, sand, silt, clay (2)	2400 (5)
Foreland Molasse Sediments	conglomerate, sand, silt, clay (2)	2350 (5)
Cretaceous	claystone, limestone (2)	2640 (5)
Upper Jurassic Malm	limestone, dolomite (2)	2650 (5)
PreMalm Sediments	claystone, sandstone, marl (2)	2680 (5)
Tauern Body *	granite, gneiss, shale (3)	2780 (3) 2800*
Upper Crystalline Crust *	granite/ granodiorit (6)	2700 (6) 2850*
Lower Crystalline Crust *	gabbro (6)	3100 (6) 3150*

A different strategy was pursued for the crystalline crust, since no measured data was available describing the density distribution, especially in the deeper crust. To obtain a density configuration also for this layer, the lateral density distribution of the crystalline crust was calculated following the approach of isostatic equilibrium of Pratt (1855).

Isostasy is based on the theory of a rigid layer drifting in a denser subjacent layer in the earth obeying the principles of Archimedes (Watts 2011). The two layers are thereby the crust and the mantle separated by the Moho. The compensation depth in this theory is defined as the depth below which all pressures are hydrostatic and at which the weights of vertical columns are equal (Fowler 2005).

Following the approach of Pratt (1855), isostasy is achieved by a horizontal variation of crustal densities for a given crustal thickness. For the calculation of the crustal densities in our model, we have used as comparison a reference model of a standard crustal block floating on the mantle and displacing the latter by the amount h_m according to

$$\rho_c \, h_c = \rho_m \, h_m \qquad \text{(Eq 1)}$$

where ρ_c is the crustal density, h_c the crustal thickness, ρ_m the mantle density and h_m the thickness of the displaced mantle. In this approach the base of the crust (= crustal thickness) in the reference model corresponds to the compensation depth. Since the thicknesses of the sediments and the crystalline crust as well as the densities of the sediments and the mantle are given in our structural model, the crustal densities ρ_c in our model can be calculated following equation 2 (e.g. Fowler 2005):

$$\rho_{cR} \, h_{cR} + \rho_{mR} h_{mR} = \rho_s h_s + \rho_c \, h_c + \rho_m h_m \qquad \text{(Eq 2)}$$

where ρ_s is the sediment density and h_s the sediment thickness, ρ_c the crustal density and h_c the crustal thickness and ρ_m the mantle density. h_m stands for the thickness of the displaced mantle and is defined by the distance between the Moho and the compensation depth, which is zero in the reference model and laterally varying in our structural model. The $_R$ stands for the reference model. For our calculations a reference model of $\rho_{cR} = 2{,}700$ kg/m^3 and $\rho_{mR} = 3{,}340$ kg/m^3 and a constant compensation depth (= h_{cR}) of -30 km was used.

The resulting average crustal densities (Fig 5) vary across the model area and are higher, where the thickness of sediments is larger, and lower where the thickness of sediments is smaller. Furthermore, the resulting distribution of average crustal densities correlates well with the thickness of the crustal layer in most parts of the model area. The model shows high density and thickness values in the area of

the Alps and the Bohemian Massif (~3,050 kg/m^3 and ~37 km) and mean to low density and thickness values in the central, northern and western (Rhine Valley) parts (3,000 – 2,700 kg/m^3 and 26 – 33 km).

A special configuration has been derived for the Tauern Body. Since the Tauern Body consists of crustal material cut off from the crystalline crust along the Subtauern Ramp by a reverse fault, the crystalline crust sensu stricto is less thick (~20 km) below this area. This thickness minimum correlates with a density maximum under the Tauern Body of ~ 3,200 kg/m^3.

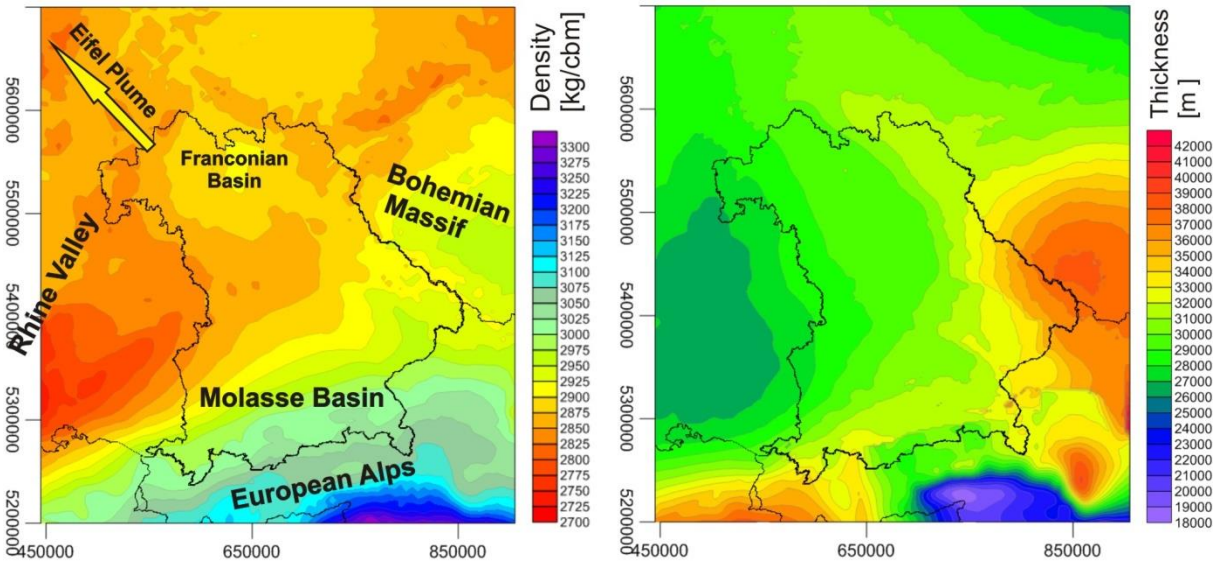

Fig 5 Calculated lateral density distribution (left) in the crystalline crust according to the approach of isostatic equilibrium of Pratt (1855) and the thickness of the crystalline crust (right). Maps are shown in UTM32N.

In a next modelling step the single crustal layer was subdivided into an upper and a lower part, by redistributing the average densities of the cumulative crystalline crust ρ_c into two new layers of different densities (ρ_{UC} and ρ_{LC}). Thereby, the crustal columns with the crustal density calculated according to the Pratt approach exert the load (P) with

$$P = g\ \rho\ h \qquad \text{(Eq 3)}$$

while g is 9,81 m/s^2. To split the whole crystalline crust (C) into an upper (UC) and a lower (LC) part, we define

$$P_C = P_{UC} + P_{LC} \qquad \text{(Eq 4)}$$

and

$$h_C = h_{UC} + h_{LC} \quad \text{(Eq 5)}$$

Considering equation 6, with some adjustments, we get equations 7 and 8 which allow the calculation of the thickness of the two crustal parts while maintaining the total load deduced from the Pratt calculations and the total crustal thicknesses (Scheck 1997) (Fig 5 and Tab 2):

$$\rho_C\, h_C = \rho_{UC}\, h_{UC} + \rho_{LC}\, h_{LC} \quad \text{(Eq 6)}$$

$$h_{UC} = \frac{\rho_C - \rho_{UC}}{\rho_{LC} - \rho_{UC}} * h_C \quad \text{and} \quad h_{LC} = \frac{1 - (\rho_C - \rho_{UC})}{\rho_{LC} - \rho_{UC}} * h_C \quad \text{(Eq 7 and 8)}$$

For the calculation, the values of ρ_{UC} and ρ_{LC} were chosen such that crustal structures observed by seismic velocity distribution (e.g. Ebbing 2004, Bleibinhaus and Gebrande 2006, Ebbing et al. 2006) were reproduced.

The resulting thickness of the upper crystalline crust (h_{UC}) decreases from north to south, where the thickness of the lower crystalline crust (h_{LC}) shows the opposite trend (Fig 6a and b).

Besides the density distribution in the sediments and the crystalline crust, density differences in the mantle may also influence the Bouguer gravity signal. Moreover, to assess the isostatic condition of the Molasse Basin area, a crustal-scale model is not sufficiently deep. Therefore, deeper structures have to be considered during the construction of a gravity constrained 3D structural model. One possible type of data for sub-crustal depths comes from seismological investigations. Consequently, the model was extended further downward by implementing a seismologically constrained Lithosphere-Asthenosphere Boundary (LAB). This LAB (Fig 7) has been constructed integrating results of Tesauro (2009), Geissler et al. (2010), Karousova et al. (2013), Seiberlich et al. (2013) and Bianchi et al. (2014). The depth structure of this LAB correlates well with the depth structure of the Moho. Like the Moho, the LAB is deepest under the Alpine Body in the south (Moho ~ -50 km, LAB ~ -142 km), is characterised by intermediate depth values below the Bohemian Massif (Moho ~ -37 km, LAB ~ -138 km) and rises towards the northwest of the model area in the direction of the Eifel plume (Seiberlich et al. 2013) to up to - 80 km (Moho ~ -25 km, LAB ~ -80 km) (Moho Fig 4, LAB Fig 7).

The resulting lithospheric-scale model represents the starting model for the 3D gravity modelling and consists of 6 sedimentary layers, the layer of the Alpine Body, the Tauern Body, a two-parted crystalline crust and a lithospheric mantle (Fig 2, Fig 6a and b, Fig 7).

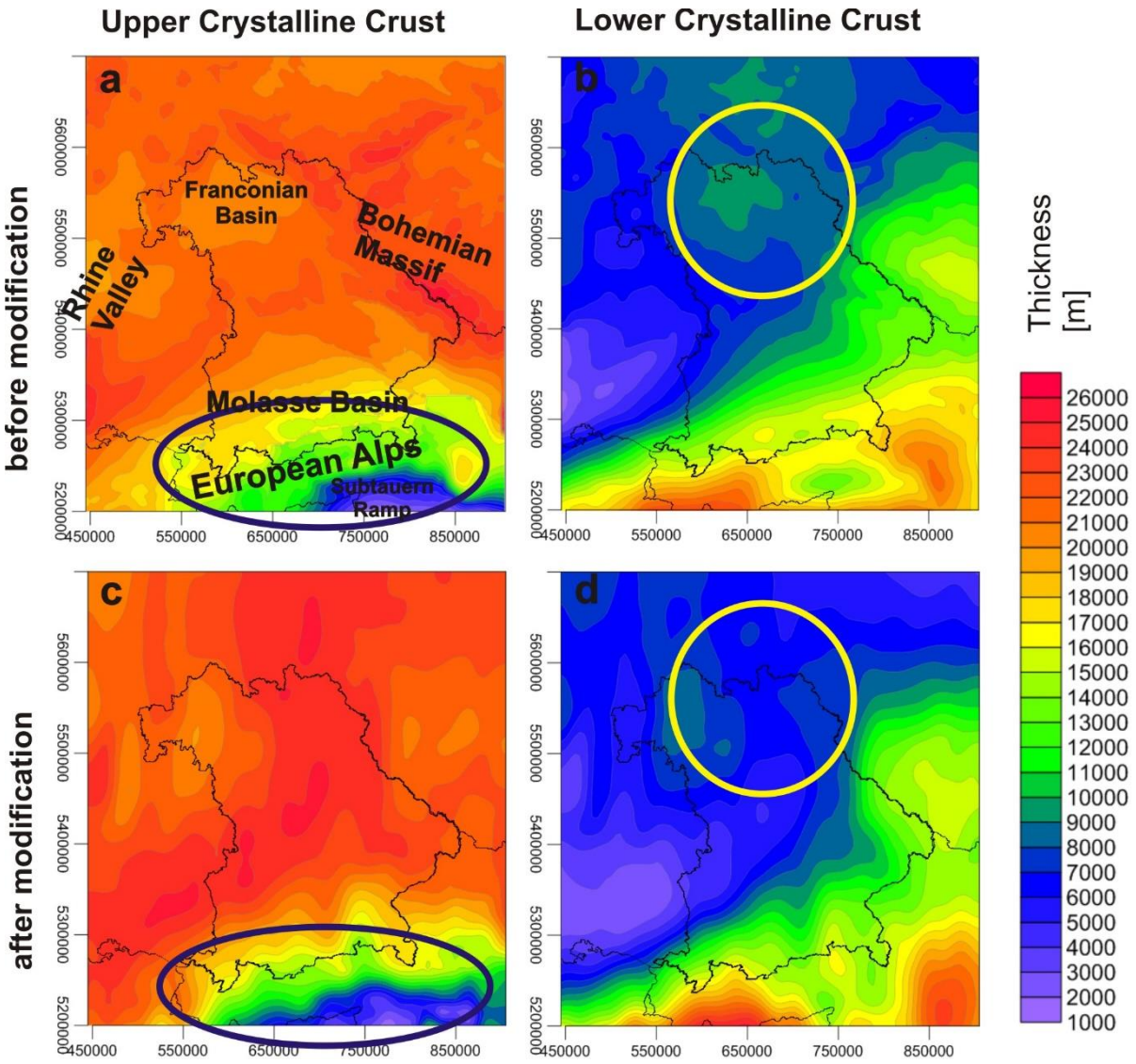

Fig 6 Thickness maps of the upper (left) and lower (right) crustal layer before (above) and after (below) the modification of the structural model by means of 3D gravity modelling. Both crustal layers show an opposite thickness distribution. Maps are shown in UTM32N.

The Nördlinger Ries (Fig 2a), a meteoric crater of 14.6 Ma in age, cuts through all sediments down to the crystalline basement, has a diameter of about 23 km and shows thicknesses of up to 650 m.

The sediments of the Folded Molasse (Fig 2b) are intensively folded and partly overridden by the Alpine Body. They occur in a narrow realm in the southern half of the model area and reach apparent thicknesses

of up to 6,000 m in response to the steep dip of the unit. The Foreland Molasse Sediments (Fig 2c) attains their maximum width of about 100 km in the central part of the model north of the Folded Molasse Sediments. Its thickness increases from 0 m at the northernmost border of the Molasse Basin proper to up to 5,000 m right in front of the Alps.

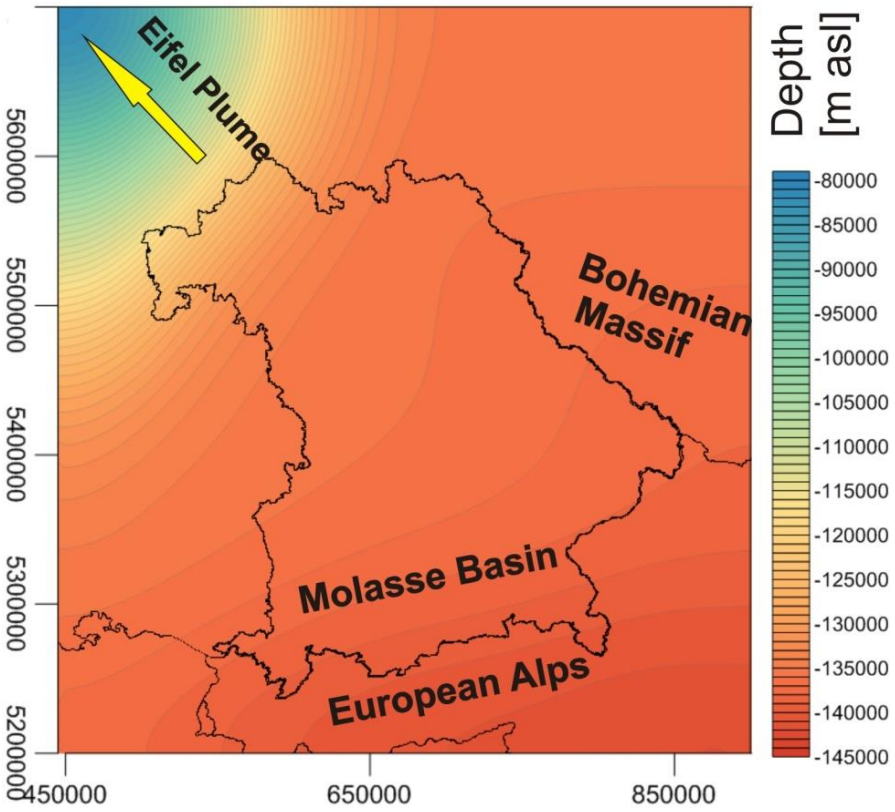

Fig 7 Depth map of the Lithosphere-Asthenosphere Boundary (LAB) in the Molasse Basin area constructed following Tesauro (2009), Geissler et al. (2010), Karousova et al. (2013), Seiberlich et al. (2013) and Bianchi et al. (2014). Map is shown in UTM32N.

Beneath the Foreland Molasse Sediments, the Cretaceous (Fig 2d) occurs only in a limited area in the south-eastern and eastern parts of Bavaria with a maximum thickness of 850 m. The Upper Jurassic (Malm, Fig 2e) shows highest thicknesses of up to 600 m at the front of the Alps and decreasing thicknesses towards the north. Furthermore, traces of the Upper Jurassic can be found in the area of the Landshut-Neuöttinger High. The Middle and Lower Jurassic as well as the Triassic have been

integrated into one unit called “PreMalm Sediments” (Fig 2f). These deposits occur in the central, western and south-western parts of the model area and attain cumulative thicknesses of up to 1,600 m in the Franconian Basin.

Since the object of interest in this study is the Molasse Basin, all (partly sedimentary) rocks of the Alpine mountain chain were integrated into one unit, the “Alpine Body” (Fig 2g). Accordingly, this unit comprises all the material in the Alpine area not belonging to the crystalline crust and the Tauern Body. The Alpine Body covers the southern part of the model area and reaches from the surface down to the crystalline basement. Its thickness increases from north to south to up to 29,000 m. The Alpine Body is cross cut by the crystalline rocks of the Tauern Body (Fig 2h) that attain maximum thicknesses of 29,000 m as well.

2.4 Gravity modelling

Density heterogeneities at different depths of the earth and of different scales cause characteristic positive or negative deviations of the gravity signal. Thereby, deep structures are causing anomalies of longer wavelengths in the gravity signal than shallow structures and high density contrasts are causing larger amplitudes in the gravity anomalies than low density contrasts. Thus, measured gravity can be used as a tool to constrain 3D structural models, especially for deep structures not covered by other data. Based on a given density distribution of a structural model, the resulting gravity response of the model can be calculated (Fowler 2005, Götze 2011). By comparing the measured gravity field of a given area to the calculated gravity response of a model, almost no residual anomaly should occur if the structural model integrates all significant structures with the appropriate geometries and densities. Deviations in the trend between the calculated and the measured gravity would point towards an inappropriate geometry of the model layers, a high positive or negative residual anomaly towards improperly chosen density values (Schmidt 2010).

To evaluate the starting model configuration resulting from isostatic calculations by means of 3D gravity modelling, we used the Bouguer gravity anomaly based on the Earth Gravitational Model 2008 (EGM2008) provided by the International Gravimetric Bureau (BGI 2012, Pavlis et al. 2012). This spherical harmonic model of the Earth´s gravitational potential represents a 5 arc-minute equiangular grid of gravity data with a mean standard deviation of ± 3.3 mGal (BGI 2012). The observed Bouguer gravity anomaly (Fig 8a) shows positive anomalies in the north, northwest and west of up to 30 mGal. Negative anomalies are observed in the central part of the model, in the area of the Rhine Valley and the Bohemian Massif (~ -45 mGal), as well as in the area of the Molasse Basin (~ -90 mGal) and the Alpine Body (~ -120 mGal). Furthermore, pronounced negative anomalies (up to -210 mGal) occur locally in the Alpine area.

To evaluate the 3D structure of the starting model the software IGMAS+ (Interactive Gravity and Magnetic Application System, Version 1.0.954.128, Götze and Schmidt 2010) was used with which the first gravitational model response was calculated (Fig 8b). Comparing the calculated model response to the measured gravity field, it is obvious that the starting model is not reproducing the measured gravity field: in the south the model shows more negative gravity values in the area of the Alpine Body pointing towards improper density values assigned to units composing this part of the model. In the central and northern part of the model area the calculated gravity response deviates from the observed gravity values indicating that a simple isostatic approach is not sufficient to derive the configuration of the crust.

To improve the gravity response of the model the densities of the Tauern Body (+ 20 kg/m^3) and the Alpine Body (+ 30 kg/m^3) were modified on the one hand (Tab 2). On the other hand the fit between the calculated and the observed gravity could be improved by locally changing the geometry of the upper crust-lower crust interface. Such changes by a few kilometers were required for the crystalline crust below the Rhine Valley, the Franconian Basin and the Tauern Body. After the modification the model intergrated a thick lower crystalline crust of up to 26 km beneath the area of the Alps (Fig 6d), a lower crystalline crust of moderate thickness below the Bohemian Massif (~ 15 km) and a thin lower crystalline crust in the central and northern part of the model (~ 6 km) and below the Rhine Valley (~ 2 km). Vice versa, the upper crystalline crust (Fig 6c) shows large thicknesses below the central and northern parts (~ 25 km) as well as in the eastern and western parts (~ 21 km) of the model. In contrast, reduced thicknesses (~ 5 km) of the upper crystalline crust are evident beneath the Alps.

The gravity response of the best-fit model (Fig 8c) reasonably reproduces the trend of the measured Bouguer gravity anomaly. Comparing the calculated gravity response of the best-fit model with the observed gravity anomaly, a short wavelength residual anomaly of ± 20 mGal can be determined for most parts of the model (Fig 8d) with locally higher values in the Alpine area. This short wavelength residual anomaly in the foreland area as well as the locally higher peaks in the Alpine area are likely caused by shallow density differences, which are not resolved in our model, neither vertically nor horizontally. Given the lithospheric-scale as well as the vertical and horizontal resolution of the model, this residual anomaly was considered acceptable. Moreover, the difference in the gravity response between the first and the best-fit model (Fig 8e) is a measure for the deviation from isostatic equilibrium as the starting model was based on the assumption of Pratt isostasy whereas the model consistent with observed gravity is not. Though this deviation is largest in the southernmost part of our model area in the Alps and the Tauern Body, a significant difference also is found for the Bohemian Massif, the Molasse Basin and the north of the model area.

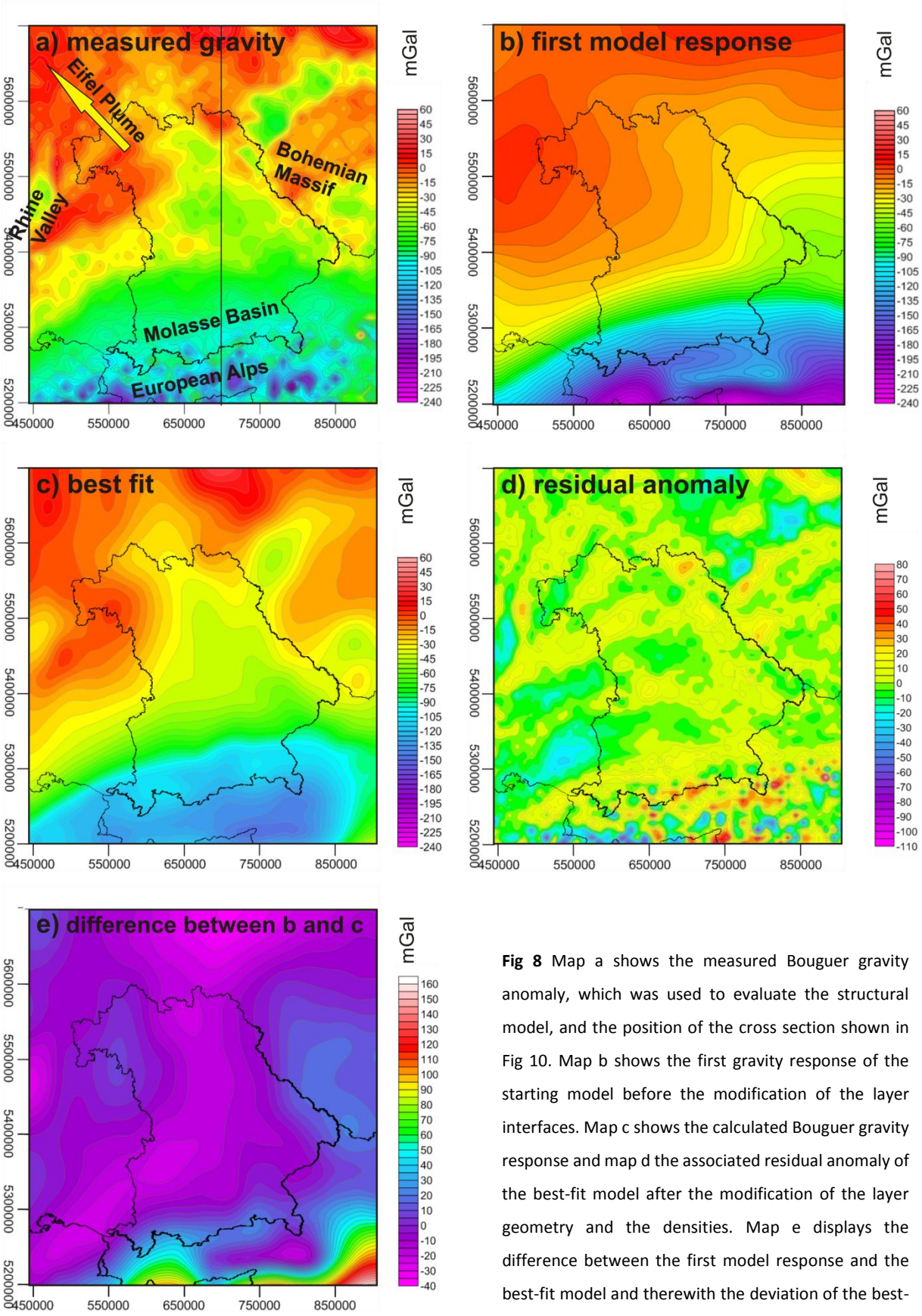

Fig 8 Map a shows the measured Bouguer gravity anomaly, which was used to evaluate the structural model, and the position of the cross section shown in Fig 10. Map b shows the first gravity response of the starting model before the modification of the layer interfaces. Map c shows the calculated Bouguer gravity response and map d the associated residual anomaly of the best-fit model after the modification of the layer geometry and the densities. Map e displays the difference between the first model response and the best-fit model and therewith the deviation of the best-fit model from the isostatically equilibrated state. Maps are shown in UTM32N.

2.5 Load calculation

The result that the gravity constrained best-fit model departs from the isostatically balanced configuration indicates that the system is not in isostatic equilibrium. To quantify the departure of the model from isostatic balance the load distribution was calculated using a 3D finite element method (Scheck and Bayer 1999, Scheck et al. 2003). A comparison of the lateral variation in load is shown in figure 9.

Two distinctly different load domains can be recognized at all depth levels of the model. One with larger load variation in the Alpine area (blue-yellow colours) and one in the central and northern model area with smaller variations (red-yellow colours). Thereby, the total lateral differences in load attains ~ 88 MPa at a depth of **0.5 km** bsl, albeit most parts of the model area are characterised by smaller load differences of less than 35 MPa (red colours). The largest differences of more than 80 MPa (yellow and blue colours) are restricted to the area of the Alps. With increasing depth the total lateral differences in load increase to ~ 96 MPa at a depth of **5 km** bsl (lower than the Molasse Sediments). Also at this depth the largest part of the model area is characterised only by smaller variations in load (~35 MPa) while the area of the Alps shows the largest variations (~80 MPa). Hence, the absolute difference in load increases with depth while the two different subdomains of the Alps (largest variations) and the rest of the model area (smaller variations) persist. At **30 km** bsl (lower than the Alpine Body) the total magnitude of lateral load variation increases to ~ 101 MPa, but the bimodal distribution of major load variations in the area of the Alps (~ 85 MPa) and minor load differences in the rest of the model area (~ 55 MPa), is preserved. However, the spread between the load variation in the mountain area and the rest of the model decreases in the deeper lithosphere (45 MPa at 5 km bsl, 30 MPa at 30 km bsl). Looking even at larger depths the magnitude of the total lateral load variation decreases to ~ 98 MPa at a depth of **60 km** bsl (lower than the deepest point of the Moho) again with major variations in the Alpine area (~ 95 MPa) and smaller variations in the rest of the model area (~ 60 MPa). Thereby, the difference between the load variations in the two domains remains constant (30 MPa). Even below 60 km bsl the total lateral load variation as well as the variation in the respective domains persist, though this part of the model consists mostly of lithospheric mantle. Finally, at a depth of **150 km** bsl (lower than the LAB), significant variations in the lateral load distribution are still evident. Summarising, the lateral load variation is significantly larger in the Alpine area than below the foreland where the smallest variation in the lateral load distribution are found. However, the absolute difference of the lateral load increases stronger with depth in the central part of the model area than in the Alps.

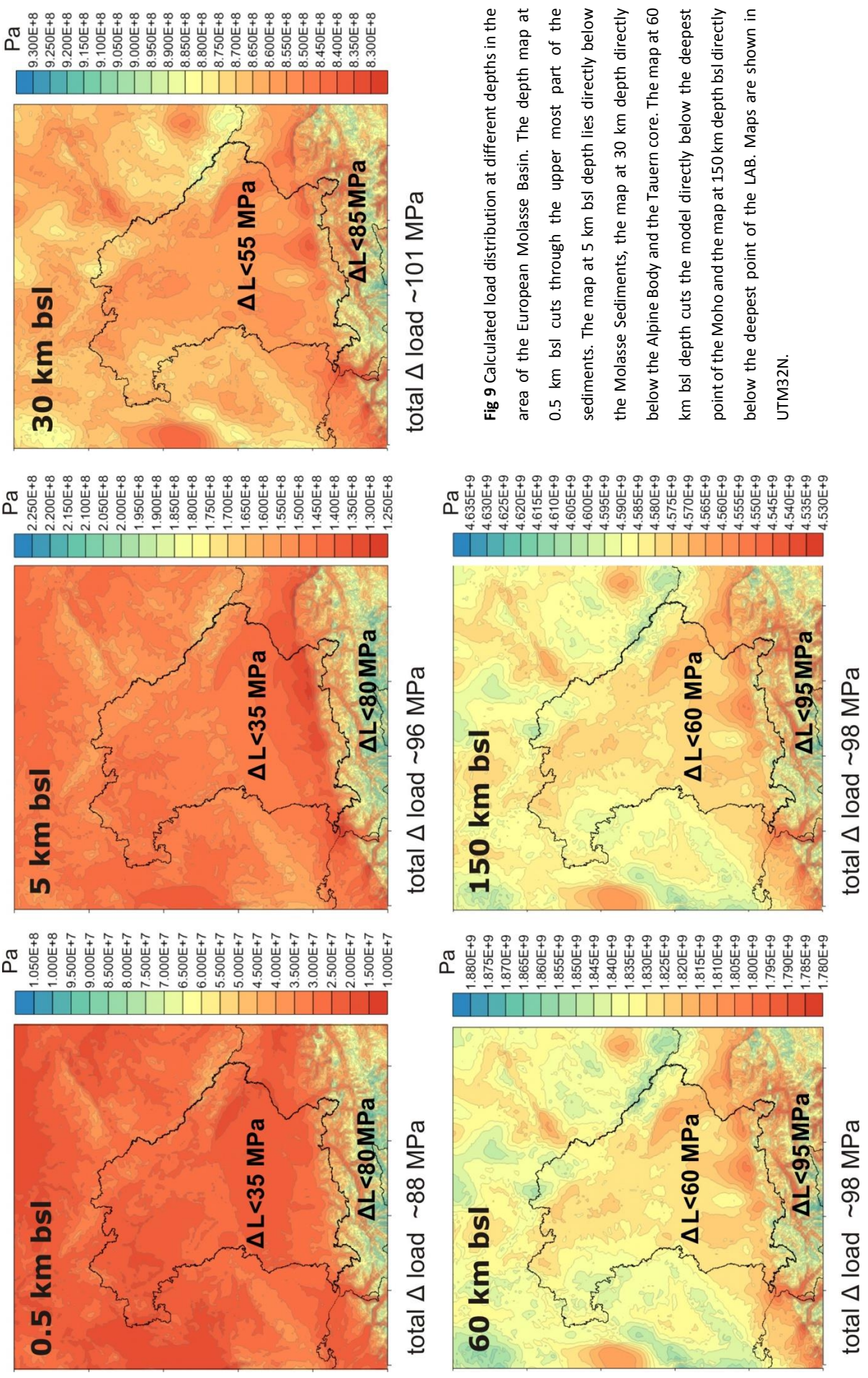

Fig 9 Calculated load distribution at different depths in the area of the European Molasse Basin. The depth map at 0.5 km bsl cuts through the upper most part of the sediments. The map at 5 km bsl depth lies directly below the Molasse Sediments, the map at 30 km depth directly below the Alpine Body and the Tauern core. The map at 60 km bsl depth cuts the model directly below the deepest point of the Moho and the map at 150 km depth bsl directly below the deepest point of the LAB. Maps are shown in UTM32N.

2.6 Interpretation and Discussion

After the 3D gravity evaluation, the lithospheric-scale 3D structural model (Fig 10) is used to derive interpretations related to the configuration of the model layers, the state of isostatic equilibrium and the stress field of the Molasse Basin area.

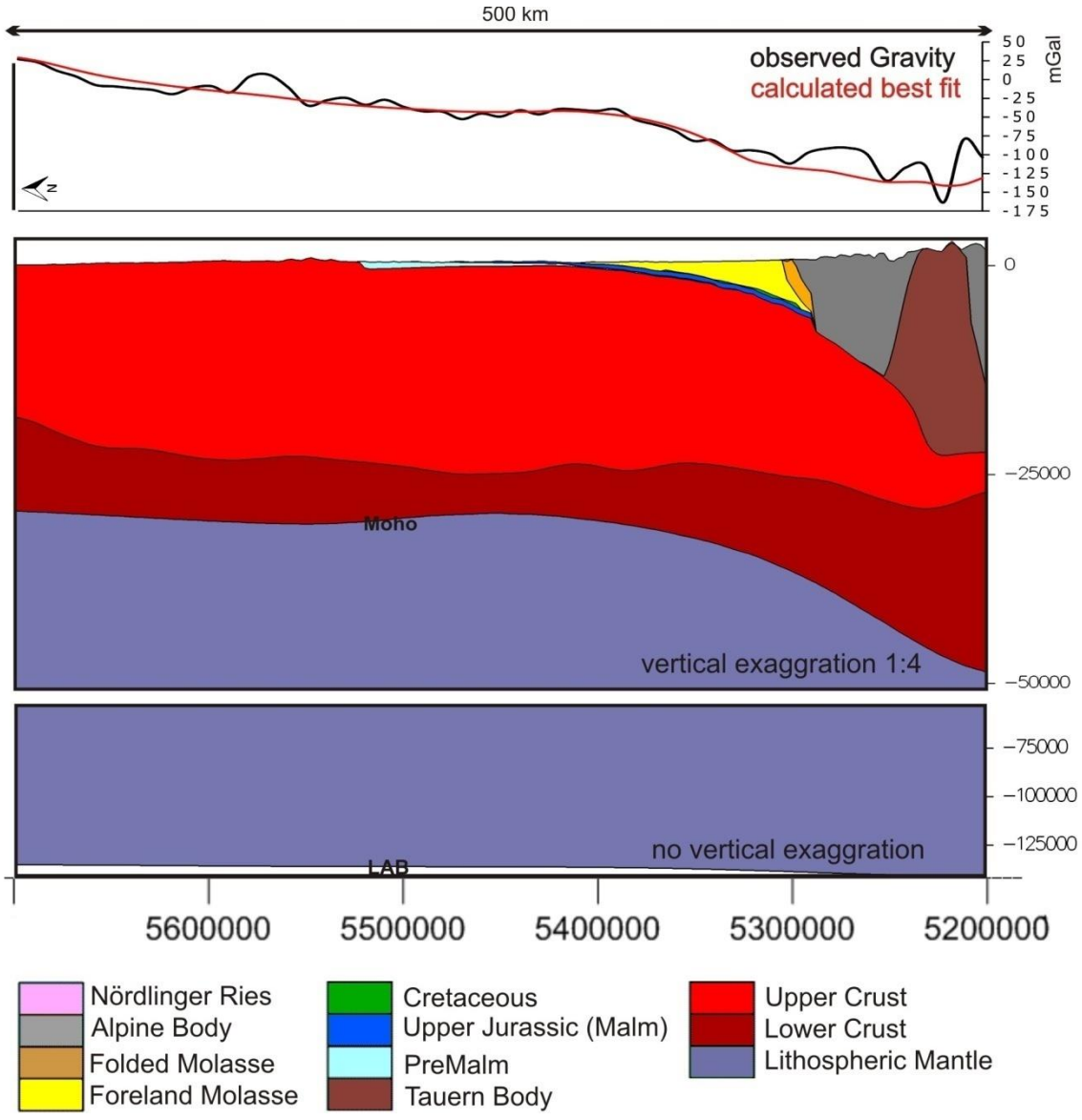

Fig 10 Cross-section through the lithospheric-scale model (below) and a zoom-in into the crustal part (middle). Above, the measured Bouguer Gravity (black) and the best-fit model response (red) are shown for this cross-section.

Concerning the sedimentary part of the model constraints are given by the implemented seismic, well and surface data. Accordingly, the geometry of these layers was not changed during gravity modelling and is consistent with other published sedimentary configurations (e.g. Ebbing 2002 and 2004, Vosteen 2003, Ebbing et al. 2006). Also the wavelength and the amplitude of the residual misfit between the

gravity response of the starting model and the observed gravity could not be significantly improved by changes of the density configuration of the sediments. Moreover, sensitivity analyses concerning variations of the sedimentary densities proved that this structural level has only a minor impact on the gravity field. Different sedimentary densities resulted only in changes of small amplitude and short wavelength in the gravity response of the model in the error range of the gravity data provided by the BGI (2012). However, in the Alpine area the density of the Alpine Body had to be increased by 30 kg/m^3 during gravity modelling, a value still within the range of published densities for the Austroalpine unit (Ebbing 2002, Simeoni and Brückl 2009, Tesauro 2009). The same holds for the Tauern Body, where the firstly chosen value of 2,780 kg/m^3 was modified to 2,800 kg/m^3 (Vosteen 2003, Ullemeyer et al. 2006, Simeoni and Brückl 2009). Both layers have a significantly higher impact on the gravity response of the model than the sedimentary units due to their large thicknesses.

The approximation of the calculated model response to the measured wavelength and amplitude of the gravity signal additionally required changing the geometry of the upper crystalline crust - lower crystalline crust interface and the density of the crustal layers. Seismic studies (e.g. Gebrande and the TRANSALP Working Group 2001) indicate that p-wave velocities increase with depth. Assuming a Nafe and Drake (1957) relationship between seismic velocities and density, this would also indicate that the densities increase with depth. It is more difficult to relate the modelled interface between the upper crystalline crust and the lower crystalline crust as well as the averaged density of both crustal layers to seismic data as respective velocity data is not available so far in 3D.

Comparing the gravity constrained 3D structure of the crystalline crust below the Molasse Basin area to published information, a good correlation of the depth to the intra-crustal interface of our model with the base of the middle crystalline crust of the Eschen-38 density model (Miller 1976) and of the density model of Ebbing (2004) is found. Assuming an equivalence of the upper crust in our model with the upper and middle crystalline crust in the mentioned earlier studies, all three models indicate lower thicknesses of the lower crystalline crust in the north than in the south and vice versa for the upper crystalline crust. On the other side both previously published density models (Miller 1976, Ebbing 2004) suggest crustal densities between 2,700 kg/m^3 in the upper crystalline crust, and 3,000 kg/m^3 in the lower crystalline crust, which are slightly smaller than our results (2,850 kg/m^3 for the upper crystalline crust and 3,150 kg/m^3 for the lower crystalline crust). Nevertheless, the density contrast between the upper crystalline crust and the lower crystalline crust is the same with ~ 300 kg/m^3, thus causing a similar impact on the gravity signal. It has to be mentioned however, that the density values chosen in our model are on the higher limit of the range given by the few available values of observed seismic p-wave velocities (Bleibinhaus et al. 2006).

Both crustal layers indicate a subdivision of the model area into a mountain region (Alps and Bohemian Massif) and a lowland region, with a transition between both in the Molasse Basin proper. The minimum thickness of the upper crystalline crust and, vice versa, the maximum thickness of the lower crystalline crust correlate thereby spatially with the rather high average density values below the Tauern Body (more than 3,250 kg/m^3) obtained from Pratt isostasy. Such high density values in the crystalline crust below the Alpine area support the hypothesis of subsurface loads in the Alps proposed earlier by Banks et al. (2001) and Ebbing et al. (2006). These deep crustal loads are needed to explain the observed maximum crustal thickness in the Alps, as the latter is larger than expected from topographic loads (Ebbing et al. 2006). However, the origin of these deep loads is still unknown, since no unusually high seismic velocities have been so far detected in the area (Ullemeyer et al. 2006). Based on our results we propose that instead of increased crustal densities in that area an increased thicknesses of the lower crystalline crust with "normal" lower crustal densities is present, and vice versa, that the thickness of the upper crystalline crust is reduced, respectively.

The modelled high densities indicate that the lower crystalline crust is mafic in character. A thick mafic lower crystalline crust beneath the Alps in turn would imply a strong lower crustal rheology. The lower crustal layer beneath the Alps is, however, not uniformly thick, but considerably thinner beneath the Tauern Body. This would imply that the rheology varies in response to thickness changes of the strong lower crustal layer. Consequently, the lithosphere should be weaker where the lower crustal layer is thinner as beneath the Tauern Body. This is in consistent with a weak lithosphere in the Alps across the Tauern Window as derived by Genser et al. (1996) and Okaya et al. (1996) from thermo-mechanical modelling studies.

On the other hand, a weaker lithosphere in the Alps compared to the foreland could also be related to the differences in the lithospheric mantle. The best-fit model presented here indicates that the lithospheric mantle is significantly thinner below the Alpine area than below the foreland and the South German Scarpland. A thinner lithospheric mantle and a thicker crystalline crust would result in an overall weaker rheology for the Alps compared to a normal crystalline crust and a thicker lithospheric mantle in the foreland. Though, at this point we admit that the Tauern and the Alpine Body are both strongly simplified in our model and that the Tauern Body does not progress further to the west under the Alpine Body as indicated by Schmid et al. (2004a). Uncertainties originating from this part of the model may propagate not only into the respective gravity response of the model but also into the calculation of the loads. This may be, besides the limited resolution of the model and the assignment of laterally uniform average densities to the layers, a source of error in our calculations.

The modified upper crust-lower crust interface required to fit the observed Bouguer gravity anomaly indicates a departure from isostatic equilibrium at least on a crustal scale. This alteration confirms two earlier hypotheses: (1) that the Molasse Basin area is not in isostatic equilibrium at crustal level, otherwise the isostatic starting model would have reproduced the measured gravity signal, and (2) that

the gravity anomalies are mainly related to density variations in the crystalline crust below the Molasse Basin area. This result is in good agreement with other published results (e.g. Wagini et al. 1988, Götze et al. 1991, Ebbing 2004). Moreover, our results show that the Alpine area and the Bohemian Massif have the largest deviations from isostatic equilibrium in the model area (Fig 8e; blue to red colours). Both areas are regions of active tectonics (e.g. Lenhardt et al. 2007, Brückl et al. 2010), thus are not expected to be isostatically balanced. In addition, the deviation from the isostatic state is larger in the Alpine area than in the Bohemian Massif. However, both domains show positive values in the map (Fig 8e) showing the difference between the gravity response of the first model result and the response of the best-fit model – an indication that they are overcompensated. In contrast, the Molasse Basin as well as the northern parts of the model show negative values in the difference map (Fig 8e) – an indication that they are undercompensated. Interestingly, the transition between domains of overcompensation and undercompensation is localized directly at the northern front of the Alpine collision zone and at the border of the Bohemian Massif with a steep gradient. This may explain why active deformation is observed along these transition zones.

The calculated 3D load distribution allows to assess the amount of stress caused by internal loads at different depth levels. Thereby, the deviatoric stress is limited to the vertical component and does not consider external forces. Furthermore, we cannot delimit the amount of stress caused by tectonic forces already introduced by the data used to build up the model (geological structures, densities). Hence, our results can only be considered as a measure of the internal potential energy of the system.

At all depths, the lateral load as well as the variation in the lateral load distribution are largest below the Alps and smaller below the area of the Molasse Basin, the South German Scarpland and the Bohemian Massif. Down to a depth of 30 km bsl, the variation in the lateral load increases from ~88 MPa to ~101 MPa in the whole model area due to the increasing proportion of (heavier) crystalline crustal material and the decreasing part of (lighter) sedimentary material with depth. Thereby, the increase in the lateral load variation with depth is more pronounced below the Molasse Basin proper, the South German Scarpland and the Bohemian Massif (+ ~ 20 MPa) than below the Alpine area (+ ~ 5 MPa). Below 30 km depth bsl the total lateral load variation decreases slightly to ~ 98 MPa at a depth of 60 km bsl, while the load variation in the two model domains increases again by + 5 MPa in the Molasse Basin, the South German Scarpland and the Bohemian Massif and by + 10 MPa in the Alpine area. This confirms the results from the gravity modelling that in general the Alpine area deviates stronger from isostatic equilibrium than the rest of the model area.

The deviation from isostatic compensation increases with depth for both domains, whereby in the Molasse Basin and the South German Scarpland this increase is more pronounced in the upper 30 km than the Alps. On the other side the deviation increases stronger in the Alpine area in the lower part of the model below 60 km bsl than in the rest of the model area. The difference between the total lateral variations in load in the upper 30 km and below this depth can be interpreted as a change in the gradient

between the two compensation domains in the model area: for the upper 30 km of the model the gradient between the undercompensated lowlands and the overcompensated Alps is higher than below 60 km depth bsl, where the gradient between the two compensation domains remains constant. Finally, the lateral load variation below the LAB (~ 98 MPa at 150 km bsl) indicates that the system is still far from isostatic equilibrium on a lithospheric scale.

An explanation for this preserved disequilibrium are the active forces due to the still ongoing collisional processes in the Alps that are known to induce tectonic horizontal stresses in the colliding tectonic plates. In case no tectonic horizontal stress (compression) was effective, the system would gravitationally collapse and areas of larger loads would impose respective vertical stresses. Thus, the deduced lateral variations in load provide a minimum estimate of the horizontal stress required to prevent gravitational collapse, a quantity we further refer to as required compensating horizontal stress. Walpersdorf et al. (2006) estimate very low (less than 1mm/yr) convergence rates from GPS measurements in the Jura Mountain Belt in France. This would indicate that the horizontal stresses in response to plate convergence are in the range or slightly higher than the ones in response to internal body forces as calculated in this study. In addition, this would support the hypothesis that the stress field in the Molasse Basin and the Alpine area is mostly controlled by internal body forces, as proposed by Delacou et al. (2004).

The differential increase of the lateral load variations with depth indicates that the horizontal stress needed to sustain the present configuration increases likewise with depth but not equally strong. Even though the Alps seem to be influenced by a larger horizontal stress, the Molasse Basin, the South German Scarpland as well as the Bohemian Massif indicate a stronger increase in the horizontal stress with depth. At larger depths, where the overall lateral load variation decreases, the difference between both domains decreases as well. This supports that also the required compensating horizontal stress becomes smaller in both domains beneath the Moho. At depths below the Moho the overall lateral load variation remains stable due to the uniform density of the lithospheric mantle and the rather small density contrast at the LAB (30 kg/m^3) assumed in the model. This stable configuration of the load variation below the Moho suggests a uniform magnitude of the required compensating horizontal stress and thus, a stable horizontal stress field below 60 km depth bsl. However, since the load variation changes non-uniformly with depth in the upper 60 km of the model, the three principal stress components ($\sigma1$, $\sigma2$ and $\sigma3$) may change as well, leading locally to a different stress pattern than assumed from simplified far-field effects. Induced by variations in the vertical stress the position of $\sigma1$, $\sigma2$ and $\sigma3$ may switch as the deviatoric stress is changing ($\sigma_{vertical}$ versus $\sigma_{minimum\ horizontal}$ and $\sigma_{maximum\ horizontal}$). Indeed, it has been shown that the stress state is orogen-perpendicular in the eastern Alps for $\sigma3$ in the inner extensional zones and for $\sigma1$ in the outer transpressional zones (Delacou et al. 2004) with strike-slip tectonics in the Alps (Willinghofer and Cloething 2003).

2.7 Conclusions

To construct a lithospheric-scale 3D structural model the integration of surface, well and seismic data helps to limit the degree of freedom in constraining the deeper parts of the earth that often are not well constrained by measurable propertys. Therefore, a combined approach of isostatic calculations and a subsequent 3D gravity evaluation of the model is a useful method to derive possible configurations of density heterogeneities in the deeper lithosphere. Using this approach also inferences about the isostatic state or deviation from the latter can be drawn.

Our calculations indicate that the crystalline crust below the Alps and the adjacent northern foreland basin is divided into two layers of different densities with lower densities in the upper part and higher densities in the lower part. The Lithosphere-Asthenosphere Boundary is deepest below the Alps and rises towards the Eifel plume in the northwest. Despite its large thickness, the configuration of the lithospheric mantle has only a minor influence on the gravity field due to the small density contrast at the LAB. The strongest influences on the gravity response of the modelled Molasse Basin area are caused by pronounced density contrasts at the upper crust-lower crust interface and at the Moho, whereas density contrasts in the sediments and the upper crystalline crust are less influential. Our investigations suggest that the Molasse Basin area is still far from isostatic equilibrium at the base of the lithosphere. Thereby, the Alps deviate strongest from the isostatic state on the scale of the lithosphere. The deduced deviation from isostatic equilibrium indicates that the Alps, as well as the Bohemian Massif, can be considered as overcompensated, whereas the Molasse Basin and the South German Scarpland appear to be undercompensated. From the calculation of the 3D load distribution we find that the Alps show the largest load variations at all depths. In contrast the Molasse Basin and the South German Scarpland are characterised by smaller load variations. The range of lateral load variations increases stronger below the Molasse Basin and the South German Scarpland than below the Alps and the Bohemian Massif. This non-uniform increase of the load with depth indicates, that the vertical stress as well as the required compensating horizontal stress preventing a gravitational collapse of the system may change with depth as well. These findings may be considered in future stress models and our results may be used as input data for such. Significant lateral load differences at the base of the lithosphere are in the range of ~ 90 - 100 MPa and thus considerably larger than commonly assumed for tectonic stresses.

3. The 3D conductive thermal field of the North Alpine Foreland Basin: influence of the deep structure and the adjacent European Alps

3.1 Abstract

We use a databased lithospheric-scale 3D structural model of the Molasse Basin area and the adjacent part of the Alpine orogen to calculate the present-day 3D thermal field of this continental collision zone. With our work we contribute to the understanding of the temperature distribution and the existence of pronounced positive and negative thermal anomalies in the Molasse Basin. We assume conductive heat transport and compare calculated temperatures to measured values and to other published 3D models. Areas, where predicted and observed temperatures match closely, are interpreted to be dominated by conductive heat transport. For areas, where a poor fit between modelled and observed temperatures has been obtained, we discuss possible reasons of this misfit. In particular, an additional contribution by fluid flow to the heat transport is likely. We conclude that the thermal field is controlled by conduction in the lithospheric mantle and the crystalline crust. Furthermore, we show that the positive and negative thermal anomalies in the Molasse Basin are partly triggered by the structural configuration of the crystalline crust. In particular, the domains of the Tauern Body and the upper part of the Alpine crust on one hand and the insulating Molasse Basin Sediments on the other hand control the shallow thermal field of the Molasse Basin area in response to their contrasting thermal properties. Our results demonstrate that the foreland basin and the adjoining Alps have to be regarded as an interdependent system that needs to be considered adequately if the present-day 3D thermal field of that area is assessed.

3.2 Background

The North Alpine Foreland Basin

The North Alpine Foreland Basin, also known as the European Molasse Basin, is a Tertiary foreland basin situated in the northern front of the European Alps (Fig 11). The formation of the basin is closely connected to the closure of the Tethys Ocean and the Alpine orogeny since the Cretaceous (Schmid et al. 2008). With the stacking of the Alpine mountains in the course of the collision process significant loads have been imposed onto the colliding tectonic plates, leading to a flexural response of the crystalline crust underlying the Alps and the creation of the wedge-shaped Molasse Basin. Today this foredeep is filled with clastic sediments, the *Molasse*, originating from erosional processes of the Alps (Roeder and Bachmann 1996). These Tertiary sediments are underlain by a Mesozoic sedimentary succession, including the Upper Jurassic aquifer (Malm) (Birner et al. 2011 and 2012), which is today intensively used for geothermal energy production, and a crystalline crust of Paleozoic age (Lemcke 1973, Freudenberger and Schwerd 1996, Schmid et al. 2004a and b, Berge and Veal 2005, Schmid et al.

2008). Roughly said the adjoining Alps consist of nappes stacked due to the collision and subduction processes in the Mediterranean area during Late Cretaceous to Cenozoic times (Schmid et al. 2004a and b, Handy and Rosenberg 2011). These calcareous nappes are punctuated by crystalline domes uplifted during the long time of tectonic activity, which are today outcropping in tectonic windows in the Alps (Tauern, Engadine and Rechnitz windows, Brückl 2011). Caused by tectonic processes related to the continental collision of Europe and Africa, large scale fault zones occur in the Molasse Basin and the Alps (Schmid et al. 2004a and b). Such fault zones might have a significant local influence on the present-day thermal field since they may act as pathways for fluid flow and could enhance fluid flow related cooling. For a more detailed description of the structural and tectonic architecture of the Alpine collision zone and the Molasse Basin we refer to Freudenberger and Schwerd (1996), Schmid et al. (2004a and b), Thomas et al. (2006) and Brückl et al. (2010).

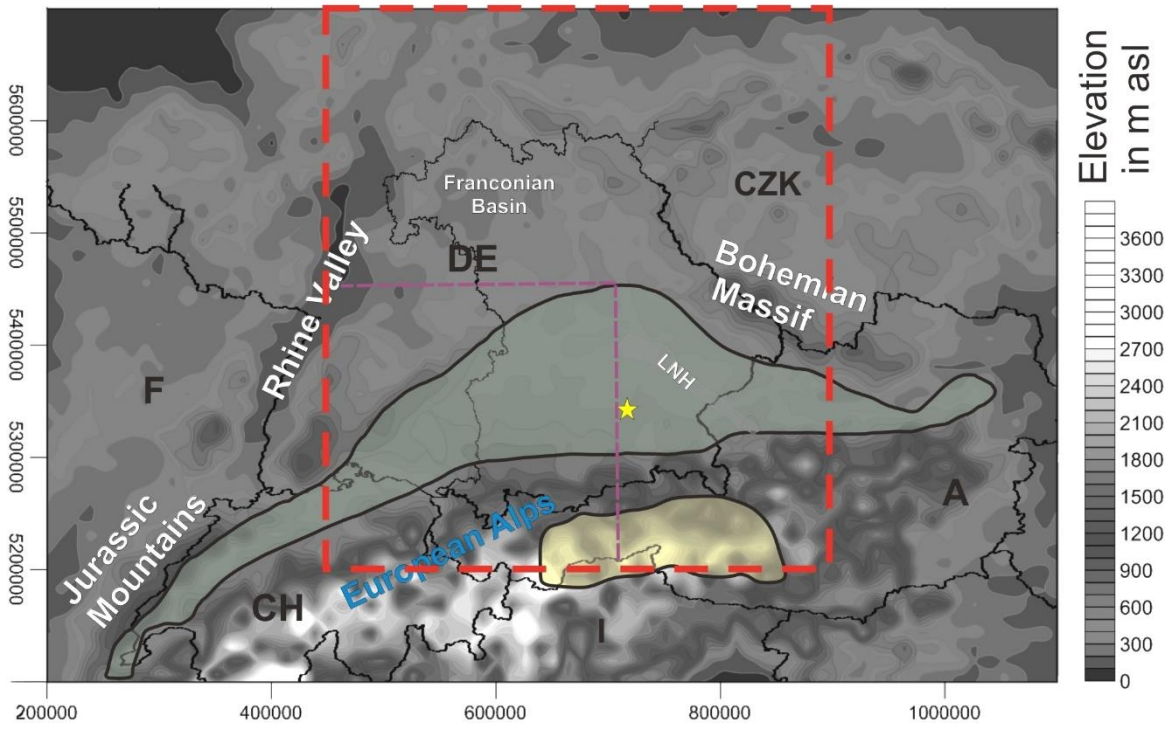

Fig 11 The North Alpine Foreland Basin in its topographic environment. The model area is marked with a red square. The basin is highlighted in green, the position of the Tauern Body is marked with yellow. LNH stands for the Landshut-Neuöttinger High, which is uplifted crust. The purple dashed line shows the position of the profile in Fig 12. Topography modified after Amante and Eakins 2009.

Geothermal field of the Molasse Basin

The North Alpine Foreland Basin and its underlying sediments have been explored for hydrocarbons since the beginning of the 20th century (Sachsenhofer et al. 2006) and subsequently for geothermal energy since the 1960´s (Bachmann et al. 1982). While the relevance of geothermal energy production

in the European Molasse Basin has increased steadily during the last decades (Roeder and Bachmann 1996, Kempf et al. 1999, Berge and Veal 2005, Jodocy and Stober 2009, Pamer and Diepolder 2010, Böhm et al. 2011, Reischenbacher and Sachsenhofer 2011, Birner et al. 2012, Cacace et al. 2013, GeoMol Team 2015,) its significance as a provider of fossil fuels has decreased (Pasternak 2015). Today the Tertiary aquifers in the European Molasse Basin and the underlying Mesozoic units are intensively used for shallow as well as for deep geothermal energy production and contribute to the provision of so-called "green energy". Unfortunately, the production rates and the potential extraction temperature may vary significantly regionally as well as locally even in a single hydraulically conductive layer, phenomena that are poorly understood. Such a case occurs in the south-eastern proximity of the city of Munich (Germany) in the Molasse Basin, where the temperature of the geothermal fluid decreases rapidly laterally within a few kilometers by 40 to 60 K (StMWIT 2010) in the Malm aquifer. Even though a huge amount of data exists for the European Molasse Basin obtained from different studies, the described strong local temperature decrease cannot be explained based on the present-day knowledge. The most decisive factors are the irregular data coverage in the basin area and the possibly deep-rooted and three-dimensional character of the causative processes. In areas of the Molasse Basin, where increased groundwater temperatures have been found in the past, the exploration effort has been increased yielding more data. In contrast, where the extracted temperatures have been disappointing, exploration efforts have been reduced resulting in a lack of further data. Even where the amount of data is large, the lateral variations in temperatures are not always understood. Significant processes of heat transport act on a basin wide scale and can be influenced by neighboring and local structures, such as the Alpine mountain chain and large fault zones, and thus have to be regarded in 3D. Until today, several studies have been conducted using different approaches addressing the temperature distribution in the Molasse Basin (e.g. numerical modelling approach: Rühaak et al. 2010; interpolation approach e.g.: Agemar et al. 2014a and b, Rühaak 2015) or the European Alps (Ebbing 2004; Ebbing et al. 2006; Vosteen et al. 2006). However, studies regarding both, the basin and the mountain chain, as an interdependent system are either two-dimensional, of local scale, or have an insufficient resolution of geological structures and tectonic elements to reproduce the local to regional temperature variations. Accordingly, it remains open which heat transport processes are acting on a regional scale.

Modelling approach

To address the problem of vertical resolution and horizontal coverage we use the databased lithospheric-scale 3D structural model of the European Molasse Basin of Przybycin et al. (2015a) to calculate the 3D conductive thermal field. The model covers the whole German part of the Molasse Basin, as well as the Northern Calcareous Alps, the Central Eastern Alps and the Tauern Body to the south and the South German Scarpland to the north. This model resolves the basin configuration with a higher resolution than previously published for such regional extent. Moreover, the model integrates all freely available depth and thickness information (wells, seismic lines) as well as faults as interpolation barriers and has

been additionally constrained by 3D gravity modelling. With our study we assess whether the measured temperatures at depth in the basin can be reproduced with a purely conductive approach, assuming that the temperature distribution over the largest parts of the model area is mostly controlled by the structural setting and the related variations in thermal properties. In consequence, for areas where the temperature field cannot be reproduced assuming purely conductive heat transport, an additional influence of heat transport related to fluid flow on the thermal field is likely, especially when taking into account large fault zones permeable for fluid flow in the basin area.

Earlier studies

As mentioned, earlier studies have dealt with the temperature field of the Molasse Basin before. Rühaak (2009) and Rühaak et al. (2010) present a temperature distribution calculated for the western Molasse Basin based on a 3D quasi steady-state conductive thermal model. They quote, that the temperature distribution in the upper crystalline crust is dominated by conductive heat transport and indicate that the thermal field in the sediments is controlled by advection and groundwater flow. They further conclude that the strong thermal anomalies in the Molasse Basin may be explained by E-W striking faults intersecting aquifers and characterised by fault parallel fluid flow. However, the model of Rühaak (2009) and Rühaak et al. (2010) was structurally based only on well information due to the lack of other data and assumed a constant basal heat flow at a fixed depth as lower thermal boundary condition. In contrast, the structural model used here integrates multidisciplinary depth and thickness information (wells, seismic lines, gravity). Moreover, we attempt to consider variations of basal heat flow in response to lithospheric heterogeneity. Instead of using a constant heat flux at a constant (shallow) depth, we use a physically motivated lower thermal boundary condition, in which we assume the thermal Lithosphere-Asthenosphere Boundary to represent the 1,300°C-isotherm, which may vary in depth across the model area. However, in conformance with Rühaak (2009) and Rühaak et al. (2010), heat transport related to fluid flow is not considered in this study. Considering advective and convective heat transport in the calculation would require a much higher horizontal and vertical resolution of the model than the one chosen for this study and thus much more information about the hydrogeological structure and property distribution, which was not accessible for this study. Though, the provided conductive part of the thermal field of the Molasse Basin area may be used as starting point for further coupled fluid and heat transport simulations to understand the origin of the distinct positive and negative thermal anomalies in the basin area.

One other project investigating the deep temperature distribution in the European Molasse Basin is the project GeotIS (Geothermal Information System; Schulz et al. 2009, Agemar et al. 2012, 2014a and b) conducted by the Leibniz Institute for Applied Geophysics (LIAG) in Germany. This internet-based geothermal information system provides information about deep aquifers and geothermal productions

sites in geothermally active areas of Germany. The data covers parts of the North German Basin, the Upper Rhine Valley and the South German Molasse Basin including more than 30,000 wells from industry and academia. GeotIS serves as a fundament for feasibility studies conducted by the geothermal industry (Schulz et al. 2009) by providing geoscientific base information in terms of depth maps of geothermally relevant aquifers, hydraulic and temperature data and is updated constantly with newly acquired information.

Based on measured data a 3D temperature model of Germany has been published for the European Molasse Basin by Agemar et al. (2014b), in which single temperature measurements have been interpolated in three dimensions. Using bottom hole temperature measurements and/or temperature data from drillstem tests these interpolations were done using 3D kriging interpolation. From the resulting model temperature information may be extracted for different depths down to 5,000 m below sea level, whereby the reliability and spatial coverage of the measurements decrease with depth due to the decreasing data density and increasing measuring uncertainties. Even though this model does not consider heterogeneities in subsurface properties or heat transport processes, it provides the most up-to-date map of the present-day deep thermal configuration of the basin. However, the 3D interpolation results may be improved in future by taking into account different quality classes of temperature measurements, an approach tested by Rühaak (2015) who used the temperature database of the Leibniz Institute of Applied Geophysics (LIAG) to assess the temperature distribution in the German Molasse Basin with weighted 3D temperature interpolations.

Since original data from temperature measurements performed by the oil and gas industry are partly confidential and thus not accessible, the thermal model of GeotIS was used as the target temperature configuration to compare modelled temperatures for the shallow part of the basin down to a depth of 4,000 m bsl. Furthermore, we compared our calculated temperatures to published values of temperature measurements from 24 geothermal production sites in Southern Germany (Tab 4).

3.3 The lithospheric-scale 3D structural model

The structural model our calculations are based on is the lithospheric-scale 3D structural model of Przybycin et al. (2015a, Fig 12), which is based on 2D maps (Freudenberger and Schwerd 1996, StMWIT 2010), on the 3D structural models of Baden-Württemberg (Rupf and Nitsch 2008) and Munich (Schulz et al. 2012) and several deep seismic profiles (TRANSALP [e.g. Gebrande and the TRANSALP working group 2001], CELEBRATION [e.g. Hrubcová et al. 2002], ALP2002 [e.g. Brückl et al. 2010], ALPASS [e.g. Mitterbauer et al. 2011]).

Thus, the model resolves six lithostratigraphic units in the sedimentary part of the basin (the Nördlinger Ries Impact structure, the Folded Molasse as well as the Foreland Molasse Sediments, the Cretaceous, the Upper Jurassic (Malm), the Middle and Lower Jurassic and Triassic Sediments summarized in one unit called the PreMalm Sediments) and two units in the Alps (the Alpine Body and the Tauern Body).

Below this sedimentary part, the structural model consists of a two-parted crust (upper and lower crystalline crust) bending towards the south and a lithospheric mantle. The bending of the crystalline crust, and with it the wedge shape of the basin, were caused by the continental collision and the rise of Alps. This wedge shape of the basin causes a non-uniform distribution of the thicknesses of the Tertiary Molasse Sediments (Fig 13). Accordingly, the sediments of the Foreland Molasse (Fig 13c) increase in their thickness from 0 m in the north to up to 5 km in the south. The Foreland Molasse Sediments are separated from the Alps by the Folded Molasse Sediments (Fig 13b), which are strongly internally deformed and party overridden by the Alps. These sediments show apparent thicknesses of up to 7 km in a thin belt in front of the Alps.

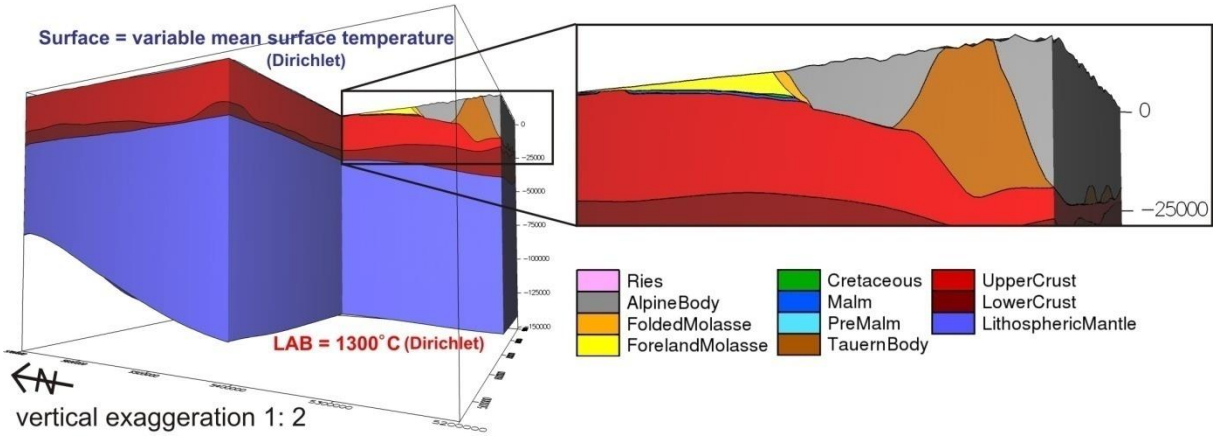

Fig 12 The lithospheric-scale 3D structural model used for the calculation of the present-day conductive thermal field (modified after Przybycin et al. 2015a). First kind boundary conditions have been used at the surface (variable mean surface temperature Fig 16) and at the LAB (1,300°C, Fig 15) for the thermal calculation.

Underlying the Molasse Sediments, the Cretaceous (Fig 13d) is only preserved in a restricted domain with thicknesses of up to 850 m with small outcropping areas of low thickness at the western rim of the Bohemian Massif. Below the Cretaceous, the Upper Jurassic (Malm, Fig 13e) shows reduced thicknesses in the outcropping domain in the north which increase southwards to up to 650 m directly in front of the orogen. The Malm is partly eroded above the uplifted crust of the Landshut-Neuöttinger High (LNH). Apart from the Malm, all Jurassic and Triassic Sediments have been summarized in one unit, the PreMalm Mesozoic Sediments (Fig 13f), which show highest thickness values (up to 1,500 m) in the Franconian Basin. At the northern rim of the Molasse Basin, the Nördlinger Ries (Fig 13a), an impact structure 14.6 Ma in age (Jankowski 1977) with a diameter of ~23 km, cuts through all units down to the crystalline crust with a maximum thickness of up to 600 m.

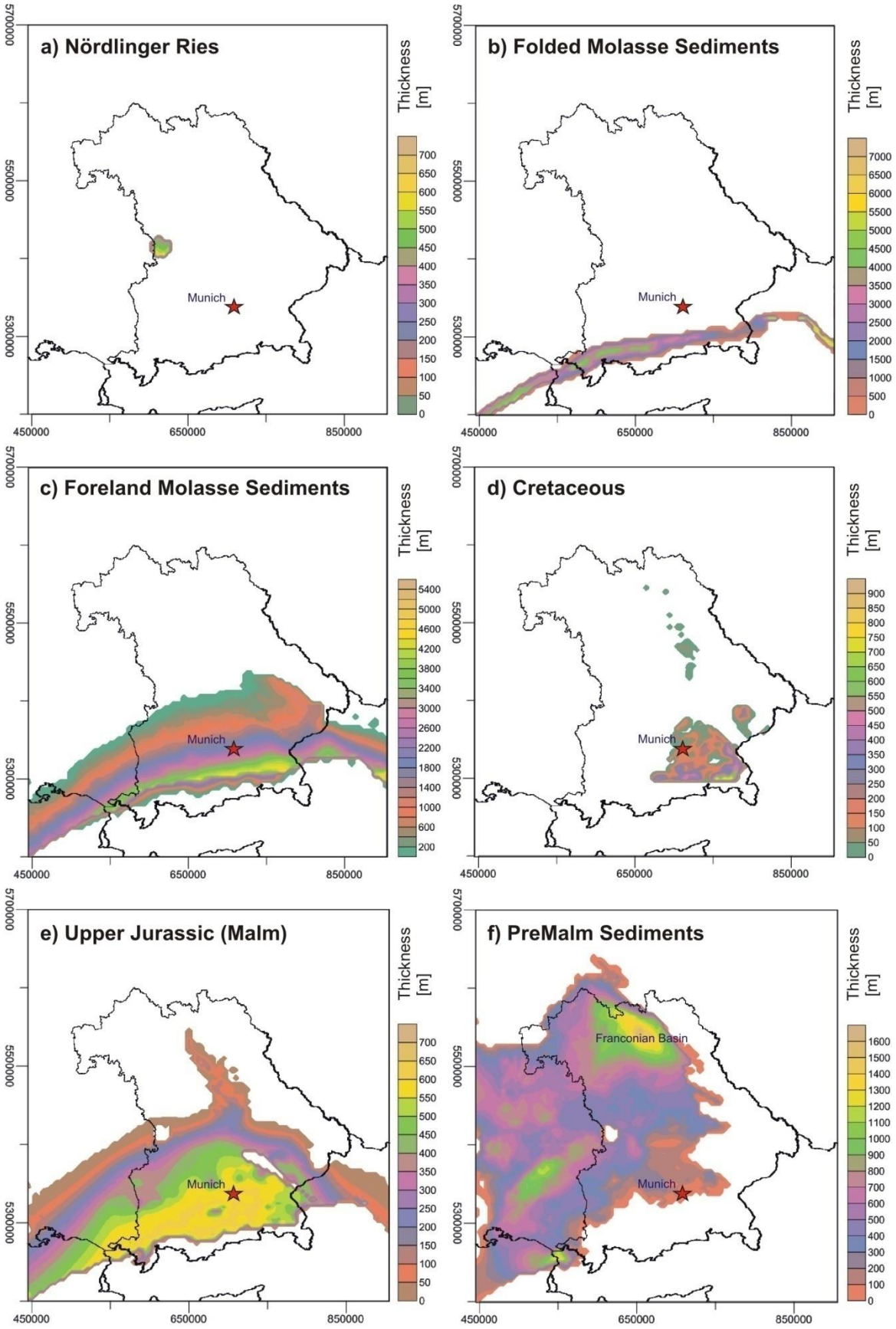

Fig 13 Thickness maps (a-f) of the sedimentary units resolved in the 3D structural model (modified after Przybycin et al. 2015a).

Since the structural model of Przybycin et al. (2015a) focuses on the Molasse Basin and considers the Alps only as first order structure, all deformed sedimentary units in the Alpine area have been summarized into one model unit, the Alpine Body (Fig 14a), with average thermal properties (Tab 3).

This Alpine Body shows thicknesses of up to 30 km at the southern model boundary and is disrupted by the Tauern Body (Fig 14b), which in turn shows thickness values of up to 30 km as well. The Tauern Body comprises all non-sedimentary units occurring within this crystalline core.

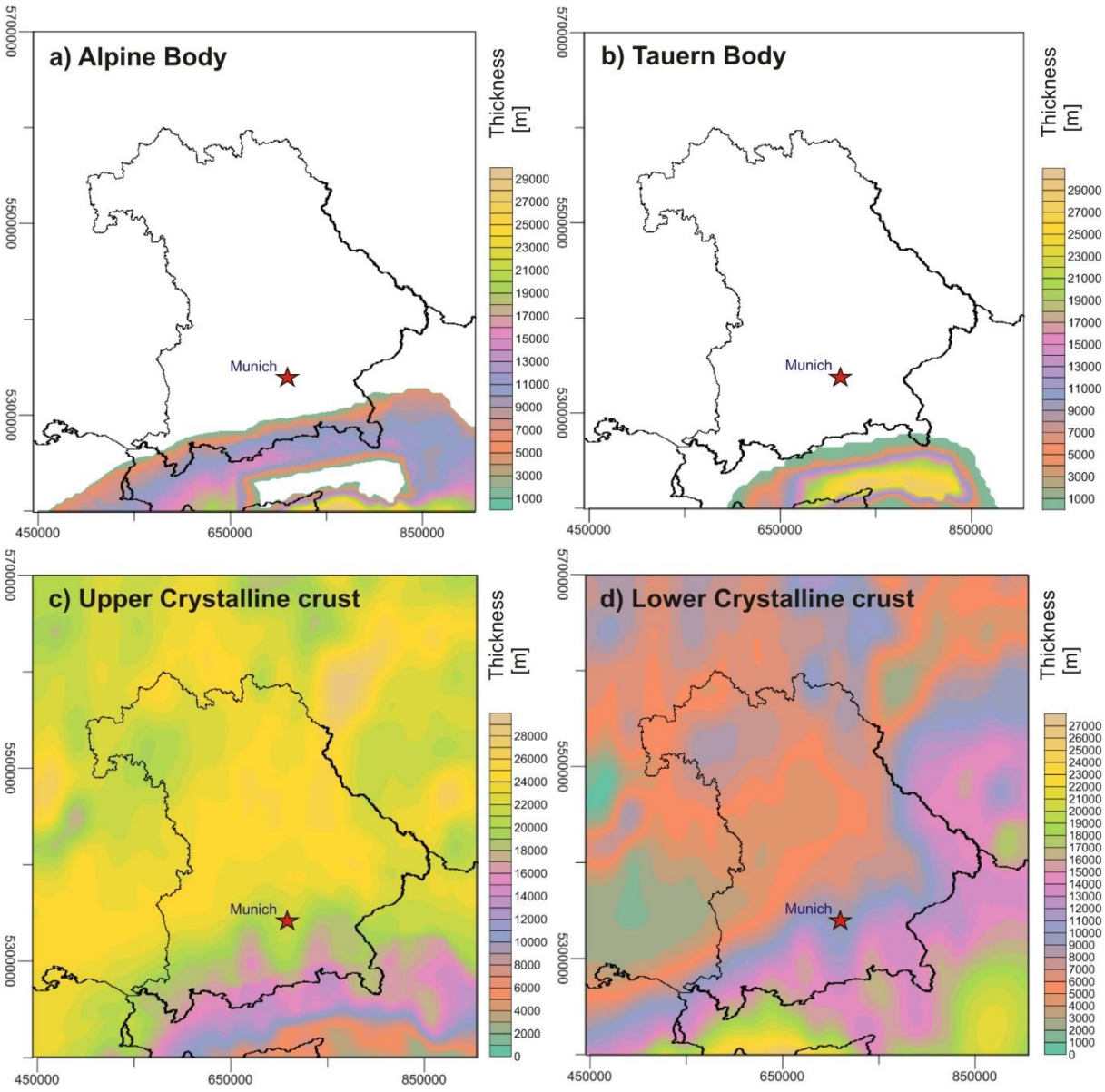

Fig 14 Thickness maps of the Alpine units (a-b) and the crustal units (c-d) resolved in the 3D structural model (modified after Przybycin et al. 2015a).

We admit that summarizing all lithological units occurring in the Alpine area into two units, the Alpine Body and the Tauern Body, is a strong simplification of the geological situation of the Alps. This was done because of two reasons: The first reason is the general goal of this study. With this study we wanted to investigate the first order interdependence of the Alpine area with the Molasse Basin related to the long wavelength thermal field. Resolving the geological structure in the Alps better would surely introduce local thermal effects in the thermal field in the Alps. However, the long wavelength thermal field and the temperature distribution in the Molasse Basin would not be significantly changed. The second reason for the strong simplification is the non-uniform distribution of geological information in the Alps, especially for deeper parts, which renders a three dimensional representation of the Alpine area with high resolution mostly challenging. To assess the influence of this simplification the different lithologies considered in the units Alpine Body and Tauern Body are summerized in table 3. Moreover a range of values for these thermal properties was tested.

The base of the crystalline crust in the model has been defined by integrating the Moho depth of Grad et al. (2009). The resulting crystalline crustal layer is split into an upper and a lower part. The depth of the upper crust-lower crust interface has been calculated using isostatic principles as well as 3D gravity modelling and is partly constrained by a deep seismic profiles (Przybycin et al. 2015a). Accordingly, the two crystalline crustal layers (Fig 14c and d) show opposed thickness distributions with a thick lower crystalline crust below the Alps, an intermediately thick lower crystalline crust below the basin and the Bohemian Massif and a thin lower crystalline crust in the north and west of the model area (vice versa for the upper crystalline crust). Gravity modelling and seismic data indicate that the seismic velocities and the densities of the upper crust correspond to an acidic (granitic to granodioritic) composition whereas the lower crust is of mafic composition (gabbro). Furthermore, a seismologically derived Lithosphere-Asthenosphere Boundary (Fig 15) has been implemented integrating results of Tesauro (2009), Geissler et al. (2010), Karousova et al. (2013), Seiberlich et al. (2013) and Bianchi et al. (2014). The LAB is deepest (up to 150 km bsl) below the Alps, moderately deep (~130 km bsl) below the Bohemian Massif and the Molasse Basin and rises towards the Eifel plume (~80 km bsl) in the northwest.

For our calculation of the thermal field we have adopted this structural model as described, to calculate the regional impact of the different lithostratigraphic units as first order structures on the temperature field.

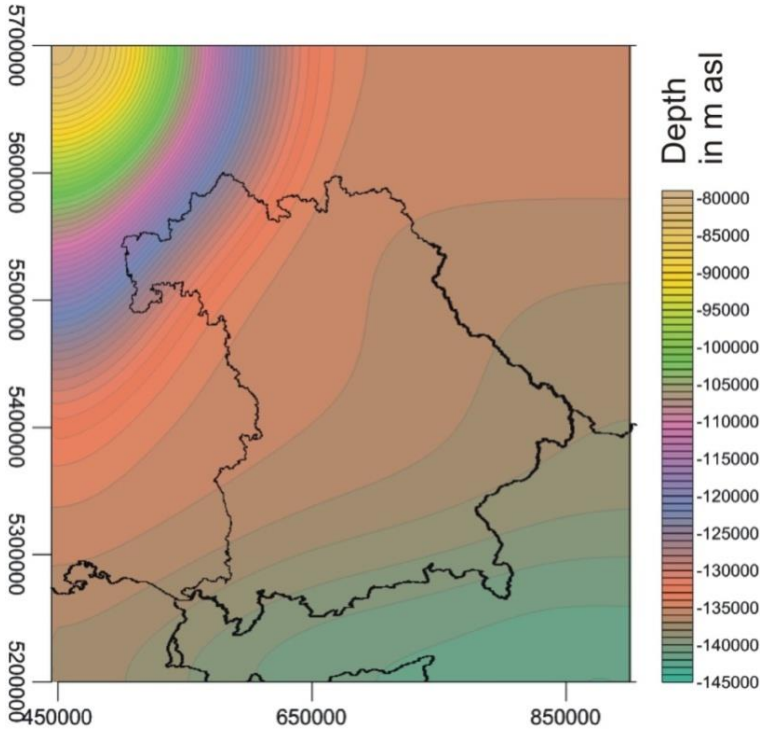

Fig 15 Depth of the Lithosphere-Asthenosphere Boundary used for this study (modified after Przybycin et al. 2015a) as the lower thermal boundary to which an isothermal temperature of 1,300°C is assigned, for the calculation of the 3D thermal field.

3.4 Method

Conductive heat transport is based on the theory of energy transfer (in this case thermal energy) by diffusion due to a temperature gradient within a body with the goal to reach thermodynamic equilibration. The base of the domain influenced by conductive heat transport is represented by the thermal Lithosphere-Asthenosphere Boundary (LAB), which is defined as the 1,300°C-isotherm. Depending on the depth of the LAB, an average geothermal gradient evolves in the lithosphere along which heat is transported to the surface. In areas where the LAB is shallower than average, a steeper thermal gradient evolves, and vice versa. In areas with steeper geothermal gradients heat is transported more efficiently towards the surface, thus causing positive thermal anomalies in shallow sedimentary successions, which are targets for geothermal projects. Additionally, the geothermal gradient is influenced by material specific parameters, as the thermal conductivity and the radiogenic heat production.

To calculate the present-day thermal field of the Molasse Basin area the conductive heat equation for steady-state conditions (Eq 9) has been solved using a 3D finite element method (Scheck and Bayer 1999; Scheck et al. 2003) with λ as the thermal conductivity, T as the temperature and S as the radiogenic heat production.

$$0 = div\,(\lambda\, gradT) + S \qquad \text{(Eq 9)}$$

Thermal conductivity is defined as the heat flow across a specific cross-section and along a specific distance for a defined temperature decrease in a defined time (Clauser 2011a). In a material with higher thermal conductivity (e.g. crustal material) heat is transported more efficiently than in a material with lower thermal conductivity (e.g. sediments). Thus, in areas where crustal material lies shallower, but is covered by insulating sediments, higher temperatures can be expected at shallower depths than in areas with deeper lying crustal material. Vice versa, where crustal material is exposed, heat can escape the system more efficiently than in areas where crustal material is covered by sediments. Hence, lower temperatures can be expected in areas where crustal material is outcropping than in areas, where crustal material is covered. Even though anisotropic conditions are not deniable even within single sedimentary layers of the Molasse Basin, we have considered all units of the model as isotropic in our calculations due to a lack of data and admit that this is a limitation of our model.

The radiogenic heat production represents the amount of thermal energy set free by the decay of radiogenic isotopes in a defined volume in a defined timespan (Clauser 2011b) and thus has to be considered as an additional heat source in the calculation. Since more additional heat is generated in the silicic upper crystalline crust because of radioactive decay than in the mafic lower crystalline crust or sediments, more additional heat is introduced into the system by crystalline material of acidic composition than by mafic material and sediments. This leads to higher temperatures in areas with thicker acidic upper crystalline crust than in areas where the upper crust is thin.

Like the thermal conductivity, the radiogenic heat production is a specific material characteristic depending on the material composition and can vary significantly for different lithologies. For the calculation of the thermal field of the basin, all lithostratigraphic units of the model have been characterised with average values for the thermal conductivity and the radiogenic heat production according to their lithological composition (Tab 3).

Tab 3 Thermal properties assigned to the lithostratigraphic units and the range of values tested in the sensitivity study. References: [1] Ernstson and Pohl 1977, [2] Freudenberger and Schwerd 1996, [3] Landolt-Börnstein 1982, [4] Ebbing 2002, [5] Marotta and Splendore 2014, [6] Allen and Allen 2005, [7] Koch et al. 2009.

Lithostratigraphic Unit	dominant Lithology	Ref	Thermal Conductivity (W/mK)	Ref	Radiogenic Heat Production (W/m^3)	Ref
Nördlinger Ries	lacustrine sediments, impact breccia	1	2.1 ± 0.6	1	$1*10^{-6} \pm 0.5*10^{-6}$	3
Alpine Body	limestone, dolomite, marl, clay, silt, conglomerate	2	2.2 ± 0.6	3	$3*10^{-7} \pm 5*10^{-7}$	3
Folded Molasse Sediments	conglomerate, sand, silt, clay	2	2.1 ± 0.6	7	$1*10^{-6} \pm 0.2*10^{-6}$	3
Foreland Molasse Sediments	conglomerate, sand, silt, clay	2	2.1 ± 0.6	7	$1*10^{-6} \pm 0.3*10^{-6}$	3
Cretaceous	claystone, limestone	2	2.4 ± 0.5	7	$1.4*10^{-6} \pm 0.3*10^{-6}$	3
Upper Jurassic Malm	limestone, dolomite	2	2.7 ± 0.5	7	$1.4*10^{-6} \pm 0.4*10^{-6}$	3
PreMalm Sediments	claystone, sandstone, marl	2	2.7 ± 0.4	7	$1*10^{-6} \pm 0.6*10^{-6}$	3
Tauern Body	granite, gneiss, shale	3	2.6 ± 0.8	5	$1.8*10^{-6} \pm 1*10^{-6}$	3
Upper Crystalline Crust	granite/ granodiorite	3	3.1 ± 0.7	5	$1.8*10^{-6} \pm 0.7*10^{-6}$	3
Lower Crystalline Crust	gabbro	4	2.7 ± 0.8	5	$7*10^{-7} \pm 3*10^{-7}$	3
Lithospheric Mantle	peridotite	6	3.0 ± 0.7	5	$3*10^{-8} \pm 5*10^{-8}$	3

Where available, measured values of the respective properties have been favored, like for the sediments. For deeper parts, where no measured values were available, average published values have been chosen for the assumed lithology (Ernstson and Pohl 1977, Landolt-Börnstein 1982, Freudenberger and Schwerd 1996, Ebbing 2002, Allen and Allen 2005, Koch et al. 2009, Marotta and Splendore 2014). Furthermore, the calculation of the thermal field not only depends on the heat conduction and the radiogenic heat production, but also on the chosen thermal boundary conditions. For our calculation we used a 1st kind upper boundary condition (Dirichlet) by assigning a variable mean surface temperature to the top surface of the model (topography) based on averaged measured surface temperature values between 1961 – 1990 (DWD 2013; InMeteo 2013; HISTALP 2013, Fig 16).

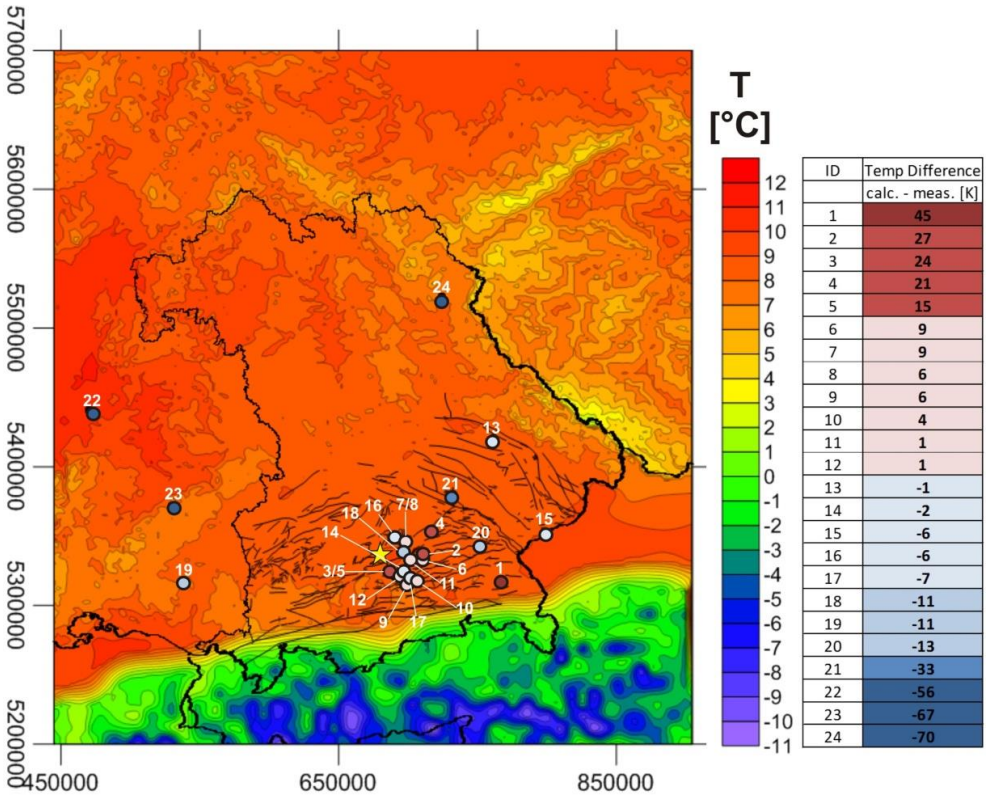

Fig 16 The mean annual surface temperature used as upper thermal boundary condition along the model surface for the calculation of the 3D thermal field (modified after DWD 2013, InMeteo 2013, HISTALP 2013).

Locations of the 24 geothermal energy production sites (Tab 4) are depicted, for which observed temperatures are available, to which our calculated temperatures have been compared. The color-coding of the locations is corresponding to the temperature difference between calculated and measured values according to the table beside. Positive values indicate that the model is too warm, negative values indicate that the model is too cold. The city of Munich is marked with a yellow star. Black lines show the locations of faults in the basin.

Besides, a 1st kind lower thermal boundary condition (Dirichlet) was assigned to the thermal LAB with a constant value of 1,300°C (Fig 15). To evaluate the influence of the assigned values for thermal conductivity and radiogenic heat production of each lithostratigraphic layer on the resulting thermal field, a sensitivity study has been carried out. Thus, a reasonable range of plausible values has been tested (Tab 3).

3.5 Results

The present-day 3D thermal field

In the calculated 3D temperature distribution (Fig 17) the temperatures increase non-uniformly with depth over the whole model area and several general thermal effects are evident (Fig 17-19).

The LAB, as the 1,300°C isotherm, lies shallower in the north and northwest than in the south of the model with a smooth transition in between (Fig 15). Accordingly, the geothermal gradient is much steeper in areas of a shallower LAB (northern and northwestern part of the model area towards the Eifel plume) than in areas of a deep LAB (Alps). This effect results in vertically closer-spaced isotherms in the north than in the south (Fig 17). Furthermore, the isotherms in the lithospheric mantle are bend upwards in the northwestern corner and flat in the northern and northeastern model part, whereas they are bent downwards in the central part of the model below the basin. In the area of the Alps, where the modelled LAB is deepest in our model, the isotherms are curved upwards in the mantle.

In the northern part of the model the isotherms are flat in the crystalline crust, illustrating a continuous decrease of temperature towards the surface. In contrast, the isotherms are bend upwards in the crystalline crust below the basin and even stronger below the Alps.
At the transition between the crystalline crust and the sediments, the shape of the isotherms changes in the domain of the Tauern Body. There, the upward-curved isotherms in the mantle and the crystalline crust flatten and even turn into a downward-curved shape when entering the Tauern Body (Fig 17b). The isotherms flatten again when entering the sediments of the Alpine Body. Accordingly, cooler temperatures are predicted in the Tauern Body than in the Alpine Body at shallow depth.
The upwards curved isotherms in the mantle and crust flatten when entering the Mesozoic sediments below the Molasse Basin (Fig 17a). This results in higher temperatures in the Mesozoic sediments under the Tertiary sediments in the Molasse Basin than in the northern parts of the model, where no insulating sediments are covering the crystalline crust.

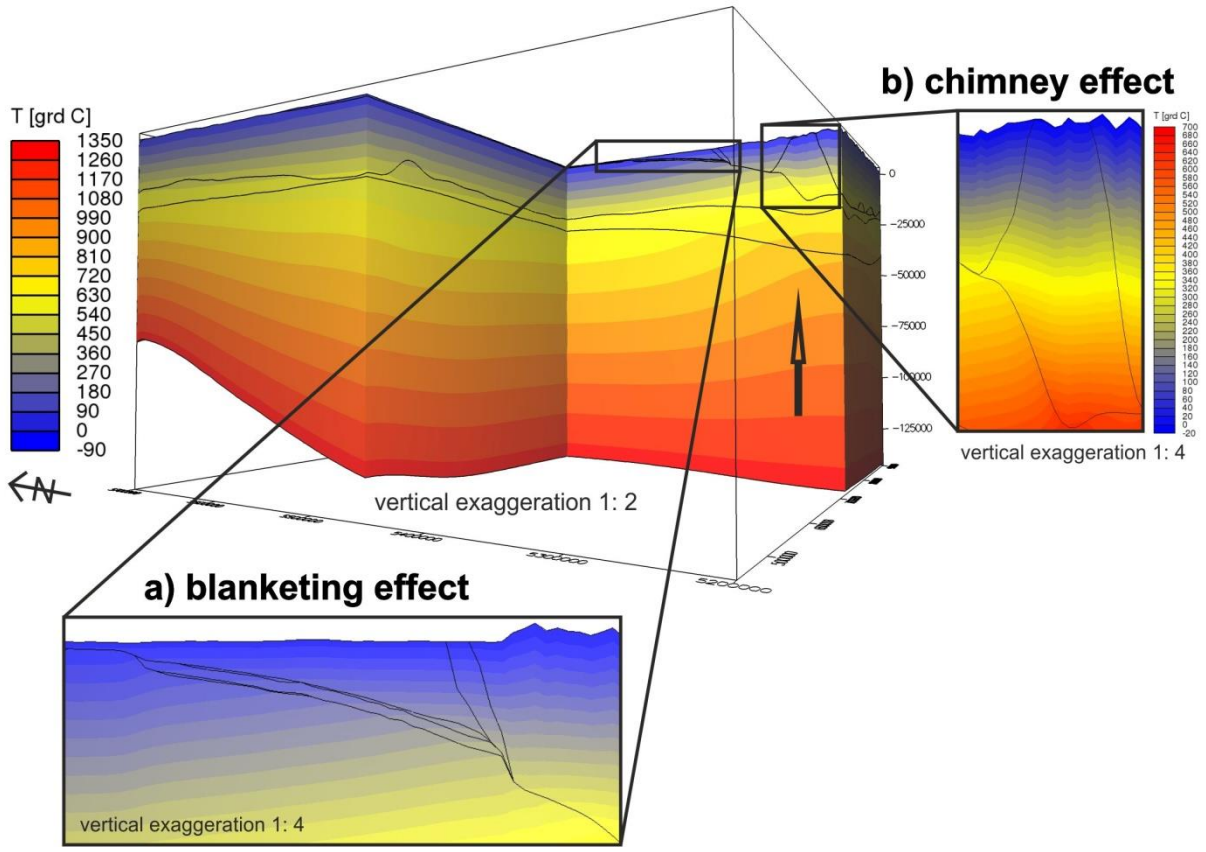

Fig 17 The resulting present-day lithospheric-scale 3D conductive thermal field of the Molasse Basin area. Subpanels a and b zoom into areas of specific thermal effects with a) thermal blanketing effect and b) chimney effect (shown with higher temperature resolution, scale shown at zoom-in b).

At all depths within the sedimentary part (Fig 18 and 19) a colder part in the north and a warmer part in the south are predicted with distinct short-wavelength temperature variations. These anomalies are in close correlation with topographic highs and can be traced in the temperature distribution at all depths in the sedimentary part.

To illustrate how the calculated temperatures change non-uniformly with depth, Fig 18 and 19 presents different temperature-depths maps.

At a depth of **1,000 m bsl** (Fig 18a) the colder part in the north shows temperatures between 25 and 50°C, while the warmer part in the south shows temperatures of up to 105°C. The outer frame of the Molasse Basin and the outcropping Mesozoic sediments can be clearly recognized in the temperature distribution. Within the basin, temperatures between 50 and 70°C are predicted with a general trend of southwards increasing temperatures. A minor negative temperature anomaly with a difference in temperature of 5-10 K is predicted south of Munich (city marked with a red star) and a short-wavelength positive anomaly is modelled in the southwestern corner of Bavaria.

The binary division of the thermal signature of the basin is also present in the temperature distribution at **2,000 m bsl** (Fig 18b), where calculated temperatures vary between 60 and 96°C. Likewise, both the colder northern part of the model as well as the Alpine area are still distinct with up to 60°C and 130°C, respectively. A positive thermal anomaly at 2,000 m bsl is predicted in the western part of the Molasse Basin with temperatures of up to 95°C. A second smaller and weaker positive thermal anomaly occurs in the eastern part of the basin in Austria. Between the hotter domains a colder area is predicted by the model.

At a depth of **3,000 m bsl** (Fig 18c) temperatures between 130 and 100°C are calculated for the basin area. The temperatures in the Alpine area increase to up to 155°C, while the northern part of the model area shows temperatures of up to 90°C with slightly warmer temperatures in the northwestern corner of the model area towards the Eifel plume. Within the basin, the positive temperature anomaly in the western part attains up to 125°C. Likewise, the thermal anomaly in the Austrian part increases to 125°C. Furthermore, a third positive temperature anomaly is visible in the south of the city of Munich with temperatures comparable to the ones of the thermal anomaly in the west of the basin.
Between these positive thermal anomalies, an area of colder temperatures is evident southeast of Munich with a temperature difference of up to 20 K with respect to the neighboring positive thermal anomalies.

At **4,000 m depth bsl** (Fig 18d) the temperature predicted in the basin ranges between 115 and 160°C, while the temperatures in the northern model area reach up to 115°C. In the Alpine area modelled temperatures are significantly higher and may reach up to 185°C. The positive thermal anomaly in the western basin as well as the anomaly in the south of Munich increase to up to 160°C. Furthermore, the smaller positive thermal anomaly in the Austrian part of the Molasse Basin has shifted westwards and shows temperatures of up to 160°C. The negative thermal anomaly in the east-southeast of Munich in between the two positive thermal anomalies shows a temperature of ~145°C, which is up to 20 K colder than the temperature within the positive thermal anomalies.

At the depth of **5,000 m bsl** (Fig 18e), the temperatures increase to up to 125°C in the northern model part and to 210°C in the Alpine area. For the basin area temperatures between 130 and 180°C are predicted with some local anomalies of higher temperature. The temperatures characterizing the positive thermal anomalies in the basin increase to up to 185°C, while the anomaly south of Munich and the one on the eastern border of the German Molasse Basin connect to form a narrow high temperature bridge. The negative thermal anomaly in the southeast of Munich is far less pronounced than at shallow levels.

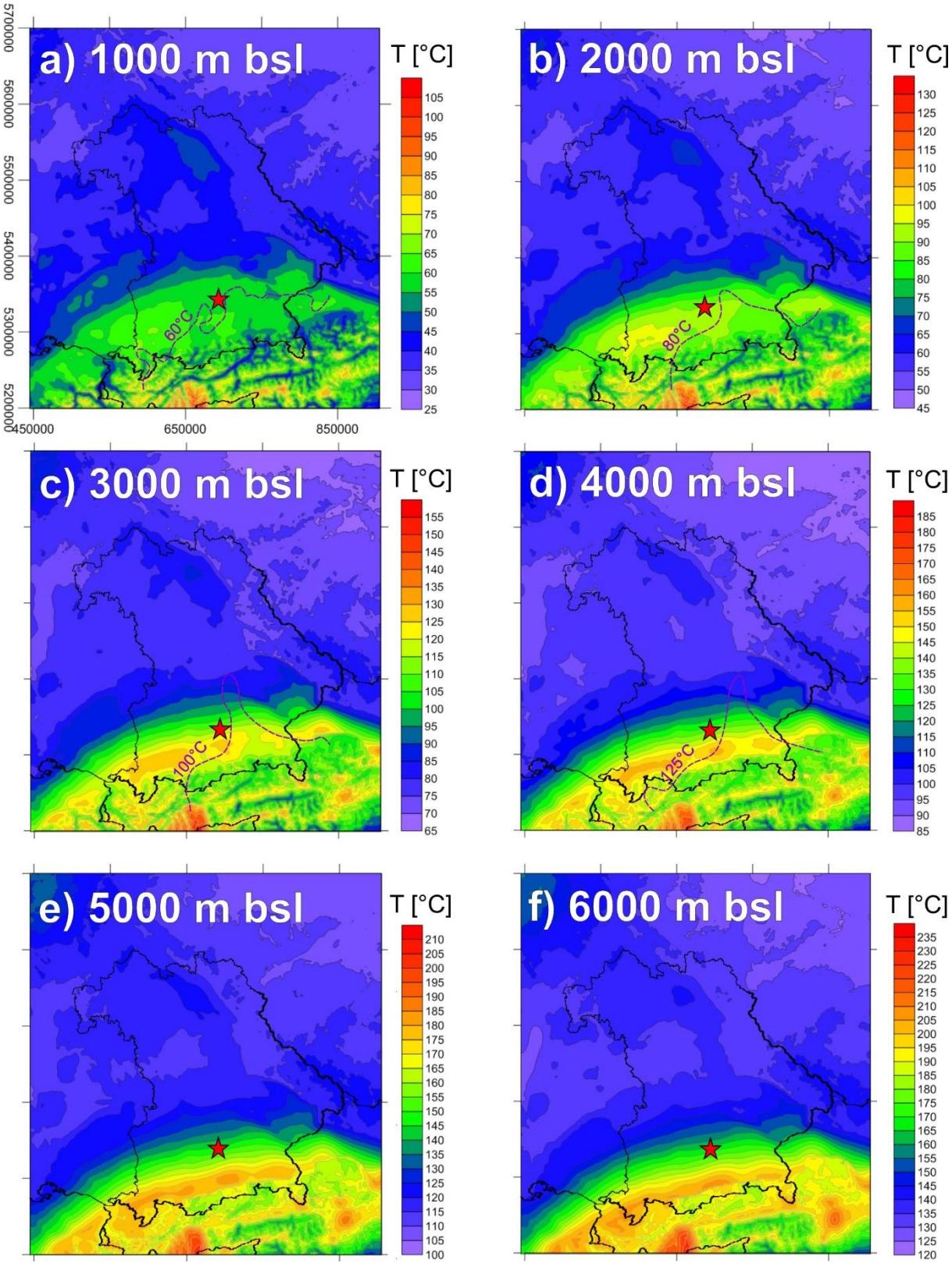

Fig 18 Temperature maps (a-f) for different depths extracted from the 3D thermal model of which maps a-d have been compared to respective temperature-depth maps of the GeotIS thermal model (Agemar et al. 2014b, purple dashed lines). Maps e-f show depths for which no observed data was available as comparison.

At **6,000 m bsl** (Fig 18f) the temperatures in the northern model part and towards the Eifel plume increase to 150°C. In the Alpine area temperatures of up to 235°C are predicted. The frame of the Molasse Basin can still be recognized clearly in the temperature distribution even at this depth. The basin shows temperatures between 150 and 210°C. The individual positive thermal anomalies distinct at shallower depths form a realm of higher temperatures at this level (up to 210°C) in the south of Munich.

At depths **below 6,000 m bsl** (Fig 19a - b) the pattern of temperature distribution is more smooth than at shallower levels though the contour of the Molasse Basin in the temperature distribution is still visible. In the area of the Molasse Basin the temperature distribution shows a continuous increase from north to south towards the Alps. At all depths a distinct temperature effect of short wavelength is predicted for the Alpine area. In this domain, the strongly varying surface temperature propagates downward causing higher temperatures in topographically high areas in the Alps. However, this effect decreases with depth and is barely visible below 6,000 m bsl. Noticeable are significantly lower temperatures in the Tauern Body than in the Alpine Body at all depths. This effect is more pronounced in the deeper parts: The temperature difference between the Tauern Body and the Alpine Body rises to up to 80 K at a depth of 10,000 m bsl.

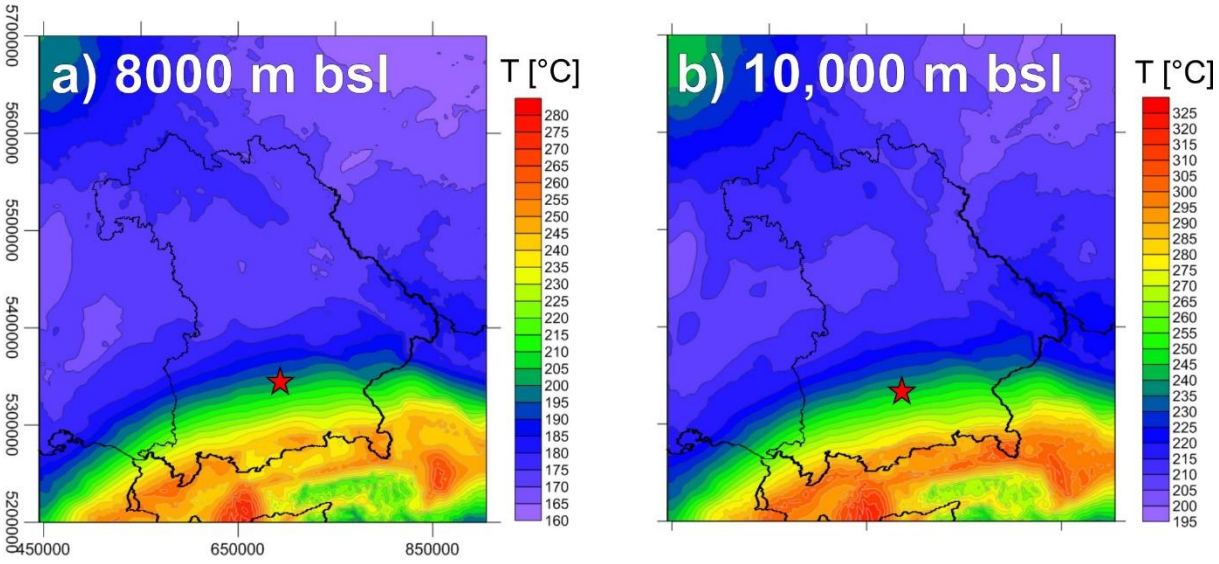

Fig 19 Temperature maps for larger depths (a-b) extracted from the 3D thermal model.

Prominent Isotherms

In case a geothermal power plant shall be used not only for heating, but as well for electric power production, a temperature threshold value of 100°C should not be undercut as reservoir temperature (Agemar et al. 2012). Looking at the depth of the **100°C isotherm** predicted by the model (Fig 20a), again a binary pattern is visible: In the northern part, the depth of the isotherm ranges between 4,800

and 3,800 m bsl. At the northern edge of the Molasse Basin the modelled depth of the 100°C isotherm decreases from 3,800 m bsl at the edge of the basin to 2,200 m bsl in the central part. Southward, the 100°C isotherms lies nearly flat at a depth of ~2,100 m bsl. Below the Alps the isotherm rises to a depth of up to 800 m bsl (but still with > 3000 m below topography) with a strongly irregular course. However, the largest depth values of the 100°C isotherm in the Alps can be found in the area of the Tauern Body with up to 3,200 m bsl.

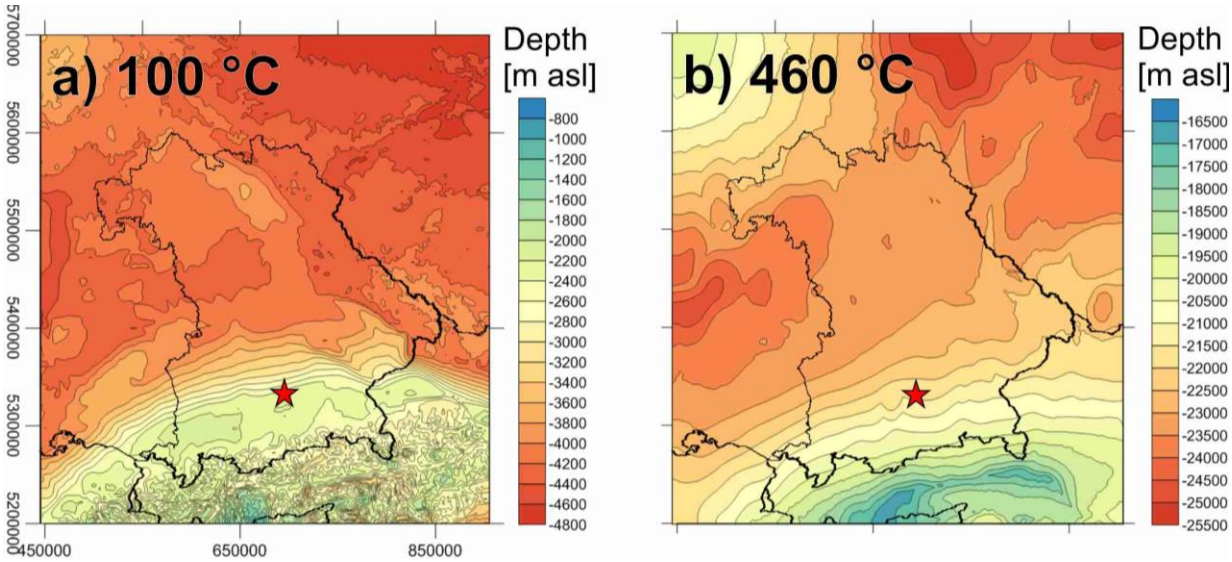

Fig 20 Depth maps (a and b) showing the depth to the 100°C and 450°C isotherms predicted by the model.

Another prominent isotherm is the **460°C isotherm**, around which, assuming an average increase of pressure with depth, the brittle-ductile transition zone of crystalline crustal material is assumed (Ranalli 1995). Around this temperature, the rheological behaviour of mainly crystalline rocks changes from brittle to ductile and therefore the depth of this isotherm sets a threshold below which no earthquakes are expected to occur (Dragoni 1993). Thus, the depth of this transition zone in a specific area is strongly affected by the geothermal gradient: the steeper the gradient the shallower the transition zone (and vice versa). According to our calculation the 460°C isotherm is at a depth of 16,500 to 25,500 m bsl in the Molasse Basin area (Fig 20b). This isotherm is deepest in the northeastern and western part of the model area with 25,500 m bsl and intermediate in the central model area with values around 23,000 m bsl. Towards the northwestern corner of the model area, in the direction of the Eifel plume (Seiberlich et al. 2013), the 460°C isotherm rises to up to 19,500 m bsl. From the northern edge of the Molasse Basin to the south the isotherm rises continuously to 20,000 m bsl depth at the margin of the Alps. Lowest depth values of this isotherm (up to 16,500 m bsl) are predicted for the area of the Alps, whereby the isotherm is deepest within the Tauern Body. Unlike the 100°C isotherm, the depth of the 460°C isotherm shows no short-wavelength variations.

3.6 Sensitivity Analysis with respect to thermal properties

To assess the influence of each model unit and the prescribed thermal properties on the predicted thermal field a sensitivity study was carried out within which different values for each property were assigned to the model layers (Tab 3) and the thermal field was calculated. In figures 21 - 23 the predicted temperature distributions at a depth of 3000 m bsl are shown for the highest and the lowest values assigned, respectively, for the model units exerting the strongest influence on the temperature distribution.

Thermal Conductivity

Figures 21a and b show the influence of the thermal conductivity of the Alpine Body on the temperature distribution in the Molasse Basin.
Assuming a low thermal conductivity of this model unit (Fig 21a, 1.6 W/mK) temperatures between 115°C and 130°C are predicted for the basin with three positive thermal anomalies (in the western part, south of Munich, and at the eastern Bavarian border) with temperatures of up to 140°C. Between the latter two positive thermal anomalies, an area with average temperatures (125°C) can be seen in the southeast of Munich.
Assuming a significantly higher thermal conductivity for the Alpine Body (Fig 21b, 2.8 W/mK) lower temperatures by 10 to 15 K are predicted by the model for the positive thermal anomalies with no pronounced cooler area in the southeast of Munich.

When decreasing the thermal conductivity of the Tauern Body to 2.3 W/mK (Fig 21c) higher temperatures in the area of the Tauern Body and the Alpine Body are predicted compared to the original model by ~20 K. The same temperature shift can be seen in the Molasse Basin, for which temperatures of up to 150°C are predicted. Assuming a higher thermal conductivity of the Tauern Body (Fig 21d, 3.5 W/mK) the area of the Tauern Body shows lower temperatures than in the original model by ~10 K. In addition, the positive thermal anomalies in the Molasse Basin decrease in size and no significant negative thermal anomaly in the southeast of Munich can be seen. Thus, removing the contrast in thermal conductivity between the Alpine and the Tauern Body also causes the negative thermal anomaly southeast of Munich to disappear.

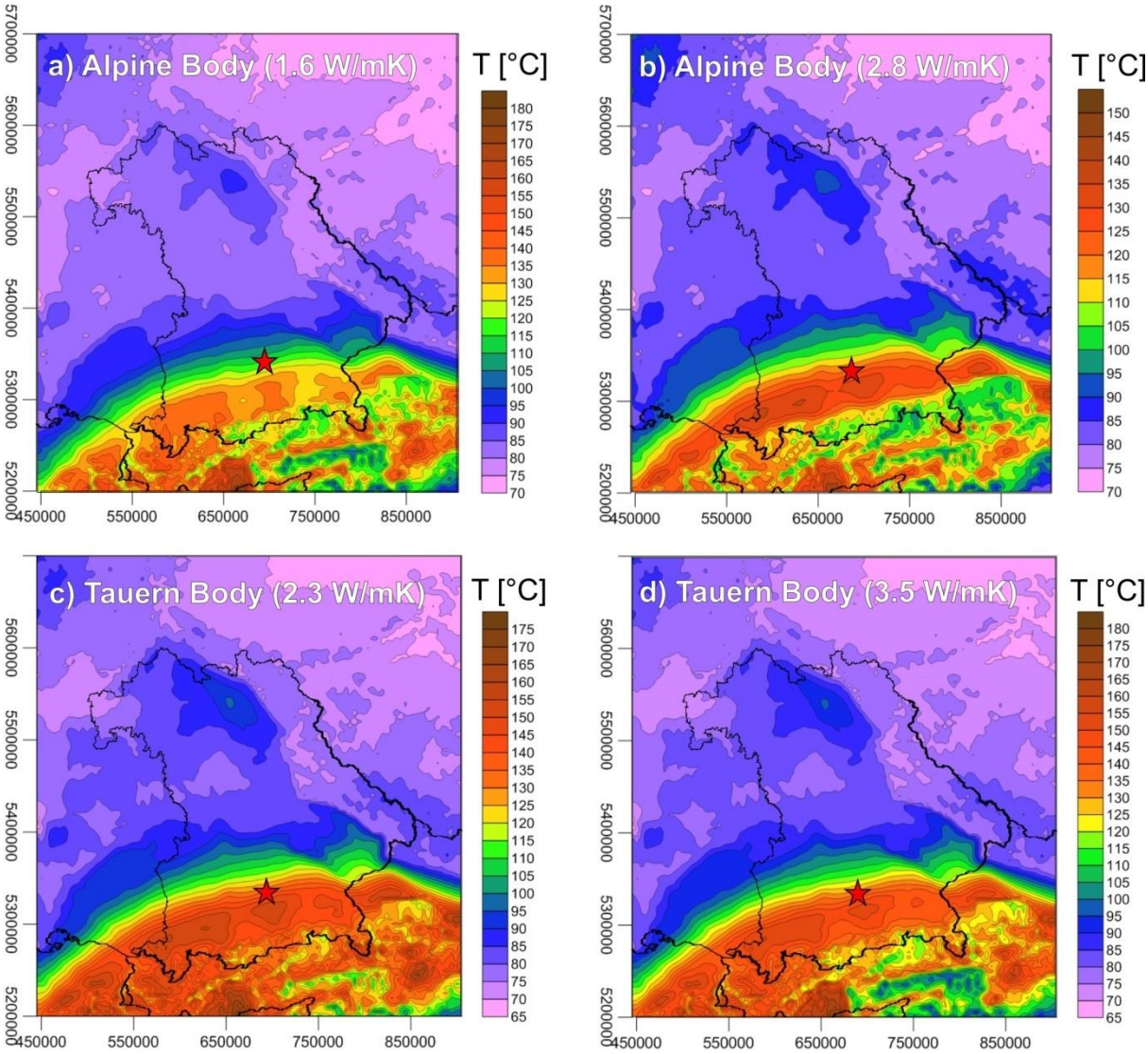

Fig 21 Temperature distribution at a depth of 3,000 m bsl predicted for different ranges of thermal properties as assessed in a sensitivity analysis. Maps a to d show the influence of the thermal conductivity of specific model units on the temperature distribution. A higher thermal conductivity of the Alpine Body leads to an average cooling of the model. A different heat conductivity of the Tauern Body mostly affects the Alpine area, while the Molasse Basin remains mostly unchanged.

Decreasing the thermal conductivity of the upper crystalline crust in the model to 2.4 W/mK (Fig 22a) the temperature increases by 10 K in average in the northern and eastern model part where the upper crystalline crust is outcropping with a stronger variation compared to the original model (Fig 18c). In the basin a temperature change of ~5 K can be recognized compared to the original model.

Increasing the thermal conductivity of the upper crystalline crust to 3.8 W/mK (Fig 22b) decreases the average temperature in the outcropping areas of the upper crystalline crust in the north and east by ~10 K. The thermal anomalies in the Molasse Basin is not significantly influenced by the changes in thermal conductivity of the upper crystalline crustal layer compared to the original model.

As visible in figure 22c and d, decreasing (1.9 W/mK) and increasing (3.5 W/mK) the thermal conductivity of the lower crystalline crust has very little influence on the predicted thermal field.

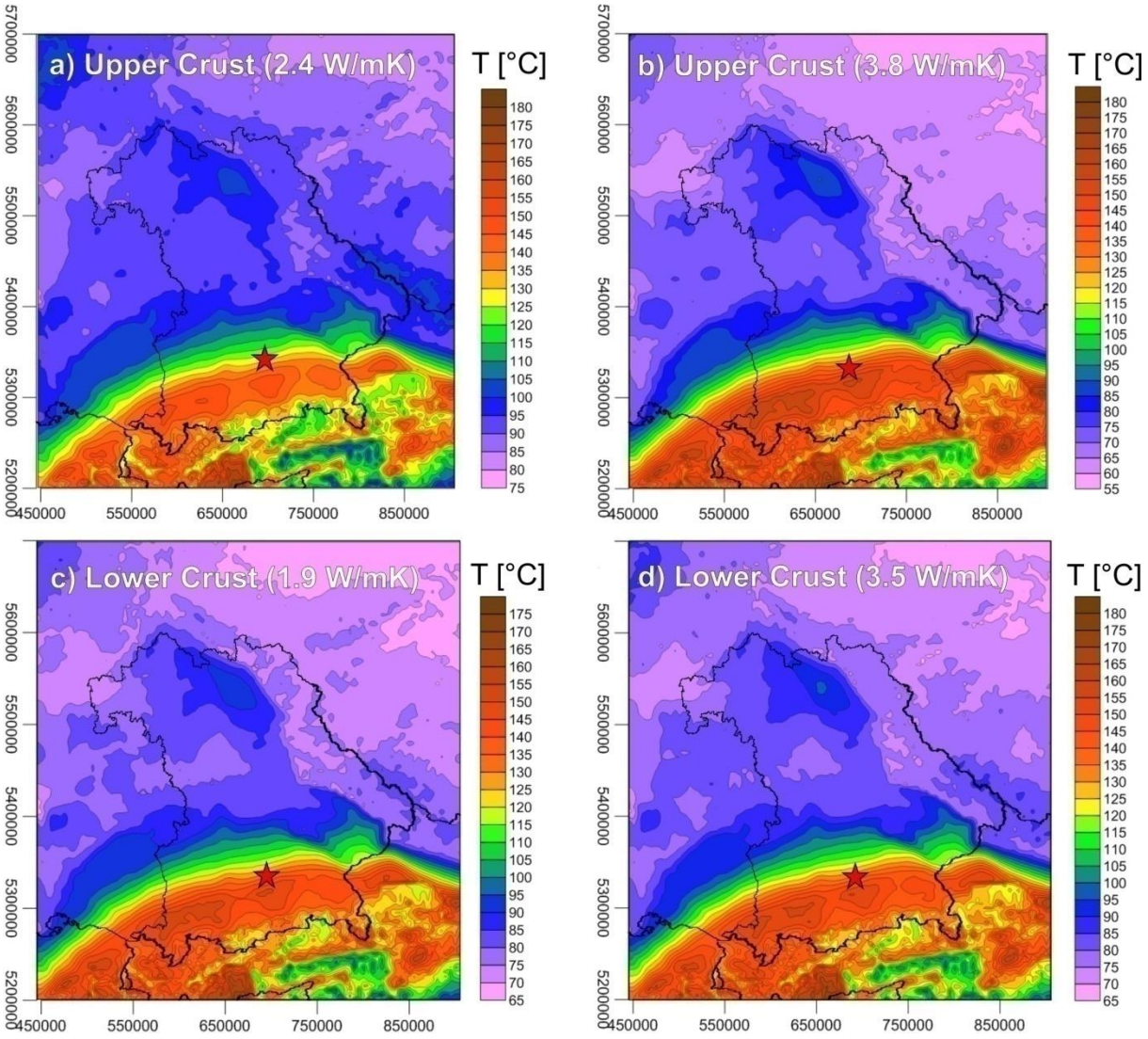

Fig 22 Temperature distribution at a depth of 3000 m bsl predicted for different ranges of thermal properties as assessed in a sensitivity analysis. Maps a - d show the influence of the thermal conductivity of the upper and lower crystalline crust on the temperature distribution. An increased thermal conductivity of the upper crystalline crust leads to higher temperatures in the Molasse Basin and the Alps, but lower temperatures in the central and northern parts of the model. Different thermal conductivities of the lower crystalline crust have only a minor influence (±5 K) on the temperature distribution in the whole model area

Radiogenic Heat Production

Decreasing the radiogenic heat production of the upper crystalline crust to $1.1*10^{-6}$ W/m^3 (Fig 23a) leads to an overall cooling of the system compared to the original model, especially in areas with a thick upper crystalline crust as in the northern and western model parts. Those areas show predicted temperatures lower by up to 25 K. The positive thermal anomalies in the Molasse Basin show decreased temperatures

by 20 K. Further south in the Alps, where the thickness of the upper crystalline crust is smaller, the temperature difference amounts ~-10 K.

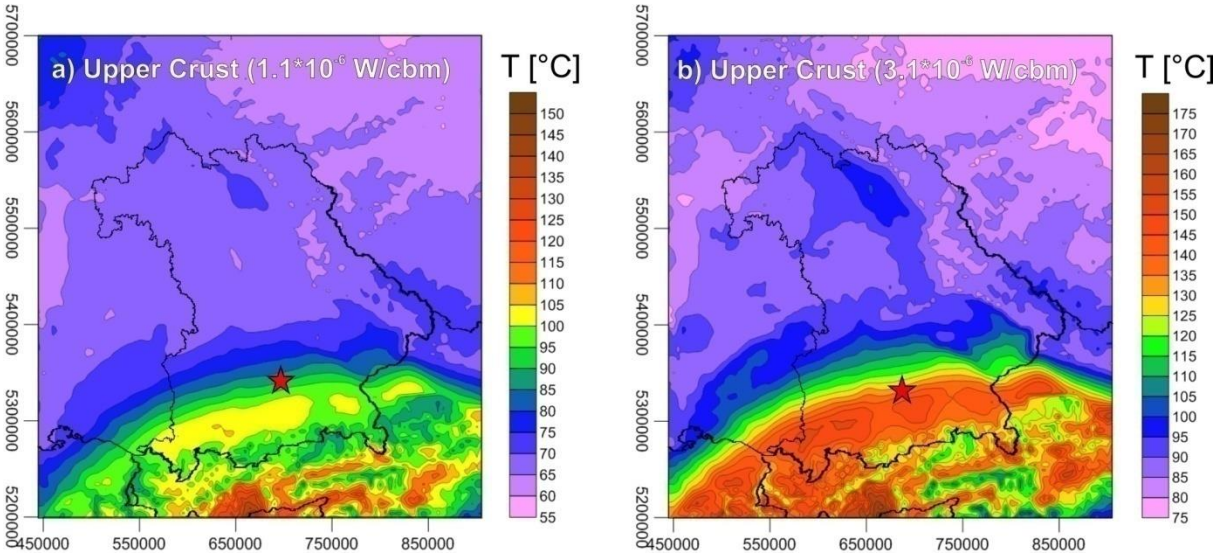

Fig 23 Temperature distribution at a depth of 3000 m bsl. Maps a and b show the impact of the radiogenic heat production of the upper crystalline crust on the thermal field. A lower radiogenic heat production of the upper crystalline crust leads to overall lower predicted temperatures in the whole model and vice versa.

Assuming an increased radiogenic heat production of the upper crystalline crust ($3.1*10^{-6}$ W/m^3, Fig 23b) the model predicts temperatures higher by up to 25 K compared to the original model in the northern and eastern parts, where the upper crystalline crust is cropping out. For the positive thermal anomalies in the basin the model would predict temperatures 15 K higher than the original model, whereas the negative thermal anomaly in the southeast of Munich is less affected.

The sensitivity analysis has shown that the thermal conductivity of the Alpine Body as well as the thermal conductivity and the radiogenic heat production of the upper crystalline crust have the strongest impact on the basin wide conductive thermal field. While the thermal conductivity of the Tauern Body shows a smaller influence on the temperature distribution in the Molasse Basin, the thermal conductivity of the lower crystalline crust has only a minor influence on the basin-wide thermal field. Both properties of the Molasse Sediments, the Upper Jurassic and the PreMalm Sediments show no significant influence on the thermal field within the range of values tested (Tab 3) and are therefore not further described.

3.7 Interpretation and Discussion

Analyzing the calculated 3D thermal field, different thermal effects can be recognized affecting the deep temperature distribution in the Molasse Basin area. Regional effects affecting the deeper part of the system and local effects having the strongest influence on the shallow thermal field can be distinguished.

Regional thermal effects

One regional effect is caused by the average **geothermal gradient** due to the depth of the **thermal LAB**. Where the LAB is shallower, as in the northern and northwestern model parts, the heat has to overcome a smaller distance to equilibrate between the two thermal boundaries (LAB: 1,300°C, Surface: -11 to +12°C) leading to an increased geothermal gradient than in areas with a deeper LAB (central model area). The switch of the bending direction of the isotherms in the mantle in the central model part from bend upwards (increasing geothermal gradient) to bend downwards (decreasing geothermal gradient) is thereby credited to the increasing depth of the LAB towards the south. Interestingly, the geothermal gradient is not smallest in the area of the Alps where the LAB is deepest, but higher than in the basin area. This is related to the compensating effect of crustal thickness. The crystalline material produces radiogenic heat adding to the total heat budget and is thinner below the Alpine foreland than below and within the orogon.

A second regional effect can be connected to the **radiogenic heat production** in the **crust**, which is an additional heat source in the system and much higher in the upper crystalline crust than in the rest of the model layers. Since the absolute amount of produced heat is dependent on the crustal volume, the intensity of this effect is in close correlation to the thickness of the upper crystalline crust, which varies between 20 and 28 km thickness in the northern model part. In contrast, below the Alpine area and the Molasse Basin the upper crystalline crust is far thinner and may locally be only 6 km thick. The Tauern Body consists predominantly of upper crystalline material and thus also represent a domain with high radiogenic heat production. Accordingly, the heat budget within the Tauern Body is larger than in the surrounding domain where the radiogenic upper crust is thinner (Fig 14c). This causes higher temperatures in the lower part of the Tauern Body compared to its neighboring areas (Fig 17b). Therefore, in spite of a uniform depth of the thermal LAB, lateral variations in temperature evolve in the upper part of the lithospheric mantle and the lower part of the crust illustrated by upward-curved isotherms in Fig 17.

A third thermal effect affecting the thermal field on a regional scale is the contrast in the **thermal conductivity** between the highly conductive crystalline **crust** and the Tauern Body and the less conductive **sediments**. In areas, where crystalline material is exposed to the surface, as in the Tauern Window (Schmid et al. 2004a), heat can escape more efficiently than in areas covered by insulating sediments. This effect is known as **chimney effect** (Fig 17b) and can be observed as downward-bend

isotherms inside the shallow Tauern Body and as lower shallow temperatures in the area of the Tauern Body compared to the surrounding area in the temperature maps (Fig 18c - f, Fig 19).

Around the Tauern Window the deformed sediments of the Alpine Body cover the crystalline crust (Fig 14a). Consisting mostly of limestone, dolomite, marl and clay, the Alpine Body has a far smaller heat conductivity that the underlying crystalline crust and the crystalline Tauern Body. Thus, the heat generated in the crust and mantle is trapped by the low conductive sediments of the Alpine Body which causes heat storage in the sediments. This effect is known as **blanketing effect** (Fig 17a) and is stronger where the sediments are thicker (as in the Alps and the basin) and weaker where sedimentary thickness is smaller (as in the north of the model). Such a blanketing effect can also be recognized in the fill of the Molasse Basin, where calcareous and clastic sediments overly the crystalline crust. This thermal blanketing leads to increasing temperatures from north to south in the Molasse Basin (Fig 18a - d) and correlates with the increasing thickness of Molasse Sediments from north to south (Fig 13c).

The chimney effect and thermal blanketing are thus results of heat refraction in response to contrasts in thermal conductivity. Such phenomena have already been described for other basins in different tectonic settings (Bayer et al. 1997, Allen and Allen 2005. Stephenson et al. 2009, Noack et al. 2010, Cherubini et al. 2014) and are laterally influencing each other. For the Alps and the Molasse Basin this implies that the heat coming from the asthenosphere together with the heat generated in the crystalline crust arrives at the base of the insulating sediments of the Alpine Body and the Molasse Basin, is stored within the sediments and causes higher temperatures within the latter. In areas where the heat is conducted directly to the surface, as within the Tauern Body, lower shallow temperatures evolve than in the surrounding areas. In summary, the binary division of the model area into a cooler northern part and a warmer southern part with a transition at the northern rim of the Molasse Basin is in close correlation with the distribution of sedimentary thicknesses (Fig 13, Fig 14), but additionally influenced by the thickness of the conductive crystalline crust (Fig 14) and the amount of radiogenic heat created in this upper part.

In addition, **topographic features** may have an effect on local subsurface temperatures which has already been quoted by Kutasov (1999) and Noack et al. (2010). In topographically high areas (e.g. summits of the Alps) the upper thermal boundary condition is prescribed at higher elevation than in topographically low areas (e.g. valleys of the Alps). This difference in elevation can reach up to 2 km. Accordingly, a temperature variation evolves in the upper few kilometers that correlates spatially with the topography. Even considering 3D heat transport such a topographic effect on the temperature distribution can be traced downwards to upper crustal levels, causing local short-wavelength temperature anomalies in the thermal field. In the deeper crust the influence of topographic effects is lost and the depth to the thermal LAB dominates the evolving temperature pattern.

The superposition of all three described effects (topographic effect, blanketing effect and chimney effect) leads to a characteristic lateral temperature distribution in the Molasse Basin area with a stronger variation (Fig 18, Fig 19) than in the temperature maps created by 3D interpolation of measured values

(Agemar et al. 2014b). This is due to the implemented structural heterogeneity considered in the thermal model of this study compared to the interpolation between measured data points in the GeotIS project (Agemar et al. 2014b) assuming a homogeneous and isotropic configuration of the subsurface. However, Agemar et al. (2012) recommend to treat the deeper temperature estimates of the thermal model of GeotIS with extra care due to possible local effects on the temperature distribution caused by a heterogeneous distribution of thermal conductivities, which have not been regarded in the temperature interpolation.

Comparing with measured temperatures

Assuming heat conduction being the main heat transport mechanism in the Molasse Basin, the observed temperature pattern and the temperature values have been reproduced to a certain degree in this study. Compared to the results of the GeotIS project (Agemar et al. 2014b) our model is too warm in the upper 5,000 m bsl. Also, the temperatures predicted in our model are too warm if compared to published temperatures measured at 24 geothermal production sites. As illustrated in Fig 16 and Tab 4, 12 sites are showing temperature differences in a range of ±10 K, a value as high as the standard deviation of bottom hole temperatures and temperature logs (Hermanrud et al. 1990, Förster 2001, Noack et al. 2010, Agemar et al. 2012 and 2014a).

At further 5 locations the model results show temperature difference of more than +10K in the area of the described negative thermal anomaly southeast of Munich, which is less cold in the model than observed. In this area, an additional effect on the thermal field by heat transport related to fluid flow is considered likely (Birner 2013). Such a phenomenon has already been assumed for the western Molasse Basin by Rühaak et al. (2010), for a similar setting with a the deep carbonate aquifer in the Po Plain in Italy (Pasquale et al. 2013), and for other structural settings as the North German Basin by Noack et al. (2010) and the Western Canada Sedimentary Basin (Majorowicz et al. 2014).

For 7 locations, the modelled temperatures are too cold compared to the measured values. One of these locations is Windischeschenbach, where the difference between modelled and observed temperature is largest (>65 K at 8,638 m bsl). A possible reason for such a high temperature difference may lay in local heterogeneities of the radiogenic heat production and thermal conductivity in the crust, which are not resolved in our model, or advective heat transport related to fluid flow, which is not considered in our approach.

Tab 4 Geothermal energy production sites with their measured and the respective calculated temperatures. The production sides are additionally depicted in Fig 16.

ID	Location	UTM Coordinates		Depth [m asl]	Temperature measured [°C]	Temperature calculated [°C]	Temp Difference calc. - meas. [K]	Reference
1	Traunreut	768326.3446	5317920.521	-4095.710	108	153	45	Agemar et al 2014a
2	Poing	709645.0836	5338567.483	-2464.960	76	103	27	Agemar et al 2014a
3	Pullach 2	687645.8845	5324767.734	-2361.960	80	104	24	Agemar et al 2014a
4	Erding	716537.888	5354505.059	-1894.809	62	83	21	Agemar et al 2014a
5	Pullach	687645.8845	5324767.734	-2920.960	104	119	15	Agemar et al 2014a
6	Aschheim	701945.275	5338366.932	-2117.904	85	94	9	Agemar et al 2014a
7	Garching	696945.2515	5346766.704	-1683.616	70	79	9	ITG (2014)
8	Garching	696945.2515	5346766.704	-1744.916	74	80	6	Agemar et al 2014a
9	Sauerlach	698045.8424	5316267.778	-3852.980	140	146	6	Agemar et al 2014a
10	Dürrnhaar	704145.653	5318768.12	-3504.876	135	139	4	Agemar et al 2014a
11	München Riem	700893.3825	5334418.605	-2155.422	95	95	1	Agemar et al 2014a
12	Oberhaching	693645.4216	5321868.061	-3232.777	128	128	1	Agemar et al 2014a
13	Straubing	761610.226	5420054.051	-500.613	37	36	-1	Agemar et al 2014a
14	Unterhaching	695375.7952	5325900.639	-3031.660	123	122	-2	Agemar et al 2014a
15	Simbach-Braunau	800291.3264	5352101.534	-1586.610	81	75	-6	Agemar et al 2014a
16	Unterschleißheim	690746.0027	5349666.83	-1484.859	78	72	-6	Agemar et al 2014a
17	Kirchstockach	699744.9973	5322467.964	-3384.942	139	132	-7	Agemar et al 2014a
18	Unterföhring	696542.4435	5340811.137	-1484.408	86	75	-11	Agemar et al 2014a
19	Bad Saulgau	537376.4201	5317524.491	-21.667	41	30	-11	Werner et al 1978
20	Waldkraiburg	752496.3402	5344579.67	-2291.049	109	96	-13	Agemar et al 2014a
21	Landshut	732766.0605	5379951.31	-72.503	60	27	-33	Agemar et al 2012
22	Bruchsal	469755.6067	5440897.013	-2409.251	120	64	-56	GTV (2014)
23	Bad Urach	529623.6519	5371419.002	-3862.813	168	101	-67	Agemar et al 2012
24	Windischeschenbach	724584.8959	5522239.823	-8638.671	253	183	-70	Agemar et al 2014a

In addition, the influences of large faults zones permeable for fluid are not considered in our approach. Such fault zones may act as pathways for fluid flow and enable convective heat transport in the basin. To investigate a potential influence of fluid flow related cooling on the thermal field of the Molasse Basin area coupled transport of fluid and heat should be considered. However, a higher vertical and horizontal resolution than used for this study and the implementation of faults into the model would be needed, which in turn would require an improved structural and (hydro)geological database.

Sensitivity

We admit that the limited model resolution and the assignment of homogenous parameters to the layers are likely to be a source of error in our approach. However, a sensitivity analysis (Fig 21 - 23) addressing the impact of different lithostratigraphic units and their respectively assigned thermal properties on the geothermal field has shown, that the lithospheric-scale thermal field mostly depends on the depth of the LAB, the configuration of the crystalline crust and the thermal properties of the Alpine and Tauern Body as well as the thickness of the Molasse Sediments. Of these, especially the radiogenic heat production of the upper crystalline crust shows a large a priori uncertainty related to the assigned values for radiogenic heat production (Vosteen et al. 2006, Vilá et al. 2010) due to lacking measurements. Variations in the thermal properties of the Nördlinger Ries, the Folded Molasse Sediments, the

Cretaceous, the Upper Jurassic Malm and the PreMalm Sediments have shown only minor influences on the long wavelength thermal field as these layers are of limited thickness and partly even discontinues. Nevertheless, a better representation of the real geological situation could be achieved by implementing varying thermal properties laterally and with depth within a model unit. Recent studies (Homuth et al. 2014 and 2015) on the nature and distribution of thermal properties of the Upper Jurassic could help to reduce the uncertainties further. However, the findings for the long wavelength thermal field of the Molasse Basin area and the thermal interdependence between the basin and the Alps are robust. Prescribing laterally varying thermal properties to the model units would lead to short wavelength thermal effects and thus not change the regional pattern of temperature distribution significantly.

Prominent isotherms

Given the mentioned limitations, the results nevertheless indicate that assuming conductive heat transport as the first order control for the thermal field is valid and give first order estimates of deep temperature variations. According to the calculated depth of the 100°C isotherm (Fig 20a), temperatures high enough for both geothermal heating and electric power production can be found at deeper levels in the north of the model area than in the south, due to the thickness distribution of the Molasse Sediments. Within the Molasse Basin this isotherm is at an average depth of 2,000 m bsl with small lateral depth variations, a result that supports the suitability of this area for electrical power production.

The second prominent temperature level is the 460°C isotherm, which marks the transition between brittle to ductile behaviour of granitic material and thus is a threshold value below which the probability of crustal rupture and associated earthquakes are strongly reduced. The larger depth of this isotherm in the northern part of the model compared to the southern part (Fig 20b) implies a weaker rheology of the lithosphere at shallower depth below the Alps than below the northern part of the model area. This in turn is consistent with earlier results from thermo-mechanical models of Genser et al. (1996) and Okaya et al. (1996). Moreover, higher temperatures at shallow depths below the Alps (compared to larger depths below the Molasse Basin) would explain the earthquake distribution described by Deichmann et al. (1999), Willinghofer and Cloething (2003) and Singer et al. (2014) with deep earthquakes in the foreland and shallow earthquakes in the Alpine area. In fact, the deepest earthquakes shown by Singer et al. (2014) correlate well with the depth of the 460°C isotherm predicted by the conductive calculations of this study.

3.8 Conclusions

Assuming conductive heat transport to be the dominand process, the lithospheric-scale 3D thermal field of the Molasse Basin area has been calculated. In the predicted temperature distribution different superposed thermal effects can be recognized, which show an interdependence between the Alps and the foreland basin with respect to the regional thermal field.

Our results indicate that the temperature distribution in the lithospheric mantle and the crystalline crust is controlled by the depth of the thermal LAB, the thickness distribution of the radiogenic crust and the contrast in thermal conductivities between crystalline and sedimentary rocks. For the Molasse Basin and the adjacent Alpine orogen this results in shallow hotter temperature where thick sedimentary rocks cover the crystalline crust (Alpine Body and Molasse Basin) and colder shallower temperatures where the crystalline crust is exposed (Tauern Body). This related chimney effect can have a significant lateral influence in response to 3D heat transport and cause local negative anomalies in neighboring domains (e.g. southeast of Munich). Together with the topographic effect, the chimney and blanketing effect control the regional scale temperature distribution in the sedimentary part of the model.

Using a conductive approach, this study was able to reproduce the measured present-day thermal field in the shallow part of the Molasse Basin area to a certain degree. Though the predicted temperatures are in average a few degrees too hot, the predicted temperature trend matches the observed temperature pattern shown by GeotIS. The respective reproduced positive and negative thermal anomalies show that this temperature pattern is caused by the structural configuration of geological units and related contrasts in thermal properties. In particular, sensitivity studies have shown that considering the configuration of the crystalline crust and the Tauern Body as well as the Alpine Body is of high significance for the regional thermal field. Lateral variations in the structure and the lateral heterogeneity of thermo-physical properties of the Molasse Sediments and the Mesozoic and Triassic Sediments have only an additional influence on the temperatures at shallow depth.

The misfit between the measured and calculated temperatures in the sediments is interpreted to be caused by additional advective and convective heat transport, mechanisms not considered in this study. To test if fluid flow related cooling is as significant for the creating of the thermal anomalies as the structural configuration, coupled fluid and heat transport simulations are required. The conductive model of this study may suit as a starting point and provide lower thermal boundary conditions for the deeper, conductive dominated parts of such coupled simulations.

4. The origin of deep geothermal anomalies in the Germany Molasse Basin assessed by 3D numerical modelling of coupled fluid flow and heat transport

4.1 Abstract

The European Molasse Basin is a wedge-shaped Tertiary foreland basin at the northern front of the Alps, which is filled with mostly clastic sediments. These Molasse Sediments are underlain by Mesozoic sedimentary successions, including the Upper Jurassic aquifer (*Malm)* which has been explored since decades due to its specific structural and thermal configuration suitable for geothermal energy production. The thermal field of the Molasse Basin area is characterised by prominent positive and negative thermal anomalies of which especially the latter ones represent a high risks for geothermal energy exploration. However, the origin of these thermal anomalies could not be explained by studies in the past satisfactorily and is still an object of debates. With our study we want to contribute to the understanding of this thermal configuration and with that help to reduce the exploration risk for future geothermal projects in the Molasse Basin. Therefore, we conducted coupled fluid and heat transport simulations for the German Molasse Basin using a basin-scale model which was based on an existing lithospheric-scale 3D structural and conductive thermal model of the basin area. Using a 3D finite element method, we aimed to reproduce the present-day thermal field of the Molasse Basin assuming conduction, advection and convection as heat driving mechanisms.

This paper focuses on the thermal field of the Molasse Basin and its dependence on regional fluid flow. Within this paper we show how the temperature distribution of the Molasse Basin including the pronounced thermal anomalies can be reproduced by coupled fluid flow und heat transport simulations following a multi-scale 3D modelling approach. We find that the shallow thermal field is strongly affected by basin-wide fluid flow. Furthermore, we show that the temperature distribution at the depth of the Malm aquifer is strongly influenced by the hydraulic conductivity of the Foreland and Folded Molasse Sediments and that possible hydraulically conductive faults have only a minor influence on the regional temperature distribution in the Molasse Basin. Moreover, we show that the positive and negative thermal anomalies in the basin are caused by the superposed effects of conductive and advective heat transport and correlated to the geological structure.

4.2 Introduction

In times of decreasing hydrocarbon resources, the provision of renewable energy is a key topic for the present-day scientific and industrial community to assure the socio-economic status of the society in the future. One type of so called “green energy” is geothermal energy, whose energy source is the earth itself. This energy can be extracted from different depths of the subsurface by geothermal power

plants and used for heating or power generation depending on the extraction temperature, which in turn depends on the geological, tectonic and hydrogeological condition of a geothermal area.

One area in Europe which is suitable for the production of geothermal energy is the European Molasse Basin.

The European Molasse Basin is a Tertiary foreland basin at the northern front the Alps and extends over parts of France, Switzerland, Germany and Austria (Fig 24). The typically wedge shape of the basin (Berge and Veal 2005) evolved in consequence of the Euro-Adriatic continental collision and the rise of the Alps since the Cretaceous.

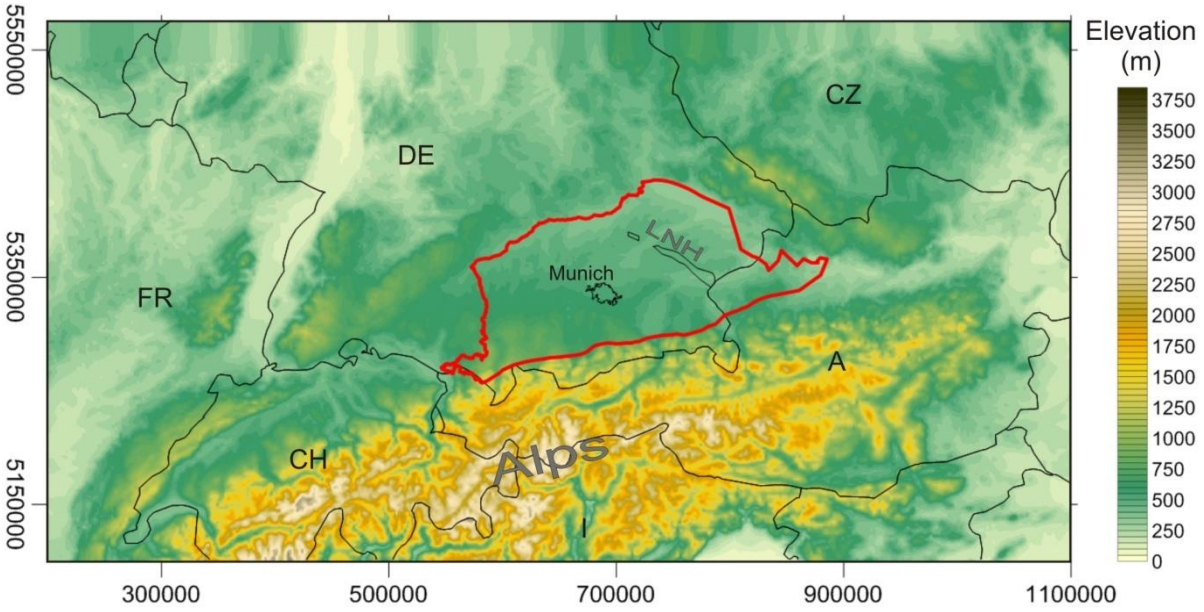

Fig 24 The model area (red frame) shown on the topography ETOPO1 (after Amante and Akins 2009). The model area of the coupled model covers the Bavarian part of the Molasse Basin and a part of the Austrian Molasse Basin.

Today the basin is filled with mostly clastic sediments originating from erosional processes of the Alps which are partly overrun and folded due to the ongoing plate movement of the Euro-Adriatic continental collision (Schmid et al. 2008). These Molasse Sediments are underlain by Mesozoic sedimentary successions, which include the Upper Jurassic Malm aquifer (Birner 2013) deposited in the Tethys Ocean. This Malm aquifer shows a high potential for geothermal energy production and is explored by the petroleum and geothermal industry as well as by the scientific community since decades (Büchi et al. 1965, Sachsenhofer et al. 2006). The exploration efforts have led to a large amount of data with which a picture of the subsurface temperature distribution of the basin could be generated by interpolation between the points of temperature measurements (GeotIS; Schulz et al. 2009, Agemar et al. 2014b). The subsurface thermal field shows increasing temperatures from north to south in the basin, as well as

prominent positive and negative thermal anomalies especially in the Bavarian part, where temperature differences of up to 60 K may occur within just a few kilometers of lateral distance (Agemar et al. 2012).

Though the knowledge about the basin has advanced in response to studies of the industry and the scientific community (Roeder and Bachmann 1996, Kempf et al. 1999, Berge and Veal 2005, Jodocy and Stober 2009, Pamer and Diepolder 2010, Böhm et al. 2011, Reischenbacher and Sachsenhofer 2011, Birner et al. 2012, Cacace et al. 2013, GeoMol Team 2015) over the last decades, the origin of this temperature pattern and the fluid flow directions in the basin are still not fully understood and a matter of debate.

Unfortunately, the distribution of data is non uniform in the Molasse Basin, leading to gaps in the pictures of the temperature and pressure field: where the extraction temperature or fluid quantity of geothermal drillings has been disappointing (Moeck et al. 2013), exploration efforts have been reduced leading to a lack of data in these areas and vice versa. To overcome such data gaps, 3D models considering structural heterogeneities are a useful tool by applying physically reliable interpolations between points of observations to fill up areas of data gaps (Cacace et al. 2010).

At present 17 major geothermal power plants are operating in the German Molasse Basin (Agemar et al. 2014a), of which the biggest part is located in the area around the city of Munich in Bavaria (Böhm et al. 2012). In this area two major thermal anomalies are located, a positive and negative one, leading to a temperature difference of up to 60 K at a depth of 3,500 m bsl (GeotIS, Agemar et al. 2012). Such strong changes in the temperature distribution over a small lateral distance represent an increased exploration risk and may reduce the willingness for further geothermal drilling projects in the Molasse Basin.

However, being aware of the complex temperature distribution at depth is not enough to reduce the exploration risk as the productivity is another key parameter for geothermal energy production. To enable a reliable temperature and pressure prediction for a geothermal reservoir, the heat transport and fluid flow mechanisms have to be understood on a bigger scale. Thereby, different types of heat transport acting in a sedimentary basin should be considered (Kaiser et al. 2011): (1) conductive heat transport, where the efficiency of heat transfer depends on the thermal conductivity of the lithology of the respective layer, (2) advective heat transport, where heat is transported passively by pressure driven fluid flow, (3) convective heat transport, where heat is transported by density driven convective fluid flow. In a fluid influenced geothermal environment, like the Molasse Basin, a combination of all three heat driving mechanisms can be expected, as has been already shown for other sedimentary basins, e.g. for the North German Basin by Kaiser et al. (2011) and Noack et al. (2013) and for the Po Plain by Pasquale et al. (2013).

Different studies have been conducted so far, based on different physical assumptions and modelling techniques, to understand the temperature and pressure field of the European Molasse Basin, of which Frisch and Huber (2000), Rühaak (2009, 2015), Rühaak et al. (2010), Agemar et al. (2012), Birner (2013) and Przybycin et al. (2015b) are just some examples.

Frisch and Huber (2000) investigated the flow field of the Upper Jurassic Malm aquifer in the German part of the basin using measurements of hydraulic potential and thermal water balancing to deduce the general flow direction. They propose a main fluid flow direction from west to east inside the Malm aquifer with a significant flattening of the hydraulic potential in the central basin area as well as discharging fluids into parts of the Danube river and in the east of the uplifted crust of the Landshut-Neuöttinger High (LNH). However, they could not explain the fluid flow pattern between the city of Munich and the LNH in the Malm aquifer.

Such a fluid flow direction could be mainly confirmed by Birner (2013), who investigated the hydrochemistry and hydraulic regime of the German Molasse Basin with a hydrogeological model of the Upper Jurassic Malm aquifer with the intention to characterize the processes driving the groundwater dynamic and the mass transport. He states that, even though the Malm aquifer shows a complex system of pores, joints and karst related cavities, it can be described with lithological units of different but homogenous hydraulical characteristics on a basin-scale.

The work of Birner (2013) has been incorporated into the Geothermal Information System (GeotIS, Schulz et al. 2009), a web-based platform integrating all available data about geological structure, lithology and temperature from outcrops, wells and seismic data for areas of geothermal interest in Germany with the intention to reduce the exploration risk for geothermal drilling projects. Based on 3D interpolation between temperature measurements, maps have been generated, available at the GeotIS platform (Agemar et al. 2012), depicting the temperature distribution at different depths in the Molasse Basin. Unfortunately, the lateral coverage and reliability of these maps is decreasing with increasing depth due to the decreasing data density and with that increasing uncertainty of interpolation. Nonetheless, the thermal model of GeotIS (Schulz et al. 2009, Agemar et al. 2012) is so far the best representation of the thermal field of the Molasse Basin according to the implemented data and has therefore been used as a reference for validation in our study.

A different approach to explain the thermal anomalies in the Molasse Basin has been used by Rühaak (2009) and Rühaak et al. (2010). They investigated the groundwater flow regime and the thermal field of the western part of the Molasse Basin using a quasi-steady-state conductive 3D modelling approach on a local-scale with the intention to compare calculated temperatures to measured values. Since they were not able to reproduce the observed thermal anomalies in the western Molasse Basin with a purely conductive approach of heat transport, they proposed E-W striking fault parallel fluid flow to cause lateral temperature differences of more than 10 K at the same depth in the basin.

Such influence of hydraulically conductive major fault zones on the thermal field has also been studied by Cherubini et al. (2014) for the area of Brandenburg in north-eastern Germany using a basin-scale 3D numerical model of coupled fluid flow and heat transport. Their results however indicate only a limited lateral influence of permeable fault zones on the regional thermal field.

Another conductive heat transport approach was followed by Przybycin et al. (2015b), who used a lithospheric-scale 3D model covering the German Molasse Basin as well as the South German Scarpland to the north and parts of the Alps including the Tauern Body in the south (Przybycin et al. 2015a) to calculate the present-day 3D conductive thermal field. By choosing a model extent which integrates a large part of the continental collision zone, Przybycin et al. (2015b) investigated the interdependence of the basin with the mountain chain with respect to the thermal field. With their approach they were able to reproduce the measured thermal field of the Molasse Basin as shown by GeotIS (Agemar et al. 2012) to a certain extent. The conductive model of Przybycin et al. (2015b) reproduces the positive and negative thermal anomalies southeast of Munich, but the predicted temperature of the negative thermal anomaly is still too high compared to the measured temperatures (GeotIS, Agemar et al. 2012). However, the conductively modelled temperature trend shows that the thermal anomalies in the Molasse Basin are generated to some extent by the structural configuration of the crust and the presence of the Tauern Body in the Alps. Przybycin et al. (2015b) propose an additional cooling influence of fluid flow in the sedimentary part of the basin as possible mechanism to explain the observed lower temperatures in the Molasse Basin, an effect already discussed for the Po Plain by Pasquale et al. (2013).

Nevertheless, a systematic assessment how far fluid flow, geological and hydrogeological heterogeneity or the presence of permeable faults may control the deep thermal field on a basin-scale in the Molasse Basin is still lacking.

To improve the understanding of the regional thermal field and the temperature controlling mechanisms in the Molasse Basin and with that decrease the exploration risk of geothermal energy projects we have conducted a systematic parameter study by simulating the coupled fluid flow and heat transport in the Bavarian part of the Molasse Basin between the Danube in the north and the Alpine front in the south using a three-dimensional basin-scale numerical FE-model.

Thereby, we followed a modelling approach whose advantages have already been demonstrated for different sedimentary basins in the past, e.g. for the North German Basin by Noack et al. (2014) and Scheck-Wenderoth et al. (2014). In this approach, a lithospheric-scale regional 3D structural model is used to calculate the present-day conductive thermal field. From this lithospheric-scale conductive model, temperatures are extracted from depths dominated by conductive heat transport (e.g. the crust)as lower thermal boundary condition for a higher resolved basin-scale model of the basin fill that considers

coupled transport of heat and fluid. Following this workflow, the obstacle of choosing a proper lower thermal boundary condition for the simulation of coupled fluid flow and heat transport on a basin-scale can be overcome. The resulting thermal and flow field may help to understand the relation between basin-scale fluid dynamics and temperature distribution. Moreover, these results from basin-scale simulations can be exploited to provide physically reliable thermal and hydraulical boundary conditions for local high-resolution reservoir-scale models as required for areas of exploitation interest. To investigate the possible influence of hydraulically conductive faults on the thermal field we have integrated three large hydraulically conductive testfaults into the model representing the main strike direction of faults in the Molasse Basin in a second modelling step.

4.3 The hydrogeological model

For the simulation of coupled fluid flow and heat transport, a basin-scale 3D structural model has been build based on the lithospheric-scale 3D structural model of Przybycin et al. (2015a). The latter integrates freely available depth and thickness information from wells and seismic lines and has been additionally constrained by 3D gravity modelling. For this study, the upper part of the lithosphere-scale model has been used. In addition, the vertical resolution of lithostratigraphical units has been increased compared to Przybycin et al. (2015a) for the basin-scale model by additionally distinguishing the Purbeck formation (Lower Cretaceous) from the Cretaceous layer according to StMWIT (2010) and the different Malm layers (Zeta - Alpha, Schulz and Thomas 2012). The base of the structural model was defined at a constant depth of 7,500 m bsl, a depth at and below which conduction is the dominant mechanism of heat transport. This basin-scale 3D structural model covers an area of 180 km in N-S direction and 340 km in E-W direction with a horizontal resolution of ~1 x ~1.7 km corresponding to 185 x 201 grid points. In the vertical direction the structural model contains 12 lithostratigraphic units from the topography downwards (Fig 25):

At the southern border of the model, the Folded Molasse Sediments occur in a thin band along the mountain chain. Due to the tectonical imprint of the moving Alps these sediments are strongly folded and steeply erected. They consist of conglomerate and sand as well as silt and clay with a moderate average permeability (Fig 25a, Tab 5). They show apparent thicknesses of up to 7,000 m directly in front of the Alps and represent therefore a possible pathway for fluid flow from the surface into larger depths.

The northwards following Foreland Molasse Sediments (Fig 25b) consist of mostly unconsolidated conglomerate and sand with intercalated silt and clay layers originating from erosional processes of the Alps (Handy et al. 2010, Bousquet et al. 2012b). These Molasse Sediments are considered as highly permeable for fluid flow (Tab 5) and show increasing thicknesses from 0 m in the north to up to 5,000 m in the south at the Alpine front.

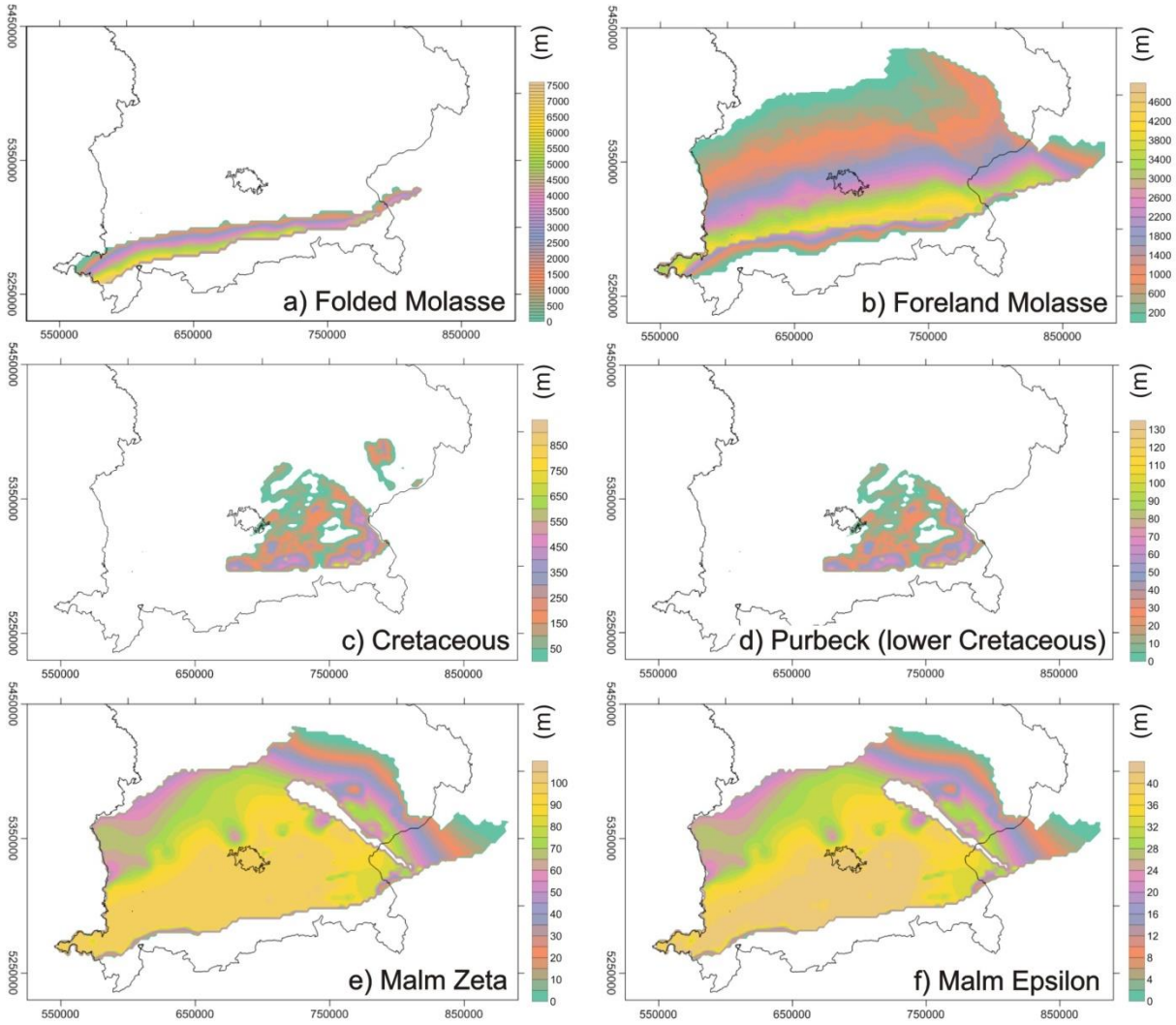

Fig 25 Thickness maps of lithostratigraphic units implemented into the coupled model. The main structure has been extracted from the 3D lithospheric-scale structural model of Przybycin et al. (2015a). In addition, the vertical resolution of the Cretaceous and the Upper Jurassic Malm aquifer has been increased by distinguishing the Purbeck formation (Lower Cretaceous) from the Upper and Middle Cretaceous and the single Malm layers (Alpha-Zeta) following StMWIT (2010), Schulz and Thomas (2012) and Birner et al. (2009).

Below the Molasse Sediments the Cretaceous (Fig 25c) consists mostly of claystone and limestone and is only preserved in a limited area between the city of Munich and the Landshut-Neuöttinger High with thicknesses of up to 850 m and in a small area east of the Landshut-Neuöttinger High with up to 150 m thickness. This unit has an average hydraulic conductivity even higher than the Molasse Sediments (Tab 5).

According to deviating hydraulic properties (higher porosity, but lower hydraulic conductivity) and a different lithology (mainly limestone) compared to the (Upper and Middle) Cretaceous, the Purbeck formation (Lower Cretaceous, Fig 25d) resembles more the Upper Jurassic and has therefore been implemented as a separate unit in the hydrogeological model.

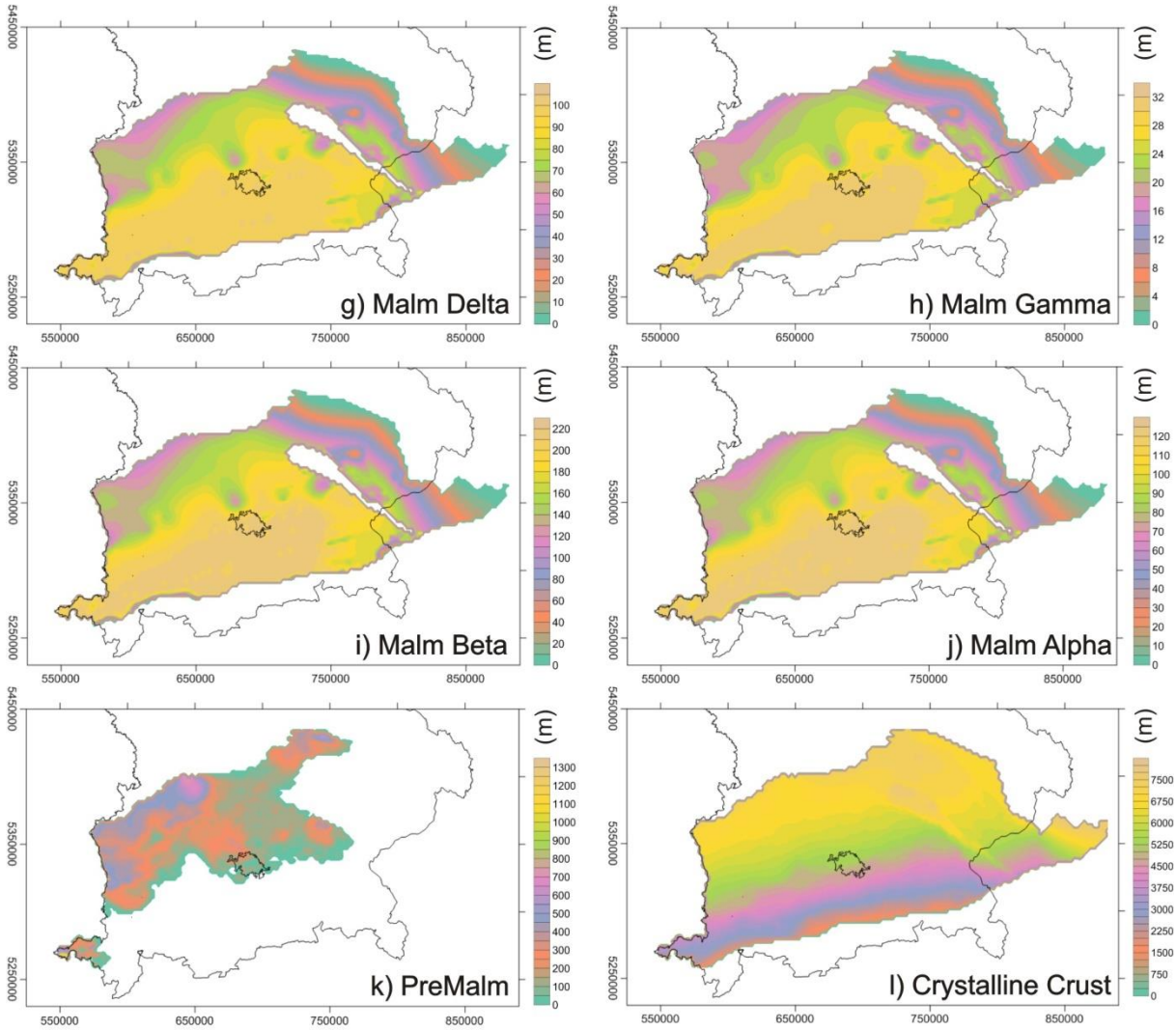

Fig 25 continued

Like the Cretaceous, the Purbeck formation is preserved in a small area between the city of Munich and the Landshut-Neuöttinger High but with smaller thicknesses of 10 - 40 m.

The Upper Jurassic Malm aquifer consists of mostly limestone and dolomite with small appearance of clay and has been separated into 6 single layers (overlying Zeta – underlying Alpha, Fig 25e - j) according to the composition and average permeability (Birner et al. 2009, StMWIT 2010, Schulz and Thomas 2012). While the lower two Malm layers (Alpha and Beta) have been regarded as impervious, the upper four Malm layers (Zeta –Gamma) have been considered as a continuous aquifer with a laterally varying hydraulic conductivity.

Tab 5 The thermal and hydraulic properties prescribed to the layers of the numerical model.

References: 1) Schulz and Thomas 2012, 2) Koch et al. 2009, 3) Homuth et al. 2014, 4) StMWIT 2010, 5) Birner 2013, 6) Birner et al. 2009, 7) Noack et al. 2013, 8) Freudenberger and Schwerd 1996, 9) Scheck 1997, 10) Cherubini et at. 2014. The terms *Massen*, *Schicht* and *Helvetic* describe different facies of the Upper Jurassic Malm aquifer accorind to StMVIT (2010).

Layer		dominant Lithology	Ref	Porosity [-]	Ref	Hydraulic Conductivity [m/s]	Ref	Heat Capacity [MJ/(kgK)]	Ref	Heat Conductivity [W/(mK)]	Ref	Heat Production [W/cbm]	Ref
1-6	FoldedMolasse	conglomerate, sand, silt, clay	8	0,029	1	2,00E-08	4	2,5	1	2,1	2	1,45E-06	1
7-13	ForelandMolasse	conglomerate, sand, silt, clay	8	0,029	1	2,00E-07	4	2,5	1	2,12	2	1,45E-06	1
14	Cretaceous	claystone, limestone	8	0,0286	1	5,00E-05	4	2,5	1	2,8	1	1,50E-06	1
15	Purbeck	limestone, claystone	8	0,06	2	1,00E-06	1	2,3	1	2,7	1	1,50E-06	1
16	MalmZeta (Massen)	limestone, dolomite	8	0,075	2	variable	5	2,3	1	2,6	3	1,50E-06	1
	MalmZeta (Schicht)	limestone, dolomite	8	0,035	3	variable	5	2,3	1	2,6	3	1,50E-06	1
17	MalmEpsilon (Massen)	limestone, dolomite	8	0,075	2	variable	5	2,3	1	2,6	3	1,50E-06	1
	MalmEpsilon (Schicht)	limestone, dolomite	8	0,035	3	variable	5	2,3	1	2,6	3	1,50E-06	1
18	MalmDelta (Massen)	limestone, dolomite	8	0,075	2	variable	5	2,3	1	2,6	3	1,50E-06	1
	MalmDelta (Schicht)	limestone, dolomite	8	0,035	3	variable	5	2,3	1	2,6	3	1,50E-06	1
19	MalmGamma (Massen)	limestone, dolomite	8	0,051	1	variable	5	2,3	1	2,22	1	1,50E-06	1
	MalmGamma (Schicht)	limestone, dolomite	8	0,035	3	variable	5	2,3	1	2,22	1	1,50E-06	1
20	MalmBeta (Massen)	limestone, dolomite	8	0,051	1	1,00E-09	6	2,3	1	2,22	1	1,55E-06	1
	MalmBeta (Schicht)	limestone, dolomite	8	0,035	3	1,00E-09	6	2,3	1	2,22	1	1,55E-06	1
21	MalmAlpha (Massen)	limestone, dolomite , claystone	8	0,051	1	1,00E-09	6	2,3	1	2,22	1	1,55E-06	1
	MalmAlpha (Schicht)	limestone, dolomite, claystone	8	0,035	3	1,00E-09	6	2,3	1	1,9	3	1,55E-06	1
	Helvetic	limestone, dolomite, claystone	8	0,035	3	1,00E-09	1	2,3	1	1,9	3	1,55E-06	1
22-23	PreMalm	claystone, sandstone, marl	8	0,051	1	5,00E-06	4	2,3	1	2,2	1	1,55E-06	1
24-26	crystalline crust	granite/ granodiorit	9	1,00E-09	9	1,00E-21	4	3,2	1	3,1	1	1,50E-06	7

Faults	0,2	10; 1	5,00E-05	10; 1	2,56	10; 1	2,6	10; 1

For this aquifer the hydraulic conductivity has been prescribed according to the degree of dolomitisation, karstification and different hydraulic properties determined by Birner (2013, Fig 26) based on well data. A high hydraulic conductivity was prescribed to the Malm aquifer in the central northern and the most eastern part, with 10^{-4} m/s. Towards the south, the aquifer has been characterised by average hydraulic conductivities (10^{-6} m/s). To the west, lowest hydraulic conductivities are prescribed to the Malm aquifer with 10^{-9} m/s. The underlying layers Malm Beta and Malm Alpha have been characterised as low-conductive with hydraulic conductivities of 10^{-9} m/s according to Birner et al. (2009).

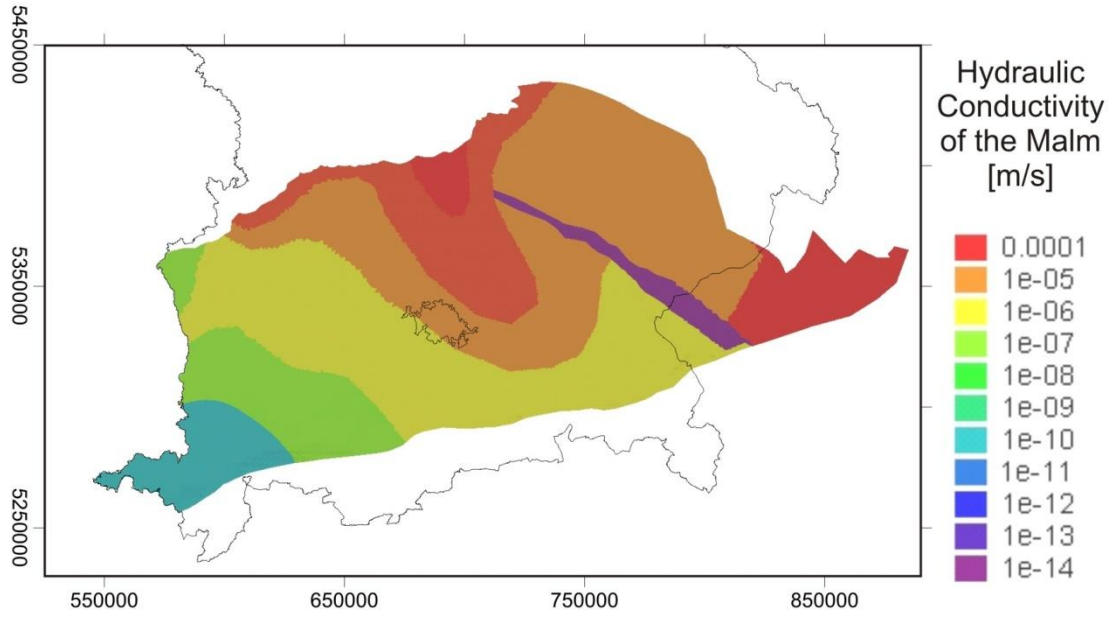

Fig 26 The hydraulic conductivity of the Malm Gamma-Zeta following Birner (2013) implemented into the 3D numerical model. As shown in the map the hydraulic conductivity is highest in the northern and eastern part of the model and decreases to the south and west. In the area of the Landhut Neuöttinger High, where the Malm is eroded, lowerst hydraulic conductivities are prescribed.

All Malm layers show increasing thicknesses from north to south with a maximum in the central model area and are eroded around the uplifted crust of the Landshut-Neuöttinger High. In particular, Malm Zeta (Fig 25e) shows maximum thicknesses of up to 100 m, whereby Malm Epsilon (Fig 25f) shows thicknesses of up to 40 m in the central model area. Lower, Malm Delta (Fig 25g) is thicker with up to 100 m in the central basin, and is, in turn, followed by a much thinner Malm Gamma (Fig 25h) with thicknesses of up to 32 m. The two lowermost Malm layers show maximum thicknesses of up to 220 m (Malm Beta, Fig 25i) and 120 m (Malm Zeta, Fig 25j) in the central part of the basin, respectively.

Below the Upper Jurassic Malm, the PreMalm layer (Fig 25k) is summarizes all sediments of the Middle and Lower Jurassic as well as Triassic and is assumed to consist of mostly claystone, sandstone and marl. This layer is restricted to the model area north and northwest of the city of Munich and is characterised by an average thickness of 200 - 500 m with locally higher thickness values.

The lowermost layer of the model is represented by the crystalline crust, which is assumed to be impermeable for fluid (Fig 25l, Tab 5). In response to the constant depth of the model of 7,500 m bsl at the model base, the thickness of this layer decreases from north to south with a maximum thickness of up to 7,500 m directly at the northern border and less than 500 m at the southern border of the model.

4.4 The numerical approach

The simulations of the coupled fluid flow and heat transport have been carried out using the commercial software package FELOW® (Version 6.2, Diersch 2009), which is based on a finite element method (FEM) and allows the consideration of different processes of heat transport in natural porous media, as conductive, advective and convective heat transport.

For the case of conductive heat transport, kinetic energy is transported along a geothermal gradient through the earth by molecule collision (Turcotte and Schubert 2014). The efficiency of conductive heat transfer is thereby only dependent on the thermal conductivity of the medium.

Both, the advective as well as the convective heat transport are related to fluid flow. While heat is transported passively by fluid flow along a hydraulic gradient in case of advection, convective heat transport occurs due to differences in fluid temperature and with that density and is a form of buoyant flow (Bjørlykke 2010). A combination of all heat driving mechanism is called mixed convection. The coupled calculation of the flow and temperature field in a saturated porous media with FEFLOW® is done solving three partial differential equations based on Darcy´s law, on mass conservation as well as on energy conservation (e.g. Nield and Bejan 2006) which are described in the following part.

Governing Equations

Here, the governing equations solved for the calculation of the coupled fluid and heat transport as given by Diersch (2009) are briefly summarized.

The generalized Darcy law (Eq 10) and the mass conservation of the fluid (Eq 11) are solved as a system of flow equations with variable fluid density ρ^f and viscosity μ^f.

Since FEFLOW® uses the hydraulic head as primary variable in the mathematical formulation, the Darcy law (Eq 10) is written in terms of hydraulic head rather than pressure:

$$q^f = -\boldsymbol{K}\left(\nabla h + \frac{\rho^f - \rho_0^f}{\rho_0^f}\frac{g}{|g|}\right)$$ (Eq 10, Darcy Law)

$$\frac{\partial(\varepsilon\rho^f)}{\partial t} + \nabla\cdot\left(\rho^f q^f\right) = \varepsilon Q_\rho$$ (Eq 11, Mass Conservation)

Thereby, q^f stands for the specific discharge (Darcy velocity) and $\boldsymbol{K}$ for the hydraulic conductivity tensor of the porous media; g describes the gravity acceleration and ρ^f the mass density of the fluid.

Further, $\boldsymbol{K}$ can be described with $\boldsymbol{K} = \frac{\rho_0^f g}{\mu^f}\boldsymbol{k}$ with $\boldsymbol{k}$ as the permeability tensor and μ^f as the fluid viscosity. In Eq 11, ε is defined as the porosity and Q_ρ as the sink-source term for mass.

Applying the law of energy conservation under the condition of thermal equilibrium between the fluid and the porous medium ($Tf = T = Ts$) and neglecting density gradients, the following heat transport equations are solved:

$$(\rho c)_{fs}\frac{\partial T}{\partial t} + \rho^f c^f \nabla\cdot\left(q^f T\right) - \nabla\cdot(\lambda\nabla\mathrm{T}) = \mathrm{Q_T}$$ (Eq 12, Energy Conservation)

$\mathrm{Q_T}$ is the heat source-sink function with λ as the equivalent thermal conductivity tensor of the fluid and the porous medium.

$(\rho c)_{fs}$ is defined as the bulk specific heat capacity of the fluid (f) and solid (s) phase system, whereby the phase system is defined as

$$(\rho c)_{fs} = \left[\varepsilon\rho^f c^f + (1-\varepsilon)\rho^s c^s\right]$$ (Eq 13)

Since taking into account the conductive (Fourier) and thermodispersive (mixing) effects, the thermal conductivity tensor of the fluid and the porous medium λ can be subdivided into two separate components:

$$\lambda = \lambda_{DISP} + \lambda_{COND} \quad \text{(Eq 14)}$$

where λ_{DISP} is the thermodispersive term and λ_{COND} the conductive term with a_L and a_T as the longitudinal and transversal dispersion length, respectively. λ^f and λ^s represent the thermal conductivity of the fluid and solid phase with I as the unit matrix in Eq 15 and 16:

$$\lambda_{DISP} = \rho^f c^f \left[a_T \sqrt{\left(q_i^f q_i^f\right)}\, \mathbf{I} + (a_L - a_T) \frac{q_i^f q_i^f}{\sqrt{\left(q_i^f q_i^f\right)}} \right] \quad \text{(Eq 15)}$$

$$\lambda_{COND} = \varepsilon \lambda^f + (I - \varepsilon)\lambda^s \quad \text{(Eq 16)}$$

The coupling of heat transport and fluid flow via the density of the fluid was done according to an equation of state using the *brine-density ifm* of Magri et al. (2009).

The FE model

To transform the geological model into a numerical one for the software FEFLOW®, all geological layers have been converted into continuous layers and discretized as a three dimensional finite element mesh with irregular triangular elements horizontally and prismatic elements vertically. While the horizontal resolution was defined as 600 m in average, the vertical resolution depends on the thickness of the lithostratigraphic units. To avoid a high aspect ratio (horizontal : vertical resolution), layers with large thicknesses, as the Folded Molasse Sediments, the Foreland Molasse Sediments and the crystalline crust, have been subdivided into sublayers with maximum thicknesses of 1.5 km resulting all in all in 26 numerical layers. The resolution of the horizontal discretization was closely connected to the facies distribution of the Upper Jurassic Malm aquifer, as given by StMWIT (2010) in the Geothermal Atlas of Bavaria: In areas where no or little fluid flow is expected due to a low permeability of the Malm aquifer a courser discretization (element size up to 1,000 m) has been chosen than in areas of high permeability. As for the latter central model area, where more vigorous fluid flow is expected, smaller mesh elements had been implemented to assure numerical stability (element size down to ~400 m).

To assess the influence of fluid flow along permeable fault zones on the thermal field in the basin (Fig 27) three faults have been integrated into the numerical model as discrete feature elements - finite elements with lower dimensionality inserted at element faces and edges (Diersch 2009). For those vertical 2D elements a horizontal buffer zone of 40 m on both sides of the faults has been implemented

to which a higher horizontal resolution of up to 20 m was set to assure stable calculation during simulations. For these domains (faults and buffer zones) fluid flow according to Darcy´s law was assumed.

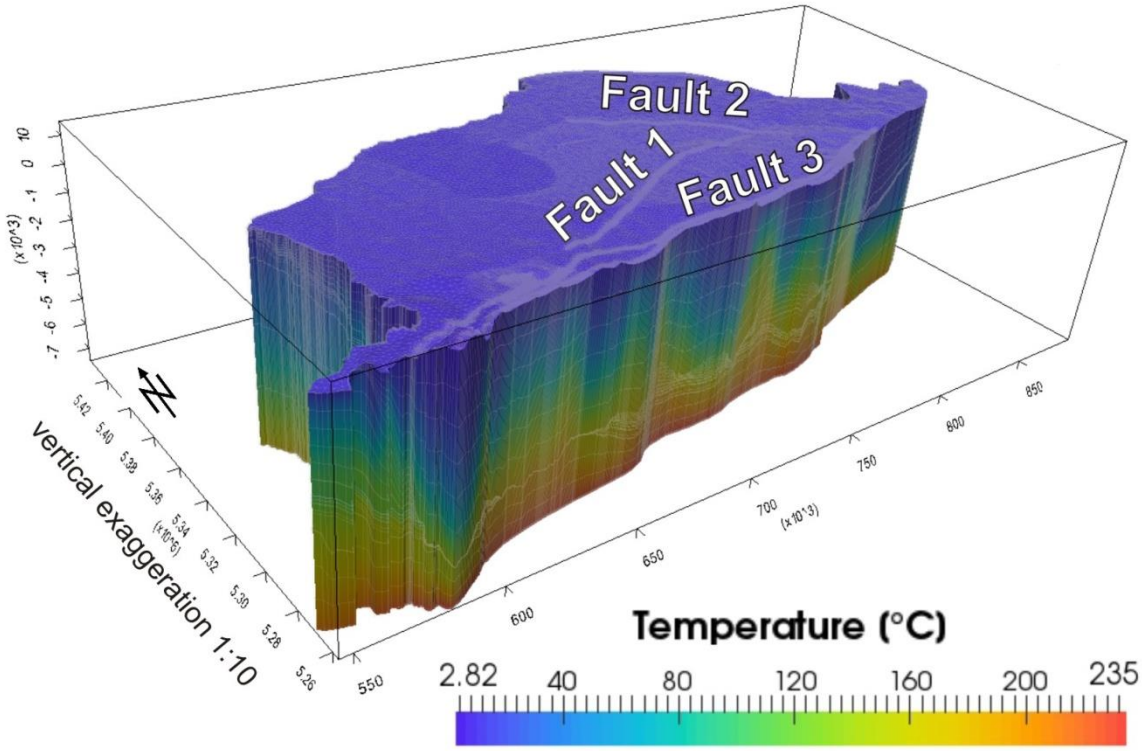

Fig 27 The 3D numerical model used for the coupled simulations of fluid flow and heat transport. The different horizontal mesh resolution was chosen according to the facies distribution of the Malm aquifer (StMWIT 2010). The color-coding shows the resulting thermal field in the model area. The faults (1, 2 and 3) have been implemented as discrete features and can be seen as areas with higher vertical resolution.

These faults are simplified representations of known fault zones in the Molasse Basin and are oriented in the main fault direction, respectively. Fault 1 has been integrated south of the city of Munich to represent the east-west oriented fault system in the Malm aquifer (StMWIT 2010). It can be traced vertically from the middle of the Foreland Molasse Sediments down to Malm Epsilon. It represents a normal fault created due to the flexural bending of the European plate in response to the load exerted by the Alps. Fault 2 has been integrated at the southern border of the model representing the east-west oriented fault system along the Alpine front in the Folded Molasse Sediments as the tectonical boundary between the Molasse Basin and the Alps. This fault can be traced from the topography down to the top of the crystalline crust (Schmid et al. 2008). Fault 3 has been integrated at the western side of the Landshut-Neuöttinger-High and represents a possible flow pathway along the tectonic border between the Malm and the uplifted crust of the Landshut-Neuöttinger-High.

The influence of each permeable fault on the fluid flow and the temperature field has been investigated separately at first. In a second step all faults were included simultaneously as permeable to investigate a possible interdependence.

All in all, the numerical model including the three faults consists of 2,432,560 prismatic mesh elements and 1,283,391 mesh nodes subdivided into 26 layers and 27 slices and three vertical faults (Fig 27).

To achieve quasi-steady-state conditions in the numerical simulations and with that predict the present-day thermal and flow field, a simulation time of 100,000 years was chosen with an automatic time step control with a limited maximum time step size of 50,000 days and a first-order accurate predictor-corrector-scheme. For the iterative calculations we chose the SAMG solver for the symmetric matrix and the BICGSTABP solver for the unsymmetric matrix as well as full upwinding for the model stabilization.

Parametrisation

For the simulations all layers have been characterised by thermal (heat capacity, thermal conductivity, radiogenic heat production), mechanical (porosity) as well as hydraulical properties (hydraulic conductivity) according to their dominant lithology (Tab 5). Measured values have been favoured. However, is case no measured values were available, average lithology-based values have been assigned. Every layer has been assigned with one uniform value for each property apart from the Upper Jurassic Malm aquifer. For the upper four layers of the Malm (Gamma - Zeta) a variable hydraulic conductivity was adopted following Birner (2013, Fig 26). Accordingly, high hydraulic conductivities prevail in the northern and eastern-most model parts, and decreasing hydraulic conductivities towards the south and west. Malm Alpha and Beta have been considered as homogeneously low-conductive.

Like the layers, all faults have been characterised with hydraulic properties following Schulz and Thomas (2012) and Cherubini et al. (2014). Thereby a hydraulic conductivity much higher than of any other layer of the model was assumed for the faults to open permeable fluid flow paths along the latter.

Detailed sensitivity analyses have been carried out to assess the level of influence of all assigned physical properties.

Boundary Conditions and Initial Conditions

To solve the partial differential equations thermal as well as hydraulic upper and lower boundary conditions are required. The thermal boundary conditions at the base and the top of the model have been defined as fixed temperatures (Dirichlet). At the surface a mean variable surface temperature measured over 30 years (1960 – 1990) in the area of interest (DWD 2013, Fig 28) has been prescribed as upper

thermal boundary condition. Thereby, the surface temperature ranges between -2°C in the south-western corner and +12°C in the northern most and eastern part of the model area.

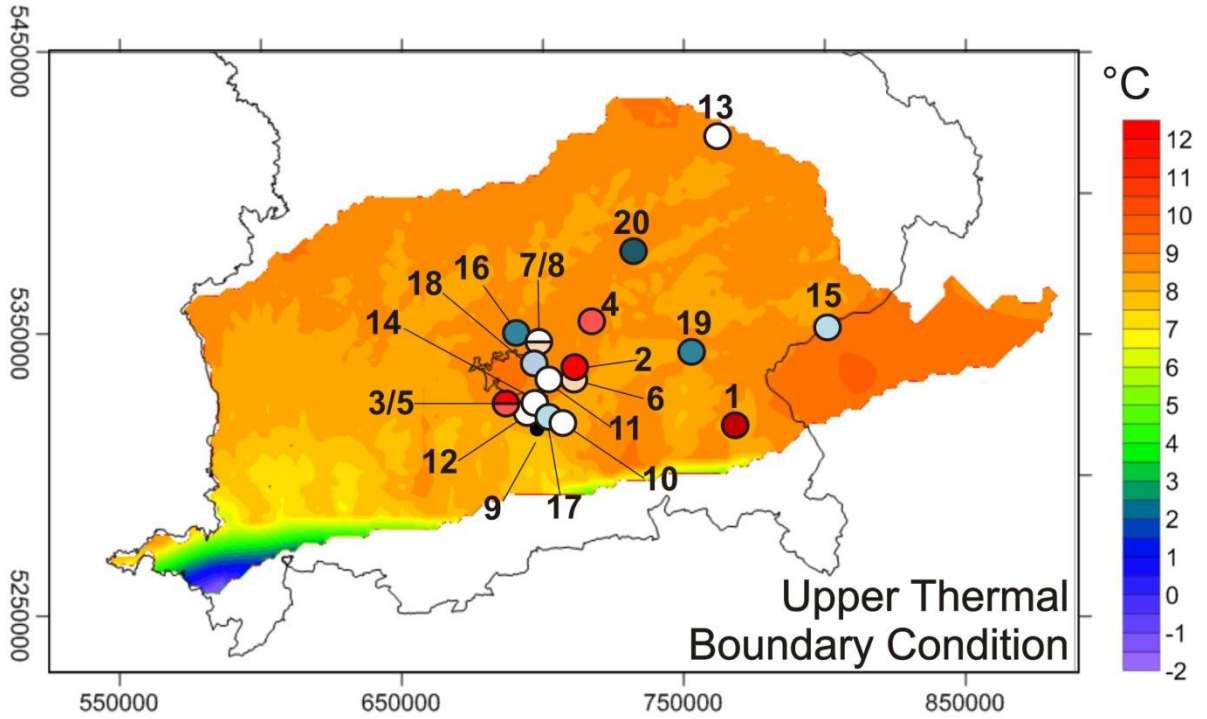

Fig 28 The upper thermal boundary condition implemented into the numerical model. The map shows a variable mean annual surface temperature over the last 30 years (DWD 2013) and was assigned as Dirichlet boundary condition to the topography. 20 locations of geothermal energy production sites are shown for which observed temperatures are available. To these observations our predicted temperatures have been compared. The color-coding of the locations is corresponding to the temperature difference between calculated and measured values given in table 6. A red colour coding means temperatures are predicted too warm by the model, blue colour coding means predicted temperatures are too cold compared to the observed ones.

A laterally variable temperature distribution, which has been extracted from a 3D lithospheric-scale conductive thermal model of the Molasse Basin and the adjoining Alps (Przybycin et al. 2015b) has also been implemented as lower thermal boundary condition. The latter considers the influence of a varying depth of the thermal Lithosphere-Asthenosphere Boundary, a heterogeneous internal structure of the crystalline crust as well as variations in thermal properties in response to the geological structure. Accordingly, the interdependence between the Alps, the Tauern Body and the Molasse Basin with respect to the basin-wide thermal field is captured by the 3D lithospheric-scale conductive model from which the temperature distribution at 7,500 m bsl has been extracted.

Hence, lower temperature values in the north (~150°C) and higher temperature values in the south (~240°C, Fig 29) are prescribed at the base as lower thermal boundary condition for the coupled model.

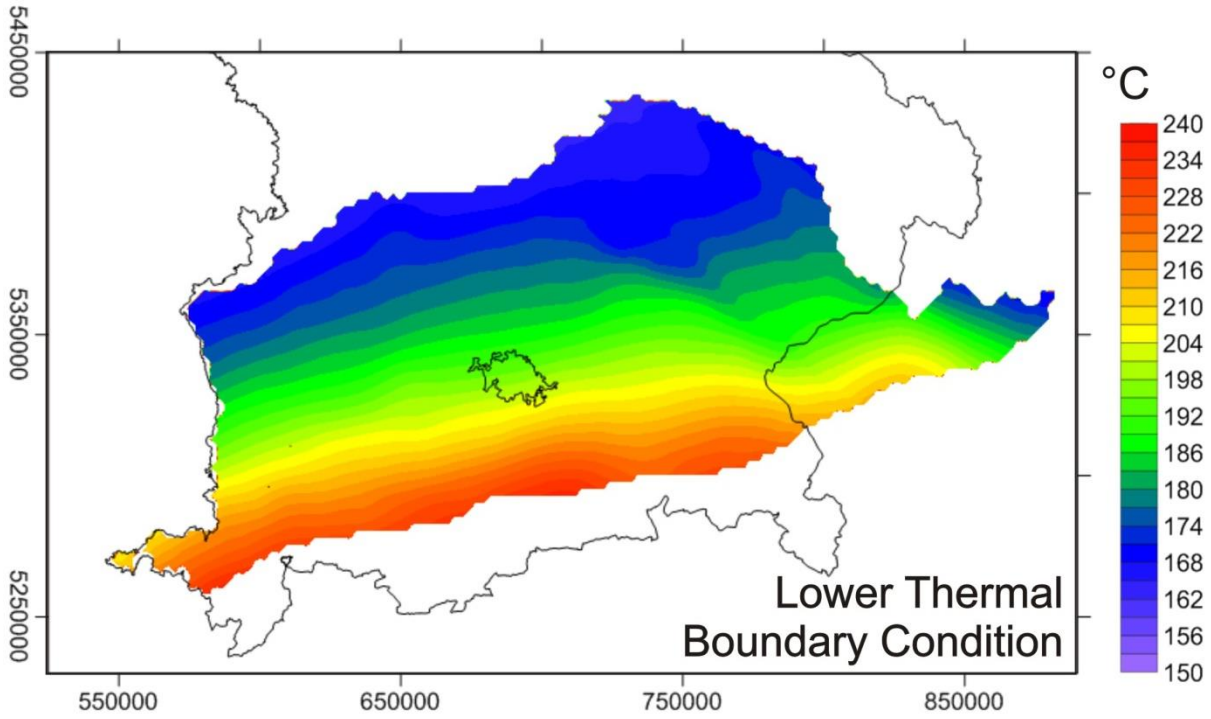

Fig 29 Temperatures distribution at a depth of 7,500 m bsl which has been extracted from the 3D lithospheric-scale conductive thermal model of Przybycin et al. (2015b) and prescribed as lower thermal boundary condition (Dirichlet) to the base slice of the coupled model.

As upper boundary conditions for fluid flow a constant pressure head (0 Pa, Dirichlet) was assigned to the topography (Fig 24). Further, fixed hydraulic heads (Dirichlet) were assigned to the river Danube and to the lateral borders of the Malm aquifer in the east and west according to Frisch and Huber (2000).

Furthermore, thermal and pressure initial conditions have been calculated with uncoupled fluid and heat transport simulations for steady-state conditions.

4.5 Results and Interpretation

In the following chapter the resulting thermal field of the Molasse Basin predicted by the coupled fluid and heart transport simulations is presented with temperature maps at different depths and prominent thermal effects are highlighted. At first, the results of model 1 without considering faults are presented and compared to an alternative version of the model obtained during the sensitivity study (model 2). Afterwards, the results of the simulations considering hydraulically conductive faults (model 3) are presented.

The basin-scale thermal field (model 1)

Figure 30 shows the temperature distribution predicted by model 1 (without faults) at depths for which temperature maps from GeotIS (Schulz et al. 2009, StMWIT 2010) are available for validation. Compared to the maps of GeotIS (StMWIT 2010), the maps produced in this study show temperature variations changing at a much smaller wavelength at all depths. This effect is related to the assumption of a homogeneous space in GeotIS whereas this study considered heterogeneities related to geological structures. Also, the grid resolution is far higher in this study compared to the GeotIS interpolation grid of measured data (Schulz et al. 2009).

At a depth of **500 m bsl** (Fig 30a) temperatures between 8 and 35°C are predicted for most parts of the model area with the coolest values in the area of the Folded Molasse Sediments. In addition, some positive thermal anomalies of smaller lateral extent with temperatures of up 63°C are present at the southern border of the model area, in the western part of the model, at the eastern border of Bavaria as well as in the area of the city of Munich. Of those the latter one shows the highest temperatures at this depth. A comparable distribution of temperatures and thermal anomalies is shown in the temperature map of GeotIS (StMWIT 2010).

At a depth of **1,500 m bsl** (Fig 30b) modelled temperatures range between 10 and 90°C, though most parts of the model area are not warmer than 50°C. The lowest temperatures are bound to the negative thermal anomalies at the southern border of the model area (~10°C) and to the negative thermal anomaly predicted in the southeast of Munich (up to 15°C). The highest temperature values are limited to the positive thermal anomalies, which, compared to the 500 m depth bsl, increased in size and temperatures. At 1,500 m bsl three positive thermal anomalies are visible in the western part of the model, one big and two smaller anomalies, with highest temperatures of up to 90°C. For the positive thermal anomaly in the area of Munich temperatures of up to 75°C are predicted by the model, which again is comparable to the temperature distribution shown by GeotIS (StMWIT 2010). Further, some smaller positive thermal anomalies are predicted in between the negative thermal anomalies at the southern model border with temperatures between 50 and 70°C. The positive thermal anomaly at the eastern border of Bavaria shows temperatures of ~60°C.

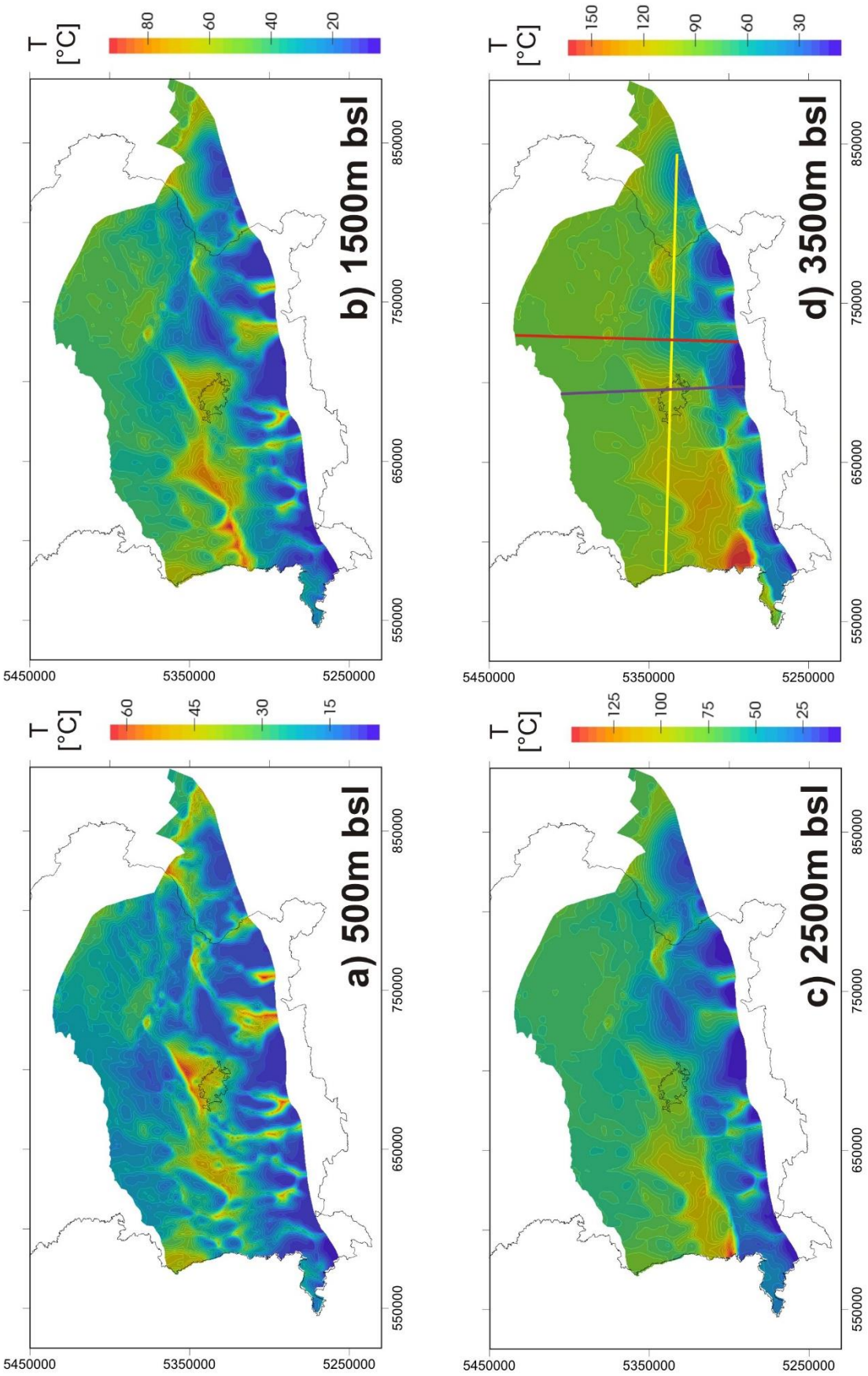
a) 500m bsl
b) 1500m bsl
c) 2500m bsl
d) 3500m bsl
T [°C]
5450000
5350000
5250000
550000
650000
750000
850000

◀**Fig 30** Predicted temperatures by the coupled fluid flow and heat transport simulations without considering faults in the system (model 1) shown with temperature maps at different depths. The model predicts widespread negative thermal anomalies (blue colours) at shallower depths within the whole basin. These negative thermal anomalies decrease with increasing depth in most parts of the basin area. Only the negative thermal anomalies in the area of the Folded Molasse Sediments, directly at the border to the Alps, are predicted even in bigger depths. These cold anomalies are caused by an inflow of cold water into depths through the hydraulically (too high?) conductive Folded Molasse Sediments. The small positive thermal anomalies (reddish colours) from shallower depths increase in size with increasing depth.
At all depths the predicted temperatures show a pronounced negative thermal anomaly in the southeast of Munich bounded by two positive thermal anomalies to the west and east. Even though the predicted temperatures are slightly lower than the observed ones, the observed temperature trend could be reproduced with the coupled fluid flow and heat transport simulations without any consideration of faults. Map d) shows the locations of the profiles shown in figure 32.

At **2,500 m bsl** (Fig 30c) the coupled simulations predict temperatures between 15 and 140°C. At this depth the northern model area shows mean temperature values of ~75°C, while the southern model area shows lowest temperature values of 15°C within the negative thermal anomalies in the Foreland Molasse Sediments. Compared to shallower levels these negative thermal anomalies have increased in size as has the negative thermal anomaly southeast of Munich, which shows a temperature of ~25°C. Likewise, the positive thermal anomalies are larger in size than at shallower levels. While at the depth of 1,500 m bsl the three positive thermal anomalies in the west appear as distinct features, they have merged into one bigger anomaly at the depth of 2,500 m bsl and show temperatures of up to 140°C. The small positive thermal anomaly at the eastern border of Bavaria shows temperatures of ~100°C. For the positive thermal anomaly around the city of Munich temperatures between 80 and 100°C are predicted, which is colder than the temperatures predicted by GeotIS (StMWIT 2010) by ~10 K. However, the trend of the measured temperature distribution could be reproduced even for this depth.

Deeper, at **3,500 m bsl** (Fig 30d), temperatures between 20 and 160°C are predicted by the model, with average temperatures of ~90°C apart from the thermal anomalies. At this depth, the coldest temperatures are limited to the negative thermal anomalies in the Folded Molasse Sediments at the southern border of the model area. The negative thermal anomaly to the southeast of Munich is characterised by temperatures of ~60°C. The positive thermal anomaly in the west of the model area increased in size compared to 2,500 m bsl and displays highest temperature values with up to 160°C. For the positive thermal anomaly in the area of Munich the simulations predict a temperature of ~120°C, and the anomaly is larger in size compared to shallower depths. The temperature of the positive thermal anomaly at the eastern border of Bavaria increased as well to 130°C. Compared to the measured temperatures shown in the GeotIS maps (StMWIT 2010), the simulations of this study predict temperatures 10 K lower in average for this depth. Nonetheless, the temperature trend of GeotIS is reproduced.

At a depth of **4,500 m bsl** (Fig 30e) average temperatures of ~100°C are predicted for the Molasse Basin. The negative thermal anomalies along the southern border of the model area decrease in size and show low temperatures of up to 20°C. For the negative thermal anomaly in the southeast of Munich the model predicts temperatures of ~90°C. To the west the positive thermal anomaly reaches temperatures to up to 170°C. The temperature of the warm thermal anomaly around Munich rises to 135°C. For this depth, no map from GeotIS (StMWIT 2010) is available anymore for comparison.

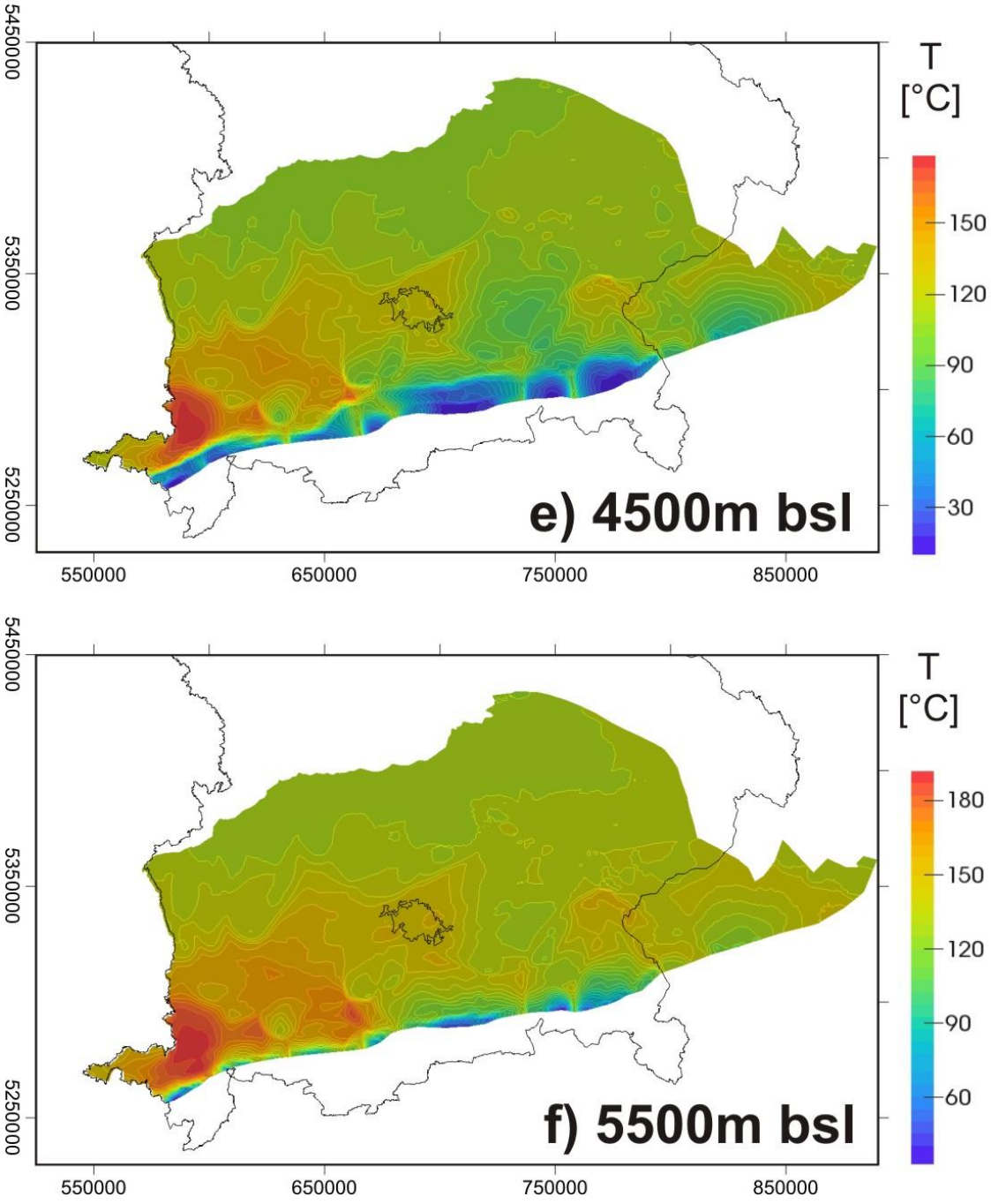

Fig 30 continued

The last temperature map (Fig 30f) shows the temperature distribution at a depth of **5,500 m bsl**. At this depth, an average temperature of 140 to 150°C is predicted by the coupled simulations. The negative thermal anomaly at the southern border of the model area decreased strongly in size and predicted temperatures are about 50°C. Highest temperatures are predicted for the positive thermal anomaly in the most western corner of the model area with up to 190°C. While the positive thermal anomaly around Munich shows temperatures of up to 170°C, the negative thermal anomaly southeast of Munich is less pronounced than at shallower depths with values of ~130 - 140°C.

All predicted temperatures have been additionally compared to measured bottom hole or extraction temperatures from different depths of 20 measurements (e.g. Agemar et al. 2014a). For 12 sites the modelled temperatures lie in a range of ±10 K of the measured temperatures (Fig 28, Tab 6). For two sites west of the Landshut-Neuöttinger High the model predicts temperatures more than 10 K lower and for two sites temperatures higher than the measured ones. For four sites in the area of Munich temperatures more than 10 K higher and for one site temperatures more than 10 K lower than the measured ones are modelled.

Tab 6 Comparison of observed and calculated temperatures for the location of 20 geothermal production sites at different depths. The locations of measurements are shown in figure 28. A red colour coding means temperatures are predicted too warm by the model, blue colour coding means predicted temperatures are too cold compared to observed ones.

ID	Location	UTM Coordinates		Depth [m asl]	Temperature measured [°C]	Temperature calculated [°C]	Residual Temp calc. - meas. [K]	Reference
1	Traunreut	768326,3446	5317920,521	-4095,710	108	151	43	Agemar et al 2014a
2	Poing	709645,0836	5338567,483	-2464,960	76	101	25	Agemar et al 2014a
3	Pullach 2	687645,8845	5324767,734	-2361,960	80	101	21	Agemar et al 2014a
4	Erding	716537,888	5354505,059	-1894,809	62	81	19	Agemar et al 2014a
5	Pullach	687645,8845	5324767,734	-2920,960	104	117	13	Agemar et al 2014a
6	Aschheim	701945,275	5338366,932	-2117,904	85	91	6	Agemar et al 2014a
7	Garching	696945,2515	5346766,704	-1683,616	70	76	6	ITG 2014
8	Garching	696945,2515	5346766,704	-1744,916	74	78	4	Agemar et al 2014a
9	Sauerlach	698045,8424	5316267,778	-3852,980	140	143	3	Agemar et al 2014a
10	Dürrnhaar	704145,653	5318768,12	-3504,876	135	135	0	Agemar et al 2014a
11	München Riem	700893,3825	5334418,605	-2155,422	95	92	-2	Agemar et al 2014a
12	Oberhaching	693645,4216	5321868,061	-3232,777	128	126	-2	Agemar et al 2014a
13	Straubing	761610,226	5420054,051	-500,613	37	35	-2	Agemar et al 2014a
14	Unterhaching	695375,7952	5325900,639	-3031,660	123	119	-4	Agemar et al 2014a
15	Simbach-Braunau	800291,3264	5352101,534	-1586,610	81	72	-8	Agemar et al 2014a
16	Unterschleißheim	690746,0027	5349666,83	-1484,859	78	70	-8	Agemar et al 2014a
17	Kirchstockach	699744,9973	5322467,964	-3384,942	139	129	-10	Agemar et al 2014a
18	Unterföhring	696542,4435	5340811,137	-1484,408	86	72	-14	Agemar et al 2014a
19	Waldkraiburg	752496,3402	5344579,67	-2291,049	109	95	-14	Agemar et al 2014a
20	Landshut	732766,0605	5379951,31	-72,503	60	26	-34	Agemar et al 2012

Interpretation: Influence of deep fluid flow on the thermal field

To compare the temperatures predicted by the coupled simulations to a purely conductive approach as followed by Przybycin et al. (2015b), the temperature distribution in the model area at a depth of 3,500 m bsl calculated considering only conductive heat transport is shown in figure 31.

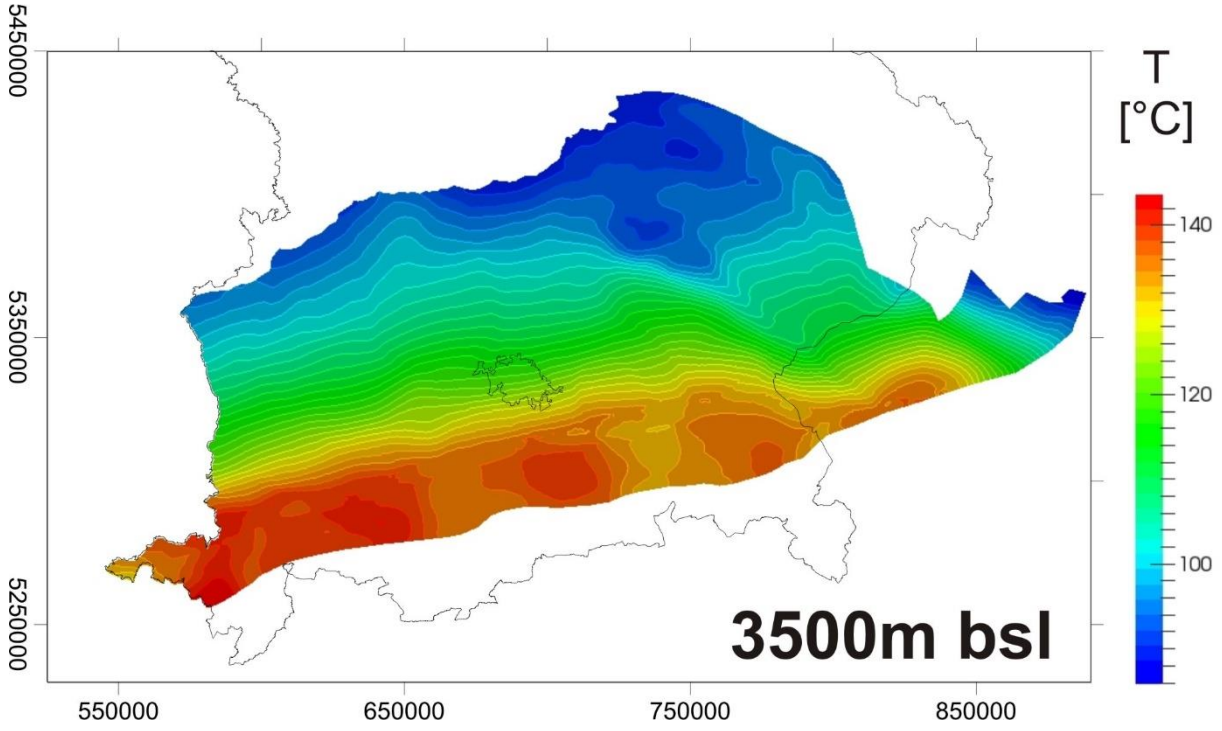

Fig 31 Temperature map at a depth of 3,500 m bsl showing the temperature distribution calculated considering only conductive heat transport following the approach of Przybycin et al. (2015b).

This temperature map shows increasing temperatures from the north (~80°C) to the south with ~120°C around Munich. South of Munich three prominent positive thermal anomalies with temperatures of ~140°C are predicted in the area of the Folded Molasse Sediments by the conductive model with lower temperatures (~130°C) in between. Compared to this conductive model, the coupled model 1 predicts a more diverse temperature distribution with a variation of much smaller wavelength for the depth of 3,500 m bsl (Fig 30d). Where a continuous increase of temperatures from north to south is calculated with the conductive model, an irregular temperature distribution is predicted by the coupled model. Moreover, the positive thermal anomalies predicted by the conductive model in the south of Munich are shifted to the north in the coupled model representing the positive thermal anomalies in the west, around Munich and at the eastern border of Bavaria. In turn, at the position of the positive thermal anomalies in the conductive model at the southern model boundary, negative ones are predicted by the coupled model. This shift of the positive thermal anomalies in the coupled model compared to the conductive case is caused by the downward directed fluid flow through the Folded Molasse Sediments in the

coupled case. This fluid inflow from the surface displaces hotter fluid at depth and thus relocates the heat coming from deeper parts of the basin by advective heat transport from the south to the north. This relocation can also be seen in the profiles through the model area depicting the temperature distribution in the basin (Fig 32).

The first profile (Fig 32a) runs west-east through the model and directly cuts the positive thermal anomaly around Munich and the negative thermal anomaly southeast of Munich. In this profile, areas where cold temperatures reach larger depths represent domains of downward flowing fluid (recharge). In contrast, areas of higher temperatures at shallower depth represent domains of upwards flowing fluids (discharge). For the negative thermal anomaly southeast of Munich this profile illustrates that the fluid turnover creating the negative thermal anomaly is limited to a local area and a comparable shallow depth (~2,000 m). At this depth, the Purbeck formation hydraulically decouples the Foreland Molasse Sediments from the Upper Jurassic (Fig 30c and d) due to its low hydraulic conductivity, and thus prevents deeper penetration of cold water from the surface. Nevertheless, the overall colder upper 2 km also affect the deeper layers via conductive heat transfer. Profile b (Fig 32b) shows the temperature distribution in north-south direction through the negative thermal anomaly southeast of Munich. Also from this perspective the prevented inflow of cold fluid from the surface to the larger depth is evident. In addition, upward directed flow of warmer fluid from larger depths is prevented as well by the Purbeck layer. This upward directed flow of warm fluid diverts to the west and east and creates the positive thermal anomalies around Munich and at the western border of Bavaria, as illustrated in profile c (Fig 32c). In particular, stream tracers show that the positive thermal anomalies are closely related to fluid entering the system vertically through the Folded Molasse Sediments due to a high topographic gradient. This fluid flows to deeper levels until it reaches the impervious crystalline crust. At that depth, the fluid flow direction changes to northward directed fluid flow. This in turn causes a general northward flow pattern through the Malm aquifer and the Molasse Sediments between Munich and the Landshut-Neuöttinger High parallel to the tilted top of the crystalline crust and around the Purbeck formation. Thereby, the heat from deeper levels is relocated compared to the conductive case by northward directed flow under advective conditions, leading to the positive thermal anomalies around Munich and at the eastern border of Bavaria and the strong negative thermal anomalies in the Folded Molasse Sediments.

While the negative thermal anomaly in the east of Munich is related to locally restricted downward flow of cold fluids, the positive thermal anomaly around Munich is caused by regional flow of fluid that initially entered the model through the Folded Molasse Sediments. This indicates that the Folded Molasse Sediments have a significant influence on the regional thermal field of the Molasse Basin and the underlying Upper Jurassic Malm aquifer even at larger depths.

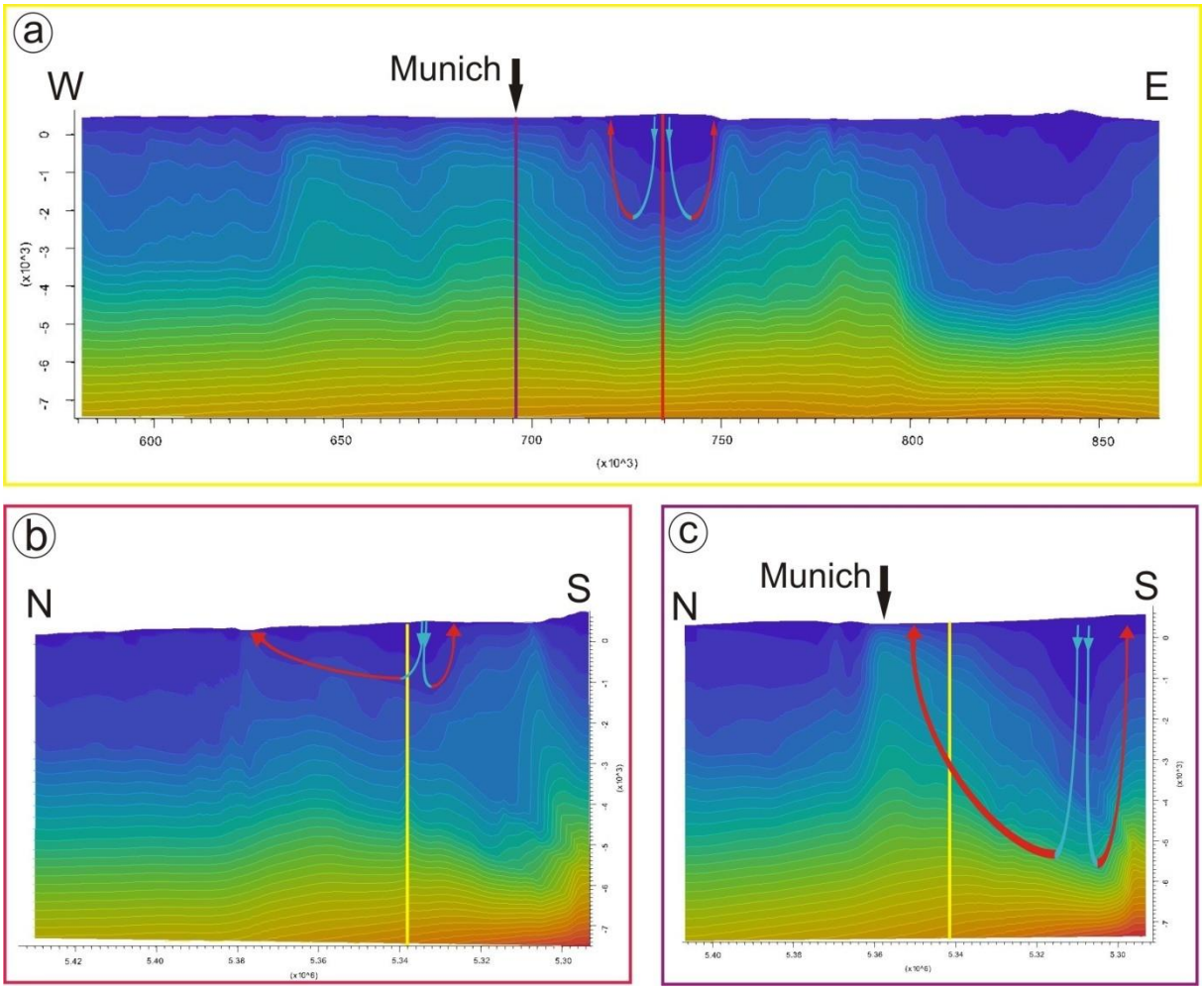

Fig 32 The predicted temperature distribution shown on profiles (vertical exaggeration 1:10) through the model area. The location of the profiles is shown in figure 30 (map d). The crosscuttings of profile b) (red frame) and c) (purple frame) are marked in profile a).

Profile a (yellow frame) shows the temperature distribution from west to east cutting through the pronounced thermal anomalies around Munich. Profile b) (red frame) shows the temperature distribution along a profile from north to south running through the cold thermal anomaly in the southeast of Munich. It shows that the negative thermal anomaly in the southeast of Munich is cause by fluid flow restricted to a small area and a shallow depth. This limitation can be correlated to the lateral distribution of the Purbeck formation occurring in that area. Profile c) (purple frame) shows the temperature distribution along a profile running from north to south through the positive thermal anomaly around the city of Munich. It shows that the positive thermal anomaly is caused by basin-wide advective heat transport bound to rising fluid flow from deeper depth.

Even though the Folded Molasse Sediments are characterised by the lowest hydraulic conductivity of all sediments, their large thickness of up to 7,000 m (Fig 25a) in combination with the high hydraulic gradient caused by the topography in front of the Alps, results in an overall flow pathway for cold fluid to larger depths. This combination of factors (hydraulic conductivity, thickness and high hydraulic gradient) leads to the very low temperatures at large depths. This result is however difficult to validate as no temperature measurements are available for comparison. To assess, how strong the influence of

the hydraulic conductivity of the Folded Molasse Sediments is on the thermal field in the whole basin, we decreased the hydraulic conductivity of the Folded Molasse Sediment even further by two orders of magnitude compared to the original model to $2*10^{-10}$ m/s. A temperature map at a depth of 3,500 m bsl (Fig 33) for this second model is shown. At this depth a much lower average temperature of ~60°C is obtained in the second model compared to the model 1. While the positive temperature anomalies at the southern model border, which were small in model 1, increase in size and value in the second model, the strong negative thermal anomalies in turn disappear nearly completely. The Folded Molasse Sediments, which were cold in average in model 1, are warm in the second model. The positive thermal anomalies in the west, around Munich and at the eastern border of Bavaria are much colder (~90°C) than in model 1. Likewise, the negative thermal anomaly southeast of Munich also shows lower temperatures in the second model (~30°C) than in model 1.

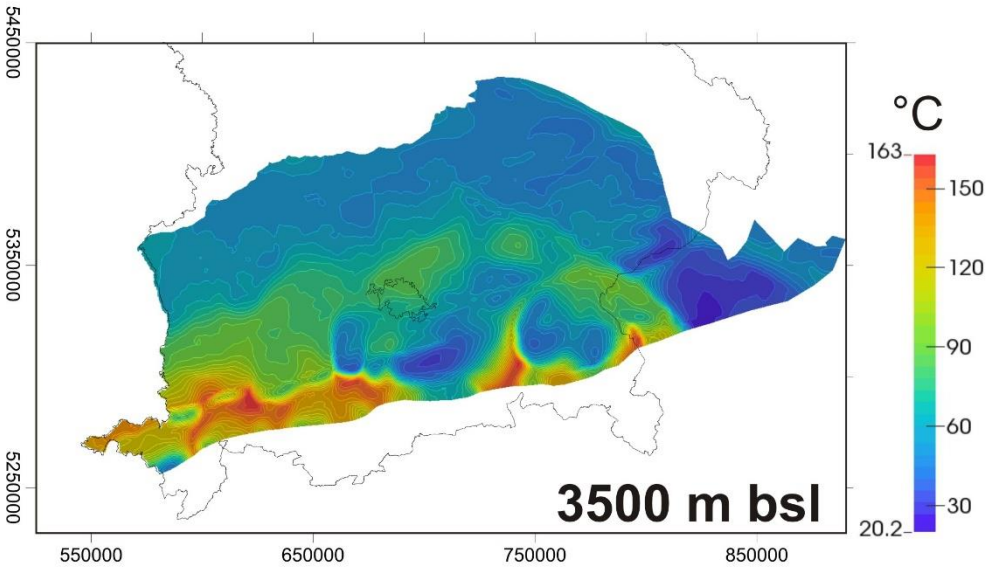

Fig 33 The temperature distribution at a depth of 3,500 m bsl calculated using a lower (by two two orders of magnitude) hydraulic conductivity of the Folded Molasse Sediments compared to model 1. The pronounced negative thermal anomalies along the Alpine border decreased significantly in size, the positive thermal anomalies increased. The central and northern model part is colder compared to the original model. The positive and negative thermal anomalies in the central model area are predicted by model 2 even though showing a lower temperatures compared to model 1.

Obviously, a lower hydraulic conductivity of the Folded Molasse Sediments leads to warmer temperatures in the Folded Molasse Sediments, but colder temperatures in the rest of the model. Though, the general temperature trend remains the same and consistent with GeotIS (StMWIT 2010) the absolute values are better reproduced by model 1.

The influence of permeable faults on the thermal field (model 3)

Even though the measured thermal field of the Molasse Basin could be reasonably well reproduced already by coupled fluid flow and heat transport simulations without considering fault related fluid flow, a possible influence of permeable faults on the temperature distribution cannot be excluded, at least on a local scale. Therefore, three permeable testfaults have been implemented into the model as described earlier to simulate the potential influence of large permeable faults on the thermal field. First, the effects of each fault have been simulated separately, before all three faults have been included simultaneously (model 3). In figure 34 the resulting temperature distributions of these simulations are presented with temperature maps at a depth of 3,500 m bsl, respectively.

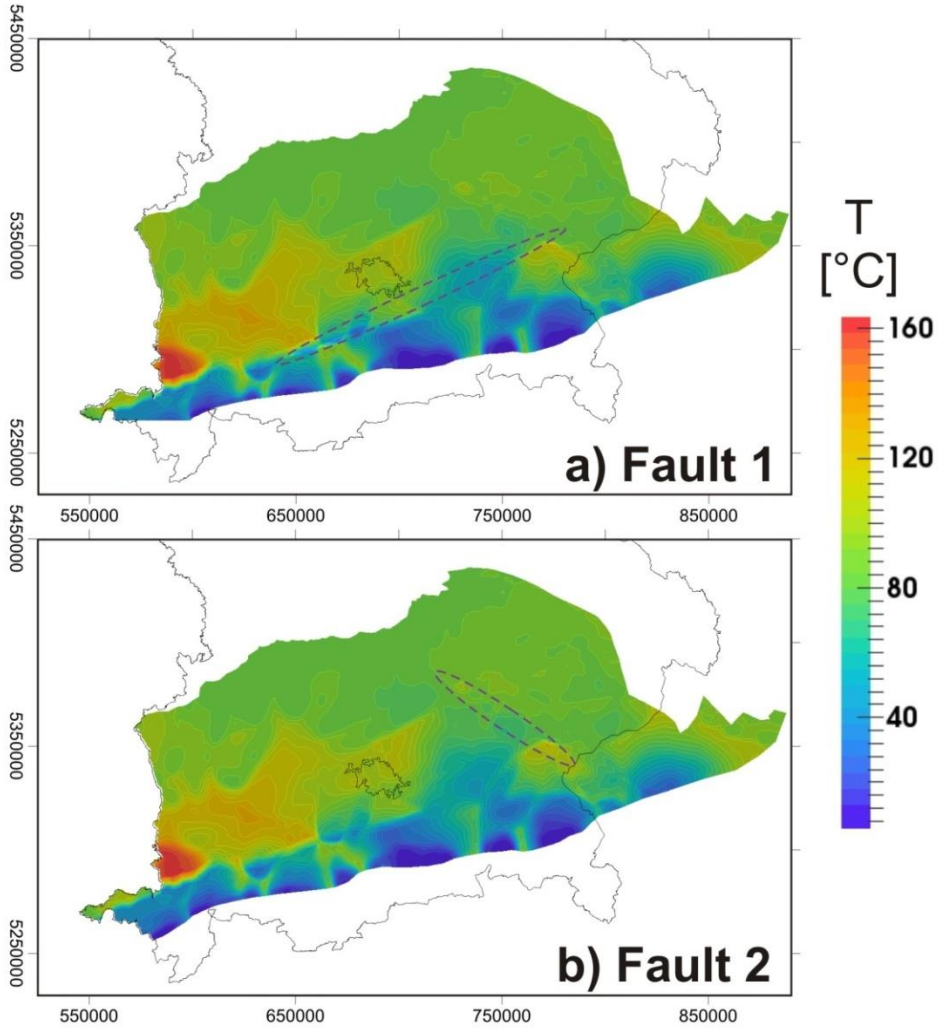

Fig 34 Temperature maps at a depth of 3,500 m bsl showing the influence of different hydraulically conducive testfaults on the thermal field, which have been included stepwise and subsequently all together in model 3. Besides a minor cooling impact on the temperature distribution in the proximity of the fault by fault related advective or convective heat transport no significant influence can be seen on the basin-wide thermal field by single and combined included faults.

Compared to the temperature distribution at the corresponding depth of model 1 only minor changes of the temperature distribution are observable for all versions of model 3. Each permeable fault has only a local influence on the thermal field in its direct surroundings (~1 km) by fault related fluid flow which cools down or heats up the fault-near areas, respectively. A combination of all faults in one simulation has as well only a minor influence on the regional thermal field.

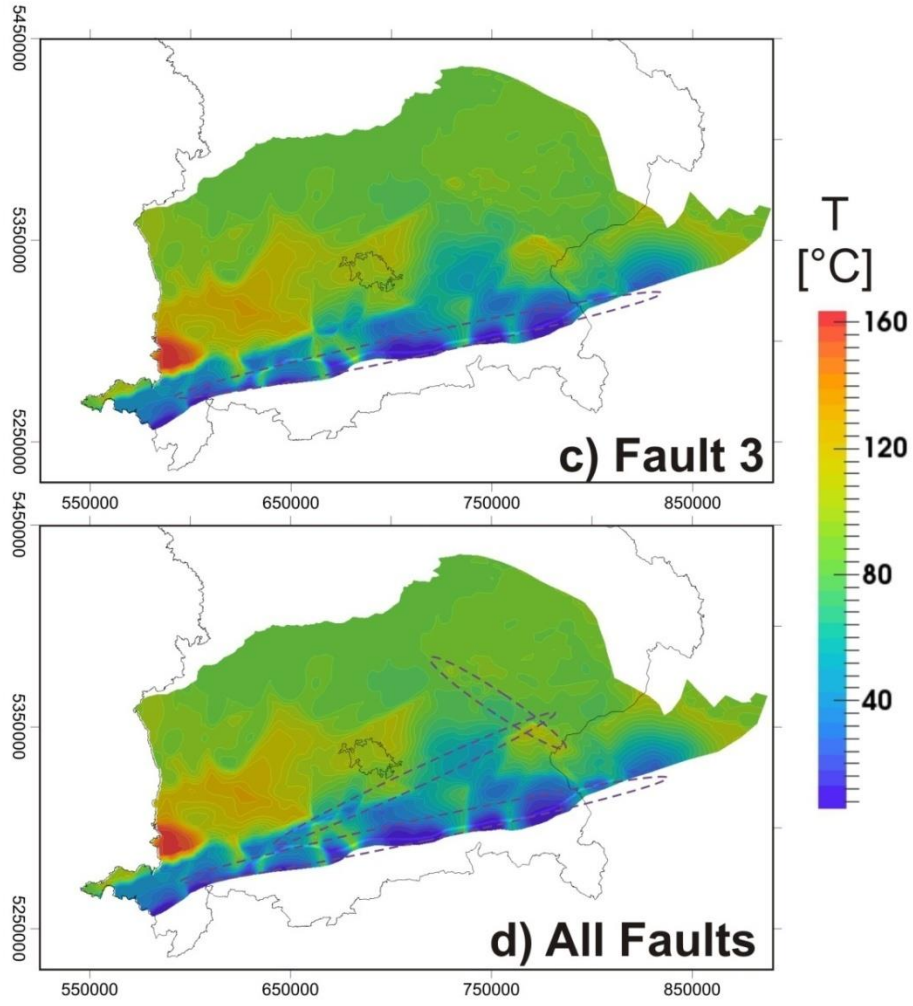

Fig 34 continued

These results indicate that permeable faults have no significant influence on the regional flow field and are not particularly necessary to reproduce the basin-wide trend of temperature distribution in the Molasse Basin area. However, the temperature misfit between measured and predicted values in model 1 of more than 10 K at the three locations in the area of the Landshut-Neuöttinger High could be decreased slightly when considering permeable faults in model 3. This indicates that permeable faults may influence the local temperature and pressure evolution and therefore should be considered for local and reservoir-scale simulations.

4.6 Discussion

As was already shown by Przybycin et al. (2015b), the long wavelength thermal field of the Molasse Basin is dominated by conductive heat transport which in turn is mostly influenced by the structural configuration of the crust and the lithosphere beneath the basin and lateral heterogeneities in the thermal conductivity. Thereby, the depth of the LAB has a distinct effect on the long wavelength thermal field: where the LAB is shallow, a steeper geothermal gradient evolves leading to higher temperature values in shallower depth than in areas where the LAB is deep. A second effect is caused by the upper crystalline crust, characterised by a much higher radiogenic heat production than the sediments or the deeper crust and the mantle: where the upper crust is thick, as in the Tauern Body, more heat from the decay of radioactive elements can be introduced into the system as an additional heat input, leading to higher temperatures in the south, where the upper crust is thicker, than in the north, where the upper crust is thinner. In addition, sensitivity analyses of thermal properties have shown that the structure and high thermal conductivity of the crystalline core of the Tauern Window cause a chimney effect between the thermally more conductive Tauern Body and the thermally less conductive Alpine Body. This effect may partly explain the positive thermal anomalies around Munich and at the eastern border of Bavaria with a negative thermal anomaly in between.

A third conductive effect is the blanketing effect (Przybycin et al. 2015b). Here, thermally more conductive material is covered by thermally less conductive sediments: higher thicknesses of insulating sediments lead to higher temperatures compared to areas with low sedimentary thicknesses at the same depth in the upper few kilometers. However, the thermal anomalies predicted by the conductive model have been too warm compared to measured data, which indicates that other than conductive effects may be relevant.

By using the lithospheric-scale 3D thermal model of Przybycin et al. (2015b) as a base for our basin-scale simulations we took into account the long wavelength conductive thermal effects by prescribing temperatures extracted from the lithospheric-scale model as lower thermal boundary condition to the coupled model. With the modelling approach of simulating coupled fluid flow and heat transport the fit of the predicted values for the thermal anomalies with observed temperatures could be improved (Fig 30) compared to the purely conductive approach (Przybycin et al. 2015b). The coupled fluid and heat transport simulations were able to reproduce not only the pattern of temperature distribution, but also the range of the measured temperatures values in the Molasse Basin area.

The remaining average temperature misfit between the measured data (GeotIS, StMWIT 2010) and the model predictions of ± 10 K lies in the range of the standard deviation of bottom hole temperatures and temperature logs (Hermanrud et al. 1990, Förster 2001, Noack et al. 2010, Agemar et al. 2012, Agemar et al. 2014a). Moreover, Agemar et al. (2012) recommends a careful treatment of the deeper temperature estimates of GeotIS (StMWIT 2010) since possible local thermal effects are not considered in the temperature interpolation. The latter assumes a homogeneous distribution of thermal conductivities in

the subsurface which does not account for lithological heterogeneities and related heat refraction. Under this consideration the reproduction of the observed temperatures in this study can be considered as satisfying for the chosen model size. Albeit, we admit that the limited vertical and horizontal resolution, the assignment of uniform physical properties to most of the layers and the prescribed first kind boundary conditions may be sources of error in our results. Therefore, the sensitivity of the modelling results on the prescribed thermal properties and the boundary conditions has been tested. The results of this analysis show that even if the predicted temperatures are strongly depending on the hydraulic conductivity prescribed to the Molasse Sediments, the temperature trend remains the same for different variations of the model. A comparable, though weaker effect could be observed for different boundary conditions.

Influence of faults

An additional consideration of permeable faults (Fig 34) had only a minor influence on the regional distribution of temperatures in the Molasse Basin. Ascending warmer fluid in the area of the positive thermal anomalies and descending colder fluid in the area of the negative thermal anomalies driven by density gradients within the faults caused insignificant (1-3 K) cooling of the system but did not lead to changes in the general temperature trend. Such a limited spatial influence of permeable fault zones on the regional thermal field has been already described by Cherubini et al. (2014). However, an implementation of permeable fault zones into reservoir-scale models might still be of high importance for the local temperature distribution. Such a local significance of permeable faults was implied by the slightly decreased temperature misfit between predicted temperatures and measured values in the area of the Landshut-Neuöttinger High after the implementation of permeable faults into model 3.

Summarizing, our results show that the basin-scale thermal field is caused by a combination of conductive and advective heat transport. In contrast to the work of Pasquale et al. (2013) for the karstified carbonate rocks in the Po Basin, we found no indication for large-scale free thermal convection in the carbonates of the Malm aquifer. This may be explained by the much smaller thickness of the upper four layers of the Upper Jurassic Malm aquifer in Germany of maximum 400 m of permeable thickness compared to the thick carbonate platform of the Po Basin with more than 4,000 m. Free thermal convection evolves only if the reservoir is sufficiently thick and lateral gradients in hydraulic head are insignificant (Kaiser et al. 2011) as otherwise pressure-driven advection suppresses density-driven fluid flow. The scenario of the Molasse Basin does not fulfil these criteria for free convection. The permeable layers of the Upper Jurassic Malm (Zeta-Gamma) are not thick enough and the lateral variations of the hydraulic head too uniform over the basin area to enable thermal convection.

Rühaak (2009) and Rühaak et al. (2010) calculated the thermal field of the western Molasse Basin using a local-scale conductive model. Since they were not able to reproduce the observed thermal anomalies in the western Molasse Basin with such a conductive approach, they presumed fluid flow along E-W striking faults to cause temperature differences of more than 10 K in the basin.

We regard the results of this study as consistent with their work, saying that fluid flow in general is needed to reproduce the detected thermal anomalies in the Molasse Basin. However, in our case the pathways for fluid flow are mainly created by the matrix porosity of the Folded and Foreland Molasse Sediments and the complex permeability variations in the Upper Jurassic Malm aquifer (Birner 2013).

More precisely, sensitivity analyses have shown that the average temperature values in the Molasse Basin are strongly influenced by the hydraulic conductivity of the Folded and Foreland Molasse Sediments (Fig 33). Hydraulically less conductive Folded Molasse Sediments would lead to higher deep temperatures at the Alpine front, but lower temperatures in the rest of the basin. Hydraulically more conductive Folded Molasse Sediments would lead more cold water to larger depths causing an overall cooling of the system. A similar effect would be caused by hydraulically more conductive Foreland Molasse Sediments, whereas a lower hydraulic conductivity of the Foreland Molasse Sediments would lead to an overall warming of the system.

Moreover, our results show that the hydraulic conductivity of the Malm aquifer has only an influence on the flow direction in the Malm aquifer, but not on the overlying layers. Accordingly, the positive thermal anomalies around Munich and at the eastern border of Bavaria appear to be caused by northward directed regional fluid flow (Fig 32) from deeper parts in the south of the model area. Furthermore, our results indicate locally restricted fluid flow related to the structural and hydraulical configuration of the Purbeck formation causing the negative thermal anomaly in the east of Munich. This combination of basin-wide regional and locally restricted fluid flow as explanation for the development of adjoining positive and negative thermal anomalies in the Molasse Basin has so far not been suggested but can have a significant influence on local and reservoir-scale studies. In particular, it may question some results derived from a local-scale 3D structural and thermal model for the area of the city of Munich (Schulz and Thomas 2012) that does not consider different hydraulic boundary conditions at the lateral model boundaries.

An investigation of real anomalies with local or reservoir-scale models may not capture the hydrothermal dynamics with sufficient detail since anomalies in the thermal field may be caused by regional fluid flow. In such cases an adoptable strategy would be to extract pressures and temperatures from basin-scale models as thermal and hydraulic boundary conditions for local and reservoir-scale models to incorporate the appropriate consideration of regional effects.

4.7 Conclusions

By following a multi-scale databased 3D modelling approach, the thermal field of the German Molasse Basin was investigated with simulations of coupled fluid flow and heat transport. Thereby, existing knowledge about the long wavelength and deep conductive thermal field of the basin was taken into account by prescribing temperatures, extracted from lithospheric-scale 3D conductive models, as the lower thermal boundary condition for the basin-scale model. The resulting thermal field reproduces the measured temperature distribution of the basin including the pronounced negative and positive thermal anomalies satisfactorily for a basin-scale approach. To reduce the remaining misfit between observed and modelled temperatures as well as remaining uncertainties, a higher vertical and horizontal structural resolution and better knowledge of the distribution of physical property is needed.

Considering the results of previous conductive studies, our results confirm that the thermal field of the German Molasse Basin is controlled by conductive heat transport in the first place, especially in the deeper parts, but strongly influenced by advective heat transport within the sediment fill bound to basin-wide fluid flow. The pronounced positive and negative thermal anomalies in the basin are partly triggered by conductive heat transport, but reinforced by a combination of regional and local fluid flow, respectively, and mostly depending on the geological structure and the hydraulic conductivity of the Molasse Sediments and the Upper Jurassic Malm. Faults appear to have only a subordinate, local influence on the thermal field. The results of this basin-wide study of coupled fluid flow and heat transport contribute to a better understanding of the origin of the thermal anomalies in the basin. In addition, the study helps to reduce the exploration risk of geothermal energy project by providing higher resolved predictions of the deep temperature conditions. Moreover, the model can be used to derive reliable pressure and temperature boundary conditions for high-resolution reservoir-scale models for areas of exploration interest.

5. Summarising Discussion

In the German Molasse Basin distinct thermal anomalies occur at depth of exploration interest and are a high risk for the geothermal energy exploration. Unfortunately, prior thermal models were not successful in reproducing these observed anomalies satisfactorily, either due to their limited model size (local) and resolution, their restriction to 2D or due to the limited consideration of different heat transport mechanisms. In fact, it remained unclear from these studies if, and in case, how significantly deep and long distance structural features may influence the thermal field of the Molasse Basin and which heat transport mechanisms create the observed temperature distribution on which scale.

The aim of this thesis was to contribute to the understanding of the temperature distribution by investigating the thermal field of the German Molasse Basin on different scales. Thereby it should be tested whether it is possible to reproduce the observed temperatures and to derive an explanation for the origin of the distinct thermal anomalies occurring in the basin by following a multi-scale modelling approach. This approach consists in lithospheric-scale structural modelling and conductive thermal calculations, which in turn provide the structural base and thermal boundary conditions for concluding basin-scale simulations of coupled fluid and heat transport.

Before the main question of this thesis could be addressed, several principle and subordinate questions had to be answered before. This chapter reviews how far the principal questions of this thesis presented in chapter 1.2 can be answered based on the results and interpretations of the three main work steps presented in the prior chapters (2-4). Finally, it will be stated how far the combined work of this study provides an answer for the major question addressed.

In a sedimentary basin at the edge of an orogen different heat driving mechanisms and thermal effects have to be taken into account. Since temperatures increase with depth due to the continuous basal heat input from the mantle (Huenges 2010) and due to the additionally generated heat in the continental crust by radiogenic heat production (Bjørlykke 2010), the average geothermal gradient may vary laterally over the area. The heat from both sources is conductively transported to the surface, whereby the efficiency of this heat transport is depending on the thermal conductivity of the respective material. The temperature pattern created by this conductive heat transport can additionally be superposed by thermal effects due advective and/or conductive heat transport. Each of this heat transport mechanisms acts on a characteristic timescale and thus has to be regarded under adapted thermodynamic and/or hydraulic conditions. While slow heat transport mechanisms, as e.g. conduction, may be investigated under steady-state conditions in some cases, faster heat transport mechanisms, as e.g. convection, should rather be investigated under transient conditions. In this thesis thermodynamic equilibrium is assumed for the calculating of the conductive thermal field under steady-state conditions. Since thermal conduction is strongly controlled by the structural configuration of an area, the state of thermodynamic equilibrium may be dependent on the isostatic state of the area in turn. However, it was unclear whether the Molasse

Basin area can be regarded as isostatically and thermally equilibrated and thus making it questionable whether steady-state condition are justified in the calculation of the conductive thermal field.

To investigate whether the Molasse Basin area is isostatically equilibrated the first principal question of this thesis was asked:

How does the lithospheric-scale 3D structure of the European Molasse Basin look like?

To answer this question, the first part of this thesis dealt with the structural configuration of the Molasse Basin on a lithospheric-scale and how it affects the vertical stress field in the model area. Thereby, a combined approach of structural modelling, isostatic calculations and 3D gravity modelling has been followed to derive the lithospheric-scale 3D structural configuration and density distribution of the Molasse Basin area with which the 3D load distribution has been calculated.

The resulting model includes key structural elements relevant for the assessment of the isostatic state of the basin and the load variations at different depths as well as for the subsequently following conductive thermal calculations.
The results indicate lower thicknesses of the lower crystalline crust in the north than in the south, and higher thicknesses of the upper crystalline crust in the north than in the south, with even smaller thicknesses directly below the Tauern Body. Accordingly, the model area can be subdivided into two regions, a mountain region and a lowland region, with a transition in the Molasse Basin (chapter 2.4).

The comparison of the structure of the isostatically calculated model with the 3D gravity constrained one (chapter 2.4) has shown, that the European Molasse Basin area is still far from isostatic equilibrium at the base of the lithosphere, which has been additionally supported by the assessment of the 3D load distribution (chapter 2.5) and is in correlation with earlier studies (Wagini et al 1988, Götze et al. 1991, Ebbing 2004). Although the Molasse Basin area is not expected to be isostatically balanced due to the still ongoing continental collision process, the results of this thesis show, that the Alps deviate the most from the isostatic equilibrium on the scale of the lithosphere followed by the Bohemian Massif. The Molasse Basin and the South German Scarpland show the smallest deviations from the isostatic equilibrium. The results from 3D gravity modelling (Fig 8e) indicated, that the smaller model units with lower densities have only of minor influence of the isostatic state as their impact is superposed by impacts of larger structures with higher densities (chapter 2.4). Moreover, the derived deviations from the isostatic equilibrium imply that the Alps and the Bohemian Massif can be considered as overcompensated. In contrast, the Molasse Basin and the South German Scarpland appear to be undercompensated. The transition between overcompensation and undercompensation proceeds directly at the northern Alpine front and the western border of the Bohemian Massif, both areas with strong structural disruption and tectonic activity and a potential of entailing permeable faults as possible pathways for fluid flow.

The calculated 3D load distribution implies a non-uniform increase of loads with depths on both sides of this transition (2.5). Such a non-uniform increase of loads with depth indicates that the vertical stress as well as the required compensating horizontal stress needed to prevent a gravitational collapse of the system may change non-uniformly with depth as well. A non-uniform change of vertical stress with depth may lead to a switch between the three principle stress axes leading to different stress patterns at different depths - a finding that challenges the general assumptions of simplified far-field effects. By changing the deviatoric stress ($\sigma_{vertical}$ versus $\sigma_{minimum\ horizontal}$ versus $\sigma_{maximum\ horizontal}$) with depth, unpermeable faults at shallower depth may change to permeable faults at deeper levels and act as pathways for fluid flow. Such areas with non-uniform changes in vertical stress have been chosen as locations for the testfaults in the coupled fluid flow and heat transport modelling step (chapter 4.4). However, it has to be mentioned that the isostatic calculations and the 3D gravity modelling (chapter 2.4) have shown that the basin area is not isostatically equilibrated, thus leaving the assumption of mechanical steady-state conditions in the calculation of the 3D load distribution questionable.

Though the first part of this thesis has shown that assuming steady-state conditions in the calculation of the load distribution may be an oversimplification, assuming a thermally equilibrated situation for the calculation of the 3D conductive thermal field may still be justified, since conductive heat transport is a very slow process. To test whether the observed thermal field of the Molasse Basin area may be reproduced based on such a simplification the work described in chapter 3 has been carried out. In this second part the second principle question ***"How does the lithospheric-scale 3D conductive thermal field of the European Molasse Basin look like?"*** was asked to distinguish the effects of heat transported by conduction from effects on the thermal field related to fluid flow. Furthermore, a temperature distribution should be derived from the conductive calculations as lower thermal boundary condition for the subsequent coupled simulations at crustal depths. Neglecting potential permeable faults in the crust, the matrix permeability of the crustal and mantle material ($< 10^{-21}$ m/s) is too low to allow large-scale fluid flow at crustal levels and deeper characterised by velocities relevant for heat transport. Thus, an influence of fluid flow related cooling/heating on the temperature distribution can be disregarded for these depths, leaving conduction as the only effective heat transport mechanism.

In the predicted thermal field of the Molasse Basin area (chapter 3.5), different conductive thermal effects could be identified of which the combination lead to the particular temperature distribution in the basin. Moreover, some of the positive and negative thermal anomalies observed in the Molasse Basin were predicted already with this purely conductive approach.

One regional effect is caused by the laterally varying **geothermal gradient** due to the variable depth of the thermal LAB below the model area. In areas with a shallower LAB, the heat from the inner parts of the earth has to overcome a smaller distance to equilibrate between two thermal boundaries (LAB and surface) leading to a steeper geothermal gradient than in areas with a deeper LAB. This leads to higher temperatures at shallower depths in areas with a shallower LAB than in areas with a deeper LAB.

Applied to the predicted thermal field of the European Molasse Basin in this study a steeper geothermal gradient and higher temperatures at deeper levels are found in the north and northwest of the model area towards the direction of the Eifel plume (Seiberlich et al. 2013). In contrast, a flatter geothermal gradient is predicted for the central model area. Interestingly, in the area with the deepest LAB below the Alps the geothermal gradient is not flattest, but steepens recognisably as upward-bend isotherms.

This divergence is in correlation with the thickness of the crystalline crust and the crystalline Tauern Body in the Alpine area and results from a second conductive effect on the thermal field. The **radiogenic heat production** in the crystalline material of the upper crust and the Tauern Body is much higher compared to the radiogenic heat produced by sediments, the lower crystalline crust and the mantle. In combination with the larger cumulative thickness of the upper crust and the Tauern Body in the south than in the north of the model, more heat is generated in the south adding to the heat budget arriving from the LAB and leading to higher temperatures at shallower depths.
Together, the upper crystalline crust and the Tauern Body are thickest in the southern part of the model area leading to higher temperatures at shallower depths compared to central and northern parts of the model area.

A third conductive thermal effect is caused by the contrast in **thermal conductivity** between the thermally highly conductive crystalline upper crustal material and the thermally less conductive sediments of the Molasse Basin fill and the sedimentary units of the Alpine Body. Due to this material characteristic heat is transported and can escape more efficiently in areas where crystalline material is exposed to the surface, like in the Tauern Window, than in areas covered by thermally less conductive sediments. Such an association of lower temperatures at shallower depths with near-surface or outcropping crustal material has already been recognized by Chopra and Holgate (2005) and Noack et al (2010) and is known as "**chimney effect**".
An opposite thermal effect occurs in areas where thermally more conductive crystalline material is covered or bordered by thermally less conductive sediments, as in the Molasse Basin or between the Alpine Body and the Tauern Body. The thermal energy coming from the crystalline crust and the mantle is trapped within the thermally less conductive sediments causing higher temperatures at shallower depths. The intensity of this so-called "**thermal banketing effect**" is thereby depending on the thickness of the insulating sediments and the contrast in the thermal conductivities between crystalline crust and sedimentary rocks.

Such influence of crustal radiogenic heat production and crustal thermal conduction on the lithospheric-scale thermal field has already been described by Mareschal and Jaupart (2013) and Maystrenko and Scheck-Wenderoth (2013) and shows the relevance of the implementation of a differentiated crust into thermal models.

All four effects may impact the shallow geothermal field of the European Molasse Basin area in superposition: The heat coming from deeper parts of the mantle and the heat generated in the crystalline

crust is stored in the insulating sediments of the Molasse Basin and the Alpine Body, whereas it is conducted directly to the surface through the Tauern Body and outcropping crystalline crust, leading to a characteristic laterally variable temperature distribution in the Molasse Basin area even at shallower depths.

In particular, sensitivity analyses with respect to the assigned thermal properties have shown that the occurrence of thermal anomalies in the Molasse Basin is strongly related to the presence of the crystalline Tauern Body within the Alpine Body and the contrast in the thermal conductivity of both units as well as to the increased radiogenic heat production of the crystalline Tauern Body and the upper crystalline crust. Though these anomalies predicted by the conductive model are too hot compared to observations, their sheer presence implies that their origin is triggered by the structural configuration of the crust and the lateral contrast in thermal properties between the Alpine area and the Molasse Basin. Since the absolute values of the thermal anomalies have been predicted too warm by the conductive model an additional influence of the heat transport related to fluid flow in the shallow part of the basin is likely.

The reproduction of the observed thermal field together with the distinct thermal anomalies occurring the basin to some extend shows that even though assuming mechanical steady-state conditions for the calculation of the 3D load distribution may be an oversimplification, following a steady-state approach for the calculation of the conductive thermal field is possible to some extent. In addition, these results imply that the Molasse Basin area deviates much stronger from the isostatic than from the thermal equilibrium on lithospheric-scale. Thus assuming steady-state conditions for thermal calculations appears to be justified on lithospheric-scale when advective and convective heat transport related to fluid flow is neglected, both much faster heat transport mechanisms compared to thermal conduction.

Comparing the resulting temperature distribution derived from conductive calculations to observed temperatures, areas were identified for which the observed temperatures could not be reproduced assuming thermal equilibrium and only conductive heat transport. To answer the third principle question of this thesis ***"Which heat driving processes are causing the present-day thermal field in the German Molasse Basin?"*** coupled fluid flow and heat transport simulations have been carried out (chapter 4). For these simulations a different workflow was followed than for the conductive calculations as investigations of different heat transport mechanisms comprise diverse requirements with respect to model simplification, resolution and computational effort. While the conductive thermal field was calculated based on a lithospheric-scale model, a basin-scale model with much higher vertical and horizontal resolution was chosen for the coupled simulation. For this, the lower, hydraulically nonconductive parts of the lithospheric-scale structural model were discarded when building the basin-scale model. Since no fluid flow related heat transport is expected in the crystalline crust and the lithospheric mantle, coupled simulations with adequate resolution on lithospheric-scale would mean a disproportional computational effort without justification. In turn, the conductive thermal effects derived

from the lithospheric-scale model were introduced into the coupled simulations by prescribing a lower thermal boundary condition extracted from the conductive model at a depth which was assumed to be dominated by conductive heat transport. Thus the cumulative deep thermal effects caused by the depth variations of the thermal Lithosphere-Asthenosphere Boundary, the internal structure of the crystalline crust as well as the interdependence between the Alps, the Tauern Body and the Molasse Basin (chapter 3.7) were transferred to the model of coupled fluid and heat transport. Following this multi-scale approach the obstacles of high computational efforts without additional benefit could be avoided without neglecting the influence of thermal effects from deeper levels on the shallow thermal field. Moreover, transient thermal and hydraulical conditions have been assumed for the simulation of the coupled fluid and heat transport by choosing a simulation time of 100,000 years. Such a simulation time is long enough to allow the fluid flow and heat transport to equilibrate within the model generating quasi-steady-state conditions, but gives the possibility to assess at which timestep steady-state conditions are reached. In fact, the evaluation of the development of the thermal anomalies in the course of these quasi-steady-state simulations has shown that first thermal anomalies emerge after 10,000 years simulation times in the basin area, and remain stable after 30,000 year simulation time. With these simulations not only the trend of the observed temperature distribution in the Molasse Basin could be reproduced, but also the absolute values of the pronounced thermal anomalies. These results imply that even though the Molasse Basin area appears to be isostatically non-equilibrated, thermal and hydraulic equilibrium may be assumed for the simulation of the coupled fluid and heat transport in the Molasse Basin area on basin-scale.

The resulting temperature distribution suggests that the deeper crystalline parts below the basin and the orogen are controlled by conductive heat transport, while the shallower thermal field is influenced by a combination of conductive and advective heat transport. However, large-scale free convective heat transport could not be recognized in the basin, what is different from the results of Pasquale et al. (2013) for a similar setting in the Po Basin. This difference may be ascribed to the much smaller thickness of the Malm aquifer in the Molasse Basin with 400 m compared to the thick carbonate platform in the Po Basin with more than 4,000 m. In particular, the limited thickness of the Malm aquifer inhibits the development of density driven instabilities.

Nevertheless, the calculated temperature distribution and the flow field indicate that the thermal field in the sedimentary part of the Molasse Basin is strongly influenced by heat transport related to pressure-driven advective fluid flow. Due to the inflow of cold fluid from the surface, the thermal field of the basin is cooled down significantly, especially in areas where the Folded Molasse Sediments are thick. There, the high hydraulic gradient generates high pressure forces in response to the first kind hydraulic boundary condition prescribed to the model. These pressure forces, in combination with the large thickness (up to 7,000 m thick) and the considerable hydraulic conductivity of the Folded Molasse Sediments result in the establishment of pathways for fluid to larger depths. Coherently, low temperatures were predicted for the deeper parts of the Molasse Basin at the southern border of the

model. These values appear unrealistically low though no comparative measurements are available from these depths at the Alpine border. However, a sensitivity analysis (chapter 4.5) of the thermal and hydraulic properties has shown that a lower hydraulic conductivity of the Folded Molasse Sediments would lead to higher temperatures at depth at the Alpine border, but considerably lower temperatures in the rest of the model area. A lower hydraulic conductivity of the Foreland Molasse Sediments would cause higher temperatures in most parts of the model area, while the temperature distribution in the Foreland Molasse Sediment would not change significantly. In both cases, the absolute temperature values would change, but the temperature pattern in the central part of the Molasse Basin would remain the same. To better assess the robustness of these values, higher resolved models, both in space and time, would be required in addition to deep temperature measurements for validation. A similar, but slightly attenuated cooling effect by advective fluid flow is caused by the considerable hydraulic conductivity of the Foreland Molasse Sediments in the central part of the model, leading to lower temperatures predicted by the coupled than by the conductive model. That such a pressure-driven cooling effect by advective heat transport significantly may influence the deep temperature field has also been described for other basins as e.g. the North German Basin (Kaiser et al. 2011, Noack et al. 2014) or the Upper Rhine Valley (Lampe and Person 2002).

Though the strongest influence on the thermal field was ascertained for the hydraulic conductivity of the Foreland and Folded Molasse Sediments, the results of the sensitivity study suggest a reasonable choice of the hydraulic conductivity to both Molasse Sedimentary units, since other values would lead to a larger misfit between observed and predicted temperatures. Furthermore, the sensitivity studies have shown that the hydraulic conductivity of the permeable parts of the Upper Jurassic Malm aquifer has only a small impact on the basin-wide thermal field. This is not surprising as the pressure differences in the fluid are insignificantly small within this aquifer.

Particle tracking has shown that the thermal anomalies caused by conductive heat transport are enhanced by basin-wide and deep fluid flow (chapter 4.5). Thereby, the fluid enters through the Folded Molasse Sediments to larger depths until it reaches the impermeable layers, along which the fluid flows northwards transporting the heat from deeper levels to shallower depths by advective heat transport. In contrast, particle tracking indicates that the negative thermal anomaly in the east of Munich is caused by locally restricted in-flow of cold surface water through the Foreland Molasse Sediments above the Purbeck formation. The structural and hydraulic configuration of the Purbeck formation in turn prevents a progression of cold fluid to deeper levels at this location, but also inhibits the ascent of warm fluid to shallower depths. In combination these two effects can explain the known local negative thermal anomaly. An additional consideration of permeable faults did not change the basin-scale thermal field of the European Molasse Basin significantly. The results of this study imply that fluid flow not only along permeable faults, but in general is needed to reproduce the thermal anomalies in the German Molasse Basin with a modelling approach reliably. However, a relevance of fault related flow should not be excluded for local- and reservoir-scale investigations with the results of this study.

Limitations of the method and need of further research

Even though it was possible to reproduce the observed temperature distribution of the European Molasse Basin with a multi-scale modelling approach, some limitations of the method cannot be concealed.

Admittedly, the vertical and horizontal **resolution** may have a strong influence on the modelling results. The vertical and horizontal resolution are both determined by the regarded geological structure, the available structural data and confined by the computational effort of a simulation. A higher resolution leads always to an increased computational effort for the simulation. Hence, a model resolution should be chosen which is suitable to resolve the respective process of interest with an acceptable amount of computational effort. Accordingly, the appropriate resolution may vary for different processes investigated and should therefore be adapted for each modelling step depending on the availability of data. The results of this thesis indicate that a multi-step refinement of the model resolution is an adequate strategy. Consequently, the resolution was successively increased progressing from conductive to coupled modelling. However, a certain influence of the layer and mesh resolution on the modelling results cannot be excluded completely, since the chosen resolution still represents a simplification of the structural geometry. Especially for deeper parts and at the margins of the model, where data coverage is low, uncertainties may arise within the results of the simulations.

Together with the resolution the accurate **geometrical description of implemented faults** is a source of errors in modelling the thermal field. In nature, faults usually have an irregular shape and a tilted dip. For this work, testfaults have been implemented as vertical structures, to test the influence of possible permeable fault zones on the coupled thermal field in principle. This is rather a conceptual approach than a realistic description. Such a simplification was necessary due to a lack of available data about the actual location, course and dip of the faults. To assess the real influence of faults on the thermal field in the Molasse Basin area, fault zones with a more realistic, ideally observed course and structure at depth should be implemented.
Moreover, only three major fault zones have been implemented into the sedimentary part of the model of this study though a high number of faults occur in the European Molasse Basin. Since it has been shown by Barton et al. (1995), Magri et al. (2010), Petitta et al. (2011) and Cherubini et al. (2014) that faults may act as pathways for fluid flow not only in sedimentary parts but also in the crust, a realistic implementation of faults in numerical models may have a significant influence in the resulting thermal field. Finally, the realistic numerical implementation of faults in 3D finite element models represents a challenge.

FE-models are based on a continuum assumption, whereas faults in general disrupt the continuum. For this work the discrete feature approach has been considered, though it is worth mentioning that alternatives exist (Nakanten et al. 2013, Tillner et at. 2013, Cherubini et al. 2014, Cacace and Blöcher 2015). Such aspects could be addressed in future studies.

Another possible source of error is the assumption of **laterally uniform isotropic properties** for the model layers. Though measured values have been favoured for all properties, units and areas without observations have been characterised with average values from literature. Indeed, it is known that large lateral heterogeneities may exist with respect to the property distribution in response to different geology and tectonic. For a more precise property assignment a better knowledge about their distribution would be necessary, than available for this study. Especially the hydraulic characteristics of the Upper Jurassic Malm have been simplified for the coupled fluid flow and heat transport simulation. Though the Upper Jurassic Malm aquifer shows a complex system of pores, joints and karst related cavities, it was described with domains with homogeneous hydraulical characteristics on basin-scale, a simplification whose feasibility was stated by Birner (2013). Furthermore, lateral variations of thermal properties in the crust have not been taken into account nor any effects of crustal composition or lithological heterogeneities in the sediments.
Obviously, it cannot be neglected that this simplified characterization of all layers may introduce errors in the modelling results. Nevertheless, this study gives a valuable insight on the first order long wavelength thermal field and can be used as a starting point for follow-up investigations considering more precise structural description. Moreover, sensitivity analyses of thermal properties have shown that changes in the thermal properties would only lead to changes in the absolute temperatures predicted by the models, but would not change the overall temperature trend.

For the calculations of the thermal field different **boundary conditions** have been prescribed to the models. In contrast to the upper thermal boundary condition, prescribed as variable averaged surface temperatures to the topography for both thermal models, different lower thermal boundary conditions were chosen for the different calculations of the lithospheric-scale conductive thermal model and the coupled transport model.
For the lithospheric-scale conductive thermal model a constant temperature of 1,300°C was prescribed at the thermal Lithosphere-Asthenosphere Boundary that varies laterally in depth between 80 and 150 km bsl. This physically justified fixed thermal boundary condition introduces variations of basal heat flow in response to lithospheric heterogeneities but still makes use of assumptions about the depth and exact temperature of this boundary that some authors may question (Houseman et al. 1981, Levin 2006, Fischer et al. 2010).

A different workflow was followed for the simulations of coupled fluid flow and heat transport, for which a temperature distribution was extracted from the lithospheric-scale thermal model and prescribed as lower thermal boundary condition (Dirichlet) at a depth of 7,500 m bsl.

Though this boundary condition introduces the influence of the varying depth of the Lithosphere-Asthenosphere Boundary, the internal structure of the crystalline crust as well as the interdependence between the Alps, the Tauern Body and the Molasse Basin on the basin-wide thermal field as derived from the conductive calculations indirectly into the coupled model, it may as well transfer possible error

sources, as insufficient vertical resolution and homogeneously assigned properties of the crust and the lithospheric mantle, into the coupled model.

The upper hydraulic boundary condition was defined as Dirichlet with a fixed 0 Pa pressure head at the topography to the coupled model. With setting the hydraulic head as equal to the topography steep pressure gradients have been imposed to areas with high topography. This surely overestimates the pressure gradient and may enforce an excessive inflow of cold fluid to larger depths, thus causing an overestimated overall cooling of the system. However, when testing other upper hydraulic boundary conditions (variations of Dirichlet, Cauchy) only the absolute temperatures changed, while the basin-wide temperature trend remained mostly unchanged. In addition, the sensitivity analysis with respect to the hydraulic conductivities of the (Folded) Molasse Sediments showed that it is mainly the latter that controls the hydraulic pressure and temperature distribution within the target Malm aquifer. As the goal of this thesis was to assess regional influencing factors for the deep thermal field, the implemented simplifications were considered as acceptable.

For future studies, however, different upper hydraulic boundary conditions should be considered, though more detailed information about the actual hydrogeological situation of the European Molasse Basin would be needed to reduce this potential source of error.

A further possible source of error is introduced into the modelling results by assuming **steady state conditions** for the calculation of the temperature distribution which neglects the temporal evolution of the thermal field with time. This was done to distinguish the dominant heat transport mechanisms at different depths in the basin from each other. Using a transient approach this task would be much more challenging. However, it has to be admitted that assuming thermal as well as hydraulical equilibrium of the system may be an oversimplification leading to overestimations of the temperatures of the positive and negative thermal anomalies in the German Molasse Basin. With only 15 Ma since the beginning of the Alpine orogeny and the crustal thickening, the related thermal signals my not yet be in steady-state (thermal time constant of the lithosphere ~60 Ma) as indicated by the non-existing isostatic balance shown in chapter 2.6. Hence, a transient consideration of heat transport when calculating the conductive thermal field may lead to a different temperature distribution. Moreover, the results of the coupled simulations have shown, that stable conditions in the thermal field may be expected not until 30,000 years of simulation time, which is twice as much as the time since the end of the last glaciation (10,000 - 15,000 years) after the the start of the Alpine collision, implying that the Molasse Basin is not yet hydraulically equilibrated.

While assuming steady-state conditions may be reasonable for conductive heat transport, since heat conduction is a comparably slow transport mechanism, in some cases, enforcing steady-state equilibrium in coupled simulations may lead to predicted temperatures much too low since advective and convective heat transport show a much faster impact on the thermal field.

For the simulations of coupled fluid flow and heat transport “pseudo” steady-state hydraulical and thermal conditions were assumed by choosing a simulation time of 100,000 years and time steps large

enough to allow the system to equilibrate and enable numerical stability. This oversimplification may have lead to unreasonably low temperatures values at deeper levels in e.g. the Folded Molasse Sediments where cold water enters with high gradients for very long time. Nevertheless, the reproduced temperature distribution has shown that this simplification can be justified in this thesis.

Finally, the predicted temperatures in this study have been compared to the interpolated temperature maps published by GeotIS (Schulz et al. 2009) and just a few measurements of bottom hole and extraction temperatures (tab 4, chapter 3.7 and tab 6, chapter 4.5). To ensure a better reliability of the modelling results, a **calibration** of the model with measured temperature and pressure data, in the best case measured temperature and pressure profiles with depth distributed regularly over the model area, should be done. This could not be done in the course of this thesis because measured temperature and pressure profiles were not accessible.

According to these limitations, some points may require further investigations to explain the temperature pattern and the origin of the thermal anomalies in the German Molasse Basin in its entirety. Such follow-up studies should comprise a further increased horizontal and especially vertical resolution of the model and implement more information about the structure of the deeper parts and at the margins of the model, which however is depending on the availability of structural data. In addition, a modified characterization of the model units with laterally varying thermal, hydraulical and mechanical properties taking into account effects of crustal composition and lithological heterogeneities in the sediments as well as more realistic boundary conditions, especially for the hydraulic upper boundary condition, should be considered to better approximate the natural condition of the Molasse Basin area. This fact accounts also for the more realistic, ideally observed course and structure of faults zones with depth, which should be implemented in future models of the Molasse Basin to assess the real influence of permeable faults of the thermal field on local- and reservoir-scale. Moreover, thermal effects caused by climate fluctuations (glaciations and interglaciations) and its remnants (permafrost) have not been considered in the calculations of the thermal field, but may have an impact in the short wavelength thermal field and should therefore be included into future studies. For such follow-up studies the results of this thesis may be used as starting point and provide reliable thermal and hydraulical boundary conditions, especially for studies on smaller scale for areas in which transregional fluid flow causes local effects in the temperature distribution. The future model should moreover be calibrated with measured temperature and pressure data and an influence on the local and reservoir-scale thermal and pressure field by operating geothermal power plants should be considered.

6. Summarising Conclusions

At the beginning of this thesis, one main question has been asked, which addressed the origin of the pronounced deep thermal anomalies in the European North Alpine Foreland Basin.

To answer this question, a multi-scale 3D modelling approach with different modelling techniques has been followed with which the basin-scale 3D thermal field of the European Molasse Basin was calculated. Thereby, different heat transport processes have been considered and the interdependence between the basin and the adjoining Alps with respect to the thermal field has been assessed. The predicted temperature distribution has been compared to published temperature maps and measured bottom hole and extraction temperatures. Moreover, different further statements could be made about the stress field, the temperature distribution and different heat transport mechanisms in the European Molasse Basin.

With respect to the main question of this thesis, this multi-scale modelling approach was able to reproduce the observed thermal field together with the distinct positive and negative thermal anomalies in the European Molasse Basin. In this thesis it has been shown that the heat budget of the North Alpine Foreland Basin is in fact controlled by a combination of different heat transport mechanisms on lithospheric-scale, though the dominant heat transport mechanism may vary laterally with depth. The evaluation of the predicted thermal field indicates that the thermal anomalies are triggered by conductive heat transport in the first place, but strongly reinforced by fluid flow related cooling. In particular, the superposition of conductive and advective heat transport can be itemised into different thermal effects and fluid flow pattern:

1) The *geothermal gradient* varies laterally over the model area due to the varying depth of the thermal Lithosphere-Asthenosphere Boundary (LAB). Where this boundary is shallow a steeper geothermal gradient leads to higher temperatures at shallower depths (northern part) than in areas with a deeper LAB (southern part).

2) The additional heat input into the system generated by the *radiogenic heat production* of the upper crystalline crust and the crustal material of the Tauern Body varies over the model area due to the varying thicknesses of the respective layers. In areas where these layers are thicker (southern part) more additional heat is added to the system than in areas where the layers are thinner (north), leading to higher average crustal temperatures in the south than in the north.

3) The combined effect of 1 and 2 lead to a geothermal gradient which is not smallest in the area of the Alps as expected, where the LAB is deepest, but higher than in the basin area visible as upwards bend isotherms below the Alps. This is related to the *compensating effect of crustal thickness*. Combined, the upper crystalline crust and the Tauern Body are thinner below the Alpine foreland than below and within the orogon. These thicker crystalline layers produce radiogenic heat adding to the total heat budget what leads to higher temperatures in the south than in the north at levels even deeper than the upper crystalline crust.

4) The efficiency of conductive heat transport varies according to the different thermal conductivities of different lithologies. Heat is transported more efficiently trough material with a higher thermal conductivity (crystalline rocks) than through material with a lower thermal conductivity (sedimentary rocks). In areas, where thermally highly conductive material is cropping out (Tauern Window) or lies shallow below the surface (northern and north-eastern model part), heat can escape the system more efficiently and lower temperatures evolve at shallower depth than in areas with thicker sedimentary cover. Such effect is known as *chimney effect*.

5) A further conductive effect related to differences of thermal conductivities is the *thermal blanketing effect*. This effect occurs in areas, where thermally highly conductive material (crystalline) is covered (basin) or bordered (Alps) by thermal less conductive sediments. In such areas, the heat coming from the mantle and generated in the crust is trapped in the low thermally conductive sediments inducing an insulation effect and causing higher temperatures in areas with thick sedimentary coverage than in areas with less sediments. Furthermore, this effect is stronger with higher contrast in the thermal conductivities in the adjoining lithologies.

6) Fluid particle tracking for coupled heat and fluid transport simulations indicates that the positive thermal anomalies in the area around the city of Munich and at the eastern border of Bavaria are reinforced by *basin-wide fluid flow*. Thereby, surface fluids enter via the thick Folded Molasse Sediment at the Alpine border and flow down into the Malm aquifer until they reaches the hydraulically nonconductive layers. At that depth, the fluid flow direction changes northwards and the warmed-up fluids flow upwards against the slope around the Purbeck formation to create the positive thermal anomalies. In this way the positive thermal anomalies predicted by the conductive model in the south of the Molasse Basin get relocated northwards. The intensity of this effect is mostly dependent on the hydraulic conductivity of the Molasse Sediments providing the buffer between the topography controlled gradient in hydraulic pressure and the pressure distribution in the deep aquifers. The hydraulic conductivity of the Malm aquifer has only a minor influence.

7) The evaluation of fluid particle tracking has further shown that the negative thermal anomaly in the southeast of the city of Munich is caused by *locally limited fluid flow* due to the structural and hydraulic configuration of the Purbeck formation. In the area of the negative thermal anomaly cold fluid enters the system through the Foreland Molasse Sediments until it reaches the hydraulically lower conductive Purbeck formation. At this point the fluid flow deviates to the east and west and contributes to the positive thermal anomalies around the city of Munich and at the eastern border of Bavaria. At the same depth, the Purbeck formation prevents the ascent of warm fluid from deeper parts. Necessarily, these deeper fluids flow round the Purbeck formation and thus additionally contribute to the positive thermal anomalies around Munich and at the eastern border of Bavaria.

The results show that the consideration of the Alps in the modelling work was of high importance to assess the thermal interdependence between the basin and the orogen and with that necessary to reproduce the observed thermal field and the distinct thermal anomalies in the European North Alpine Foreland Basin with a multi-scale modelling approach. Therewith, this workflow extends the state of the art for 3D thermal modelling of large-scale areas in continental collision zones. Moreover, the results imply that the thermal field of the Molasse Basin area can be reproduced assuming steady-state thermal conditions, even though the model area may not be isostatically equilibrated.

The proposed explanation for the distinct thermal anomalies in the basin area may help to reduce the exploration risk for further geothermal drilling projects by improving the understanding of the hydro-thermal dynamics on basin-scale and by providing appropriate lower and lateral thermal boundary conditions for local and regional scale models, an issue of high relevance in thermal modelling.

7. References

Agemar T, Schellschmidt R and Schulz R (2012) Subsurface temperature distribution in Germany. Geothermics 44: 65-77, doi: 10.1016/j.geothermics.2012.07.002.

Agemar T, Weber J and Schulz R (2014a) Deep Geothermal Energy Production in Germany. Energies 7: 4397-4416, doi:10.3390/en7074397.

Agemar T, Alten J-A, Ganz B, Kuder J, Kühne K, Schumacher S and Schulz R (2014b) The Geothermal Information System for Germany – GeotIS. Zeitschrift der Deutschen Gesellschaft für Geowissenschaften 165/2: 129-144, doi: 10.1127/1860-1804/2014/0060.

Allen and Allen (2005) Basin Analysis: Principles and Applications. Wiley-Blackwell, 2nd edition.

Amante C and Eakins BW (2009) ETOPO1: 1 Arc-Minute Global Relief Model: Procedures, Data Sources and Analysis. NOAA Technical Memorandum NESDIS NGDC-24.

Bachmann GH, Dohr G and Müller M (1982) Exploration in a classic thrust belt and its foreland: Bavarian Alps, Germany. American Association of Petroleum Geologists Bull 66: 2529-2542.

Banks RJ, Francis SC and Hipkin RG (2001) Effects of loads in the upper crust on estimates of the elastic thickness of the lithosphere. Geophysical Journal International 145: 291-299, doi: 10.1046/j.0956-540x.2001.01380.x.

Barton CA, Zoback MD and Moos D (1995) Fluid flow along potentially active faults in crystalline rock. Geology 23/8: 683-686, doi: 10.1130/0091-7613(1995)023<0683:FFAPAF>2.3.CO;2.

Bayer U, Scheck M and Koehler M (1997) Modeling of the 3-D thermal field in the northeast German Basin. Geologische Rundschau 86/2: 241–51, doi: 10.1007/s005310050137.

Berge TB and Veal SL (2005) Structure of the Alpine foreland. Tectonics 24, doi: 10.1029/2003TC001588.

BGI (2012) The International Gravimetric Bureau. In: Drewes H, Hornik H, Adam J and Rozsa S (Eds.) The Geodesist's Handbook 2012 (International Association of Geodesy). Journal of Geodesy 86: 10, doi: 10.1007/s00190-012-0584-1.

Bianchi I, Miller MS and Bokelmann G (2014) Insights on the upper mantle beneath the Eastern Alps. Earth and Planetary Science Letters 403: 199-209, doi: 10.1016/j.epsl.2014.06.051.

Birner J, Jodocy M, Fritzer T, Schneider M and Stober I (2009) Projektgebiet - Molassebecken. In: Schulz R (Ed.) Aufbau eines geothermischen Informationssystems für Deutschland (Endbericht – BMU Forschungsvorhaben 0327542), LIAG Archiv-Nr. 0128452: 44-60, Hannover.

Birner J, Mayr C, Thomas L, Schneider M, Baumann T and Winkler A (2011) Hydrochemie und Genese der tiefen Grundwässer des Malmaquifers im bayerischen Teil des süddeutschen Molassebeckens. Zeitschrift für geologische Wissenschaften 39: 291-308.

Birner J, Fritzer T, Jodocy M, Savvatis A, Schneider M and Stober I (2012) Hydraulische Eigenschaften des Malmaquifers im Süddeutschen Molassebecken und ihre Bedeutung für die geothermische Erschließung. Zeitschrift für geologische Wissenschaften 40: 133-156.

Birner J (2013) Hydrogeologisches Modell des Malmaquifers im Süddeutschen Molassebecken. Dissertation, Freie Universität Berlin.

Bjørlykke K (2010) Subsurface water and fluid flow in sedimentary basins. In: Petroleum Geoscience: From Sedimentary Environments to Rock Physics 259–279, Springer, Heidelberg, doi: 10.1007/978-3-642-02332-3_10.

Bleibinhaus F and Gebrande H (2006) Crustal structure of the Eastern Alps along the TRANSALP profile from wide-angle seismic tomography. Tectonophysics 414: 51-69, doi: 10.1016/j.tecto.2005.10.028.

Böhm F, Birner J, Steiner U, Koch R, Sobott R, Schneider M and Wand A (2011) Tafelbankiger Dolomit der Kernbohrung Moosburg SC4: Ein Schlüssel zum Verständniss der Zuflussratern in Geothermiebohrungen des Malmaquifers (Östliches Molasse-Becken; Malm Gamma – Zeta; Süddeutschland). Zeitschrift für geologische Wissenschaften 39/2: 117-157.

Böhm F, Savvatis A, Steiner U, Schneider M and Koch R (2012) Lithofazielle Reservoircharakterisierung zur geothermischen Nutzung des Malm im Großraum München. Grundwasser 18/1: 3-13, doi: 10.1007/s00767-012-0202-4.

Bousquet R, Oberhänsli R, Schmid SM, Berger A, Wiederkehr M, Robert C, Möller A, Rosenberg C, Koller F, Molli G and Zeilinger G (2012b) Metamorphic framework of the Alps. CCGM/CGMW.

Braitenberg C, Ebbing J and Götze H-J (2002) Inverse modelling of elastic thickness by convolution method - the eastern Alps as a case example. Earth and Planetary Science Letters 202: 387-404, doi: 10.1016/S0012-821X(02)00793-8.

Brückl E, Behm M, Decker K, Grad M, Guterch A, Keller GR and Thybo H (2010) Crustal structure and active tectonics in the Eastern Alps. Tectonics 29/2, doi: 10.1029/2009TC002491.

Brückl E (2011) Lithospheric Structure and Tectonics of the Eastern Alps – Evidence from New Seismic Data, Tectonics, Closson D. (Ed.), ISBN: 978-953-307-545-7, InTech, doi: 10.5772/14364.

Büchi UP, Wiener G and Hofmann F (1965) Neue Erkenntnisse im Molassebecken auf Grund von Erdöltiefbohrungen in der Zentral- und Ostschweiz. Eclogae Geologicae Helvetiae 58/1, doi: http://dx.doi.org/10.5169/seals-163259.

Cacace M and Blöcher G (2015) MeshIt - a software for three dimensional volumetric meshing of complex faulted reservoirs. Environmental Earth Sciences 74/ 6: 5191-5209, doi: 10.1007/s12665-015-4537-x.

Cacace M, Kaiser BO, Lewerenz B and Scheck-Wenderoth M (2010) Geothermal energy in sedimentary basins: What we can learn from regional numerical models. Chemie der Erde 70/3: 33-46, doi: 10.1016/j.chemer.2010.05.017.

Cacace M, Blöcher G, Watanabe N, Moeck I, Börsing N, Scheck-Wenderoth M, Kolditz O and Huenges E (2013) Modelling of fractured carbonate reservoirs: outline of a novel technique via a case study from the Molasse Basin, southern Bavaria, Germany. Environmental Earth Sciences 70: 3585–3602, doi: 10.1007/s12665-013-2402-3.

Carafa MMC and Barba S (2013) The stress field in Europe: optimal orientations with confidence limits. Geophysical Journal International 193/2: 531-548, doi: 10.1093/gji/ggt024.

Champagnac J-D, Schlunegger F, Norton K, Blankenburg F, Abbühl LM and Schwab M (2009) Erosion-driven uplift of the modern Central Alps. Tectonophysics 474: 236-249, doi: 10.1016/j.tecto.2009.02.024.

Cherubini Y, Cacace M, Scheck-Wenderoth M and Noack V (2014) Influence of major fault zones on 3-D coupled fluid and heat transport for the Brandenburg region (NE German Basin). Geothermal Energy Science 2/2: 1-20, doi: 10.5194/gtes-2-1-2014.

Chopra P and Holgate F (2005) A GIS analysis of temperature in the Australian Crust. Proceedings of the World Geothermal Congress 2005. Antalya, Turkey.

Clauser C (2011a) Thermal Storage and Transport Properties of Rocks I: Heat Capacity and Latent Heat. In: Gupta H (Ed.) Encyclopedia of Solid Earth Geophysics, Springer Heidelberg.

Clauser C (2011b) Radiogenic Heat Production of Rocks. In: Gupta H (Ed.) Encyclopedia of Solid Earth Geophysics, Springer Heidelberg.

D'Agostino N, Avallone A, Cheloni D, D´Anastasio E, Mantenuto S and Selvaggi G (2008) Active tectonics of the Adriatic region from GPS and earthquake slip vectors. Journal of Geophysical Research 113, doi: 10.1029/2008JB005860.

Deichmann N, Baer M, Braunmiller J, Ballarin D, Bay F, Delouis B, Fäh D, Giardini D, Kastrup U, Kind F, Kradolfer U, Künzle W, Röthlisberger S, Schler T, Salichon J, Sellami S, Spühler E and Wiemer S (1999) Earthquakes in Switzerland and surrounding regions during 1999. Eclogae Geologicae Helvetiae 93: 395–406.

Delacou B, Sue C, Champagnac JD and Burkhard M (2004) Present-day geodynamics in the bend of the western and central Alps as constrained by earthquake analysis. Geophysical Journal International 158: 753-774, doi: 10.1111/j.1365-246X.2004.02320.x.

Diersch HJG (2009) FEFLOW Finite Element Subsurface Flow and Transport Simulation System. Reference Manual/White Papers 1, WASY GmbH Institute for Water Resources, Planning and System Research, Berlin.

Dragoni M (1993) The brittle-ductile transition in tectonic boundary zones. Annals of Geophysics, doi: 10.4401/ag-4282.

DWD (2013) monthly mean of air temperatur, 1km grid for Germany. https://werdis.dwd.de/werdis/toSimpleSearchShowMetaData.do

Ebbing J (2002) 3-D Dichteverteilung und isostatisches Verhalten der Lithosphäre in den Ostalpen. Dissertation, Freie Universität Berlin.

Ebbing J (2004) The crustal structure of the Eastern Alps from a combination of 3D gravity modelling and isostatic investigations. Tectonophysics 380: 89-104, doi: 10.1016/j.tecto.2003.12.002.

Ebbing J, Braitenberg C and Götze H-J (2006) The lithospheric density structure of the Eastern Alps. Tectonophysics 414: 145-155, doi:10.1016/j.tecto.2005.10.015.

Ernstson K and Pohl J (1977) Neue Modelle zur Verteilung der Dichte und Geschwindigkeit im Ries-Krater. Geologica Bavarica 75: 355-371.

Fischer KM, Ford HA, Abt DL and Rychert CA (2010) The Lithosphere-Asthenosphere Boundary. Annual Review of Earth and Planetary Sciences 38: 551-575, doi: 10.1146/annurev-earth-040809-152438.

Fowler CMR (2005) The Solid Earth: An Introduction to Global Geophysics, Cambridge University Press, Cambridge.

Förster A (2001) Analysis of borehole temperature data in the Northeast German Basin: Continuous logs versus bottom-hole temperatures. Petroleum Geoscience 7: 241–254, doi: 10.1144/petgeo.7.3.241.

Freudenberger W and Schwerd K (1996) Geological Map of Bavaria (1:500,000) and its explanations. Bavarian Geological Survey, Munich.

Frisch H and Huber B (2000) A Hydrogeological Model and the Attempt of a Balance of the Thermal Water of the Malmkarst in the Southgerman and the Neighbouring Upper Austrian Molasse Basin. Hydrogeologie und Umwelt 20: 25-43.

Gebrande H und TRANSALP Working Group (2001) TRANSALP: concept and main results on the project. Geologisch-Paläontologische Mitteilungen 25: 7-8, Innbruck.

Geissler WH, Sodoudi F and Kind R (2010) Thickness of the central and eastern European lithosphere as seen by S receiver functions. Geophysical Journal Internation 181: 604-634, doi: 10.1111/j.1365-246X.2010.04548.x.

Genser J, van Wees JD, Cloething S and Neubauer F (1996) Eastern Alpine tectono-metamorphic evolution: Constraints from two-dimensional P-T-t modelling. Tectonics 15: 584-604, doi: 10.1029/95TC03289.

GeoMol Team (2015) GeoMol – Assessing subsurface potentials of the Alpine Foreland Basins for sustainable planning and use of natural resources – Project Report, Bavarian Environment Agency, Augsburg, Germany.

Gölke M and Coblentz D (1996) Origin of the European regional stress field. Tectonophysics 266: 11-24, doi: 10.1016/S0040-1951(96)00180-1.

Götze H-J, Meurers B, Schmidt S and Steinhauser P (1991) On the isostatic state of the eastern Alps and the central Andes: A statistical comparison. Geological Society of America Special Papers 265: 279-290, doi: 10.1130/SPE265-p279.

Götze HJ and Schmidt S (2010) IGMAS+: A new 3D gravity, FTG and magnetic modelling software tool. In: Lane (Ed) Airborne Gravity 2010 Workshop: Published jointly by Geoscience Australia and the Geological Survey of New South Wales, Geoscience Australia Record 2010/23 and GSNSW File GS2010/0457.

Götze H-J (2011) Gravity Methods, Principles. In: Gupta H (Ed): Encyclopedia of Solid Earth Geophysics. Volume 1: 500-504, Springer, Dordrecht, Netherlands.

Grad M, Tiira T and ESC Working Group (2009) The Moho depth map of the European Plate. Geophysical Journal International 176: 279-292, doi: 10.1111/j.1365-246X.2008.03919.x.

GTV (2014) Nutzung der Geothermie in Deutschland
http://www.geothermie.de/wissenswelt/geothermie/in-deutschland.html

Huenges E (2010) Geothermal Energy Systems. WILEY-VCH, Weinheim.

Handy MR, Schmid SM, Bousquet R, Kissling E and Bernoulli D (2010) Reconciling plate-tectonic reconstructions of the Alpine Tethys with geological-geophysical record of spreading and subduction in the Alps. Earth-Science Reviews 102: 121-158, doi: 10.1016/j.earscirev.2010.06.002.

Handy MR and Rosenberg CL (2011) From embryonic tectonics and geosynclines to modern concepts of rifting, spreading, and Alpine orogenesis: a summary of contributions to the 9th Alpine Workshop (Cologne, 2009). International Journal of Earth Sciences 100: 895–897, doi: 10.1007/s00531-011-0647-1.

Heidbach O, Tingay M, Barth A, Reinecker J, Kurfeß D and Müller B (2009) The World Stress Map based on the database release 2008, equatorial scale 1:46,000,000. Commission for the Geological Map of the World, Paris, doi: 10.1594/GFZ.WSM.Map2009 .

Hermanrud C, Cao S and Lerche I (1990) Estimates of virgin rock temperature derived from BHT measurements: Bias and error. Geophysics 55, 924–931.

HISTALP (2013) Historical Instrumental Climatological Surface Time Series Of The Greater Alpine Region: http://www.zamg.ac.at/histalp/

Homuth S, Götz AE and Sass I (2014) Lithofacies and depth dependency of thermo- and petrophysical rock parameters of the Upper Jurassic geothermal carbonate reservoirs of the Molasse Basin. Zeitschrift der Deutschen Gesellschaft für Geowissenschaften 165/3: 469-486, doi: 10.1127/1860-1804/2014/0074.

Homuth S, Götz AE and Sass I (2015) Physical Properties of the geothermal carbonate reservoirs of the Molasse Basin, German - Outcrop Analogue vs. Reservoir Data. World geothermal congress 2015, 19.04–24.04.2015, Melbourne, Australia.

Houseman GA, McKenzie DP and Molnar P (1981) Convective instability of a thickened boundary layer and its relevance for the thermal evolution of continental convergent belts. Journal of Geophysical Research: Solid Earth 86/B7: 6115–6132, doi: 10.1029/JB086iB07p06115View/save citation.

Hrubcová P, Špičák A, Švancara J, Růžek B, Hubatka F, Tomášková A and Brož M (2002) Investigation of the Deep Structure of the Bohemian Massif CELEBRATION 2000. MS Ministry of Environment, CR.

InMeteo (2013) Archiv počasí, klima České republiky
http://www.in-pocasi.cz/archiv/img/teplotap2a.png

ITG (2014) Informationsportal Tiefe Geothermie.
http://www.tiefegeothermie.de/projekte/garching

Jankowski (1977) Die Postimpakt Sedimente in der Forschungsbohrung Nördlingen 1973. Geologica Bavarica 75: 21-36.

Jodocy M and Stober I (2009) Geologisch-geothermische Tiefenprofile für den südwestlichen Teil des Süddeutschen Molassebeckens. Zeitschrift der Deutschen Gesellschaft für Geowissenschaften, 160/4: 359–366, doi: 10.1127/1860-1804/2009/0160-0359.

Kaiser BO, Cacace M, Scheck-Wenderoth M and Lewerenz B (2011) Characterization of main heat transport processes in the Northeast German Basin: Constraints from 3D numerical models. Geochemistry Geophysics Geosystems (G3) 12, C07011, doi: 10.1029/2011GC003535.

Karousova H, Plomerova J and Babuska V (2013) Upper-mantle structure beneath the southern Bohemian Massif and its surroundings imaged by high-resolution tomography. Geophysical Journal Internationa 194: 1203-1215, doi: 10.1093/gji/ggt159.

Kempf O, Matter A, Burbank DW and Mange M (1999) Depositional and structural evolution of a foreland basin margin in a magnetostratigraphic framework: the eastern Swiss Molasse Basin. International Journal of Earth Sciences 88: 253 - 275, doi: 10.1007/s005310050263.

Koch A, Jorand R, Arnold J, Pechnig R, Mottaghy D, Vogt C and Clauser C (2009) Erstellung statistisch abgesicherter thermischer und hydraulischer Gesteinseigenschaften für den flachen und tiefen Untergrund in Deutschland (Phase 2 – Westliches Nordrhein-Westfalen und bayerisches Molassebecken), Schlussbericht zum BMU-Projekt FKZ 0327563, E.ON Energy Research Center, Lehrstuhl Applied Geophysics and Geothermal Energy, RWTH Aachen.

Kutasov IM (1999) Applied Geothermics for Petroleum Engineers. Elsevier Science B.V., Netherlands.

Lampe C and Person M (2002) Advective cooling within sedimentary rift basins - application to the Upper Rhinegraben (Germany). Marine and Petroleum Geology19/3: 361-375, doi: 10.1016/S0264-8172(02)00022-3.

Landolt-Börnstein (1982) Zahlenwerte und Funktionen aus Naturwissenschaft und Technik, Band 1a, Springer Berlin, Germany.

Lemcke K (1973) Zur nachpermischen Geschichte des nördlichen Alpenvorlandes. Geologica Bavarica 69: 5-48.

Lenhardt W, Švancara J, Melichar P, Pazdírková J, Havír J and Sýkorová Z (2007) Seismic activity of the Alpine-Carpathian-Bohemian Massif region with regard to geological and potential field data. Geologica Carpathica 58: 397-412.

Levin LE (2006) Structure of the thermal lithosphere and asthenosphere beneath oceans and continents. Geotectonics 40/5: 357-366, doi: 10.1134/S0016852106050037.

Magri F, Bayer U, Maiwald U, Otto R and Thomsen C (2009) Impact of transition zones, variable fluid viscosity and anthropogenic activities on coupled fluid-transport processes in a shallow salt-dome environment. Geofluids 9: 182-194, doi: 10.1111/j.1468-8123.2009.00242.x.

Magri F, Akar T, Gemici U and Pekdeger A (2010) Deep geothermal groundwater flow in the Seferihisar-Balcova area, Turkey: results from transient numerical simulations of coupled fluid flow and heat transport processes. Geofluids 10, 388-405, doi: 10.1111/j.1468-8123.2009.00267.x.

Majorowicz J, Nieuwenhuis G, Unsworth M, Phillips and Verveda R (2014) High temperatures predicted in the granitic basement of northwest Albert - an assessment of the EGS energy potential.

Proceedings of 39th workshop on geothermal reservoir engineering Stanford University, Stanford California, SGP-TR-202.

Mareschal J-C and Jaupart C (2013) Radiogenic heat production, thermal regime and evolution of continental crust. Tectonophysics 609: 524–534, doi: 10.1016/j.tecto.2012.12.001.

Marotta AM and Splendore R (2014) 3D mechanical structure of the lithosphere below the Alps and the role of the gravitational body forces in the regional present-day stress field. Tectonophysics 631: 117-129, doi:10.1016/j.tecto.2014.04.038.

Maystrenko YP and Scheck-Wenderoth M (2013) 3D lithosphere-scale density model of the Central European Basin System and adjacent areas. Tectonophysics 601: 53-77, doi: 10.1016/j.tecto.2013.04.023.

Miller H (1976) A lithospheric seismic profile along the axis of the Alps, 1975. Pure and Applied Geophysics 114: 1109-1130, doi: 10.1007/BF00876205.

Mitterbauer U, Behm M, Brückl E, Lippitsch R, Guterch A, Randy Keller G, Koslovskaya E, Rumpfhuber E-M and Sumanovac F (2011) Shape and origin of the East-Alpine slab constrained by the ALPASS teleseismic model. Tectonophysics 510: 195-206, doi: 10.1016/j.tecto.2011.07.001.

Moeck I, Jentsch A, Steiger T, Stiller M, Tondera D and Blöcher G (2013) Geothermal field development in foreland basins: Case study Mauerstetten, Bavarian Molasse Basin (Germany). EGU General Assembly European Geosciences Union, Vienna, Austria.

Nafe JE and Drake CL (1957) Variation with Depth in Shallow and Deep Water Marine Sediments of Porosity, and the Velocities of Compressional and Shear Waves. Geophysics 22: 523-552, doi: 10.1190/1.1438386.

Nakaten B, Tillner E and Kempka T (2013) Virtual Elements for Representation of Faults, Cracks and Hydraulic Fractures in Dynamic Flow Simulations. Energy Procedia 40: 447-453, doi: 10.1016/j.egypro.2013.08.051.

Nield DA and Bejan A (2006) Convection in Porous Media. Springer, NewYork.

Noack V, Cherubini Y, Scheck-Wenderoth M, Lewerenz B, Höding T, Simon A and Moeck I (2010) Assessment of the present-day thermal field (NE German Basin) - Inferences from 3D modelling. Geochemistry, 70/3: 47-62, doi:10.1016/j.chemer.2010.05.008.

Noack V, Scheck-Wenderoth M, Cacace M and Schneider M (2013) Influence of fluid flow on the regional thermal field: results from 3D numerical modelling for the area of Brandenburg (North German Basin). Environmental Earth Sciences 70/ 8: 3523-3544, doi: 10.1007/s12665-013-2438-4.

Noack V (2014) Evaluation of main controlling factors for the recent regional thermal field in Brandenburg (North German Basin). Dissertation, Freie Universität Berlin.

Okaya N, Cloething S and Mueller St (1996) A lithospheric cross-section through the Swiss Alps – II. Constraints on the mechanical structure of a continent-continent collision zone. Geophysical Journal International 127: 399-414, doi: 10.1111/j.1365-246X.1996.tb04729.x.

Pamer RFJ and Diepolder GW (2010) 3D geological modelling in Bavaria – state-of-the-art at a State Geological Survey. Zeitschrift der Deutschen Gesellschaft für Geowissenschaften 161/2: 189 - 203, doi: 10.1127/1860-1804/2010/0161-0189.

Pasquale V, Chiozzi P and Verdoya M (2013) Evidence for thermal convection in the deep carbonate aquifer of the eastern sector of the Po Plain, Italy. Tectonophysics 594: 1-12, doi: 10.1016/j.tecto.2013.03.011.

Pasternak M (2015) Exploration und Produktion von Erdöl und Erdgas in Deutschland 2014. Erdöl Erdgas Kohle 131/7: 258 - 77.

Pavlis NK, Holmes SA, Kenyon AC and Factor JK (2012) The development and evaluation of the Earth Gravitational Model 2008 (EGM2008). Journal Geophysical Research 117, B04406, doi: 10.1029/2011JB008916.

Persaud M and Pfiffner OA (2004) Active deformation in the eastern Swiss Alps: post-glacial faults, seismicity and surface uplift. Tectonophysics 385: 59-84, doi: 10.1016/j.tecto.2004.04.020.

Petitta M, Primavera P, Tuccimei P and Aravena R (2011) Interaction between deep and shallow groundwater systems in areas affected by Quaternary tectonics (Central Italy): a geochemical and isotope approach. Environmental Earth Sciences 63: 11-30, doi: 10.1007/s12665-010-0663-7.

Pratt JH (1855) On the attraction of the Himalaya Mountains and of the elevated regions beyond them, upon the plumb line in India. Philosophical Transactions of the Royal Society London 145: 53-100.

Przybycin AM, Scheck-Wenderoth M and Schneider M (2015a) Assessment of the isostatic state and the load distribution of the European Molasse basin by means of lithospheric-scale 3D structural and gravity modelling. International Journal of Earth Sciences 104/5: 1405-1424, doi: 10.1007/s00531-014-1132-4.

Przybycin AM, Scheck-Wenderoth M and Schneider M (2015b) The 3D conductive thermal field of the North Alpine Foreland Basin: influence of the deep structure and the adjacent European Alps. Geothermal Energy 3: 17, doi: 10.1186/s40517-015-0038-0.

Ranalli G (1995) Rheology of the Earth. Second Edition, Chapman and Hall, London.

Reinecker J, Tingay M, Müller B and Heidbach O (2010) Present-day stress orientation in the Molasse Basin. Tectonophysics 482: 129-138, doi: 10.1016/j.tecto.2009.07.021.

Reischenbacher D and Sachsenhofer RF (2011) Entstehung von Erdgas in der oberösterreichischen Molassezone: Daten und offene Fragen. BHM Berg- und Hüttenmännische Monatshefte 156/11: 463 - 468, doi: 10.1007/s00501-011-0037-9.

Roeder D and Bachmann GH (1996) Evolution, structure and petroleum geology of the German Molasse Basin. In: Ziegler P and Horvath F (Ed) Peri-Tethys Memoir 2: Structure and Prospects of Alpine Basins and Forelands. Memoires Museum National d'Histoire Naturelle, 170: 263 - 284, Editions du Museum National d'Histoire Naturelle, Paris, France.

Rupf I and Nitsch E (2008) Das Geologische Landesmodell von Baden-Württemberg – Datengrundlagen, technische Umsetzung und erste geologische Ergebnisse. LGRB- Informationen 21. Freiburg.

Rühaak W (2009) Multidimensional modeling of the thermal and flow regime in the western part of the Molasse Basin, Southern Germany. Dissertation. Rheinisch-Westfälische Technische Hochschule Aachen.

Rühaak W (2015) 3-D interpolation of subsurface temperature data with measurement error using kriging. Environmental Earth Sciences 73/4: 893 - 900, doi: 10.1007/s12665-014-3554-5.

Rühaak W, Rath V and Clauser C (2010) Detecting thermal anomalies within the Molasse Basin, southern Germany. Hydrogeology Journal 18: 1897-1915, doi: 10.1007/s10040-010-0676-z.

Sachsenhofer RF, Gratzer R, Tschelaut W and Bechtel A (2006) Characterisation of non-producible oil in Eocene reservoir sandstones (Bad Hall Nord field, Alpine Foreland Basin, Austria). Marine and Petroleum Geology 23/1: 1-15, doi: 10.1016/j.marpetgeo.2005.07.002.

Scheck M (1997) Dreidimensionale Strukturmodellierung des Nordostdeutschen Beckens unter Einbeziehung von Krustenmodellen. Dissertation, Freie Universität Berlin.

Scheck M and Bayer U (1999) Evolution of the Northeast German Basin - inferences from a 3D structural model and subsidence analysis. Tectonophysics 313: 145-169, doi: 10.1016/S0040-1951(99)00194-8.

Scheck M, Bayer U and Lewerenz B (2003) Salt redistribution during extension and inversion inferred from 3D backstripping. Tectonophysics 373: 55 - 73, doi: 10.1016/S0040-1951(03)00283-X.

Scheck-Wenderoth M, Cacace M, Maystrenko YP, Cherubini Y, Noack V, Kaiser BO, Sippel J and Lewerenz B (2014) Models of heat transport in the Central European Basin System: Effective mechanisms at different scales. Marine and Petroleum Geology 55: 315-331, doi: 10.1016/j.marpetgeo.2014.03.009.

Schmid SM, Fügenschuh B, Kissling E and Schuster R (2004a) Tectonic map and overall architecture of the Alpine orogen. Eclogae Geologicae Helvetiae 97: 93-117, doi: 10.1007/s00015-004-1113-x.

Schmid S, Fügenschuh B, Kissling E and Schuster R (2004b) TRANSMED Transects IV, V and VI: Three lithospheric transects across the Alps and their forelands. In: Cavazza W, Roure F, Spakman W, Stampfli GM, and Ziegler PA (eds) The TRANSMED Atlas: The Mediterranean Region from Crust to Mantle. Springer Verlag.

Schmid S, Bernoulli D, Fügenschuh B, Matenco L, Schefer S, Schuster R, Tischler M and Ustaszewski K (2008) The Alpine-Carpathian-Dinaridic orogenic system: correlation and evolution of tectonic units. Swiss Journal of Geosciences 101: 139-183, doi: 10.1007/s00015-008-1247-3.

Schmidt F (2010) Dynamical masses in modified gravity. Physical Reviews, doi: 10.1103/PhysRevD.81.103002.

Schulz R, Agemar T, Alten J-A, Brunken, J, Heber M, Kuder J, Kühne K, Maul A-A, Pester S, Schönhofer K, Fritzer T, Birner J, Schneider M, Rauppach K, Seibt P, Wolfgramm M, Brandes J, Feldrappe H, Obst K, Jodocy M and Stober I (2009) Aufbau eines geothermischen Informationssystems für Deutschland (Endbericht BMU Forschungsvorhaben 0327542), LIAG Archiv-Nr.: 0128452: 114 S., Hannover.

Schulz R and Thomas R (2012) Geothermische Charakterisierung von karstig-klüftigen Aquiferen im Großraum München (Endbericht – BMU Forschungsvorhaben 0325013A). LIAG Archiv-Nr. 0130392: 98 S., Hannover.

Seiberlich CKA, Ritter JRR, and Wawerzinek B (2013) Topography of the lithosphere-asthenosphere boundary below the Upper Rhine Graben Rift and the volcanic Eifel region, Central Europe. Tectonophysics 603: 222-236, doi: 10.1016/j.tecto.2013.05.034.

Simeoni O and Brückl E (2009) The Effect of Gravity Stripping on the Resolution of Deep Crustal Structures in the Eastern Alps and Surrounding Regions. Austrian Journal of Earth Sciences 102: 157-169.

Singer J, Diehl T, Husen S, Kissling E and Duretz T (2014) Alpine lithosphere slab rollback causing lower crustal seismicity in northern foreland. Earth and Planetary Science Letters 397: 42 - 56, doi: 10.1016/j.epsl.2014.04.002.

Stephenson R, Egholm D, Nielsen SB and Stovba SM (2009) Role of thermal refraction in localizing intraplate deformation in southeastern Ukraine. Nature Geoscience 2: 290 - 293; doi: 10.1038/ngeo479.

StMWIT (2010) Bayerischer Geothermieatlas. Bayerisches Staatsministerium für Wirtschaft, Infrastruktur, Verkehr und Technologie München.

Tesauro M (2009) An integrated study of the structure and thermomechanical properties of the European lithosphere. Dissertation, Vrije University Amsterdam.

Tillner E, Kempka T, Nakaten B and Kühn M (2013) Brine migration through fault zones: 3D numerical simulations for a prospective CO2 storage site in Northeast Germany. International Journal of Greenhouse Gas Control 19: 689-703, doi: 10.1016/j.ijggc.2013.03.012.

Thomas R, Schwerd K, Bram K and Fertig J (2006) Shallow high-resolution seismics and reprocessing of industry profiles in southern Bavaria: The Molasse and the northern Alpine front. Tectonophysics 41: 87-96, doi: 10.1016/j.tecto.2005.10.025.

Turcotte DL and Schubert G (2014) Geodynamics. 3rd edition, Cambridge University Press, New York.

Ullemeyer K, Siegesmund S, Rasolofodaon NJ and Behrmann JH (2006) Experimental and texture-derived P-wave anisotropy of principal rocks from the TRANSALP traverse: An aid for the interpretation of seismic field data. Tectonophysics 414: 97-116, doi:10.1016/j.tecto.2005.10.024.

Vilá M, Fernández M and Jiménez-Munt I (2010) Radiogenic heat production variability of some common lithological groups and its significance to lithospheric thermal modeling. Tectonophysics 490: 152-164, doi: 10.1016/j.tecto.2010.05.003.

Vosteen H-D (2003) The thermal regime of the Eastern Alps along the TRANSALP project. Dissertation, Rheinisch-Westfälische Technische Hochschule Aachen.

Vosteen H-D, Rath V, Clauser C and Lammerer B (2006) A review of the thermal regime of the Eastern Alps with respect to the effects of paleoclimate and exhumation. Tectonophysics 414: 157–167, doi: 10.1016/j.tecto.2005.10.022.

Wagini A, Steinhauser P and Meurers B (1988) Isostatic residual gravity map of Austria. U.S. Geological Survey Open File Report, 87-402.

Walperdorf A, Baiz S, Calais E, Tregoning P and Nocquet J-M (2006) Deformation in the Jura Mountains (France): First results from semi-permanent GPS measurements. Earth and Planetary Science Letters 245: 365-372, doi: 10.1016/j.epsl.2006.02.037.

Watts A (2011) Isostasy. In: Gupta H (Ed) Encyclopedia of solid earth Geophysics. Volume 1: 647-662, Springer, Dordrecht, Netherlands.

Werner J (1978) Die Thermalwasserbohrung Saulgau (Württemberg). Abhandlung des Geologischen Langesamtes Baden-Württemberg 8: 129-164.

Willinghofer E and Cloething S (2003) Present-day lithospheric strength of the Eastern Alps and its relationship to neotectonics. Tectonics 22, 1075, doi: 10.1029/2002TC001463.

8. Appendix 1

Publications related to this thesis

Przybycin AM, Scheck-Wenderoth M and Schneider M (2015a) Assessment of the isostatic state and the load distribution of the European Molasse basin by means of lithospheric-scale 3D structural and gravity modelling.
International Journal of Earth Sciences 104/5: 1405-1424, doi: 10.1007/s00531-014-1132-4.

Przybycin AM, Scheck-Wenderoth M and Schneider M (2015b) The 3D conductive thermal field of the North Alpine Foreland Basin: influence of the deep structure and the adjacent European Alps. Geothermal Energy 3:17, doi 10.1186/s40517-015-0038-0.

Przybycin AM, Scheck-Wenderoth M and Schneider M: The origin of deep geothermal anomalies in the German Molasse basin assessed by 3D coupled numerical modelling of coupled fluid flow and heat transport.
Under peer-review at Geothermics.